Use of CFD techniques to improve the energetic efficiency of a hull form with particular reference to bulbous bows

BOUZID Tawfiq

Master Thesis

presented in partial fulfillment
of the requirements for the double degree:
“Advanced Master in Naval Architecture” conferred by University of Liege
"Master of Sciences in Applied Mechanics, specialization in Hydrodynamics, Energetics and Propulsion” conferred by Ecole Centrale de Nantes

developed at University of Genoa
in the framework of the

“EMSHIP”
Erasmus Mundus Master Course
in “Integrated Advanced Ship Design”

Ref. 159652-1-2009-1-BE-ERA MUNDUS-EMMC

Supervisor:	Prof. Dario Boote, M.Ferrando **University of Genoa**
Reviewer:	Prof: Lungu Adrian **University of Galati - Romania**

Genoa, February 2013

Use of CFD techniques to improve the energetic efficiency of a hull form with particular reference to bulbous bows

BOUZID Tawfiq

Master Thesis

presented in partial fulfillment
of the requirements for the double degree:
“Advanced Master in Naval Architecture” conferred by University of Liege
"Master of Sciences in Applied Mechanics, specialization in Hydrodynamics, Energetics and Propulsion” conferred by Ecole Centrale de Nantes

developed at University of Genoa
in the framework of the

“EMSHIP”
Erasmus Mundus Master Course
in “Integrated Advanced Ship Design”

Index:

Abstract:

After significant effort in the marine research, hydrodynamics have begun to venture into computational prediction of hydrodynamic behavior of surface ships. The flow pattern around ship hull plays an important role in its resistance. In this work CFD has been used for calculating ship resistance, and investigating its variation when changing the ship hull form due to varying the geometrical parameters of the bulbous bow, which represents a very important task in the optimization of the efficiency of the ship hull form.
Commercial software is used for grid generation and flow solution. In the present work the STARCCM+ software is used to simulate ship resistance.

Introduction:

In recent years, the design of a large motor yacht is focused on higher speeds, as it's known that in generals the yachts are working at the cruising speed. This indicates the need for focusing hull design to have less resistance rather than good hull efficiency at cruising speed. Using an optimization methods to optimize the area of immersed transom, bulbous bow and hull form…etc., it's shown that the bulbous bow has a big effect on the wave making resistance rather than on the total ship resistance. This drives to study the ship resistance and its components with particular reference to the influence of the bulbous parameters on the wave making resistance.

In order to define the influence of the bulbous parameters on the ship resistance, the Kracht theory will be use. In his method Kracht defined six parameters for the bulb, three linear and three nonlinear, each parameter having a different effect on the wave making resistance either on interference or breaking wave. This knowledge allows us to use the systematic method to optimize the bulbous bow, this method based on the modification of each parameter of the bulb separately, and note the influence of each one on the ship resistance. Unfortunately it's not the case for the bulb where it cannot modify each parameter independently.

The yacht model has been provided by AZIMUT-BENETTI shipyard, where this model has already tested in Towing tank, with initial bulb. The methodology of this project is to simulate the ship resistance using Computational Fluid Dynamics by using STARCCM+ Software which is able to solve this kind of problems (Free surface). The initial hull will simulate in STARCCM+ and the result obtained will be compared with the one obtained from experimental test, in order to check the validity of the mesh generated which is consider the main important task in ship simulation. The valid error required by the company AZIMUT-BENETTI is about of 5% of ship resistance.

Once the ship resistance simulates and the results correspond to the requirement of the company, the next task will be the optimization of the bulbous bow shape. In order to optimize the bulb the KRACHT method (theory) is used, following to this theory the bulb shape will be modify according to the criteria of the kracht experience. All alternatives shapes of the bulb will be tested and the optimum bulb will be compared with the initial bulb shape in order to appreciate the influence of the bulb on the wave making resistance further than total ship resistance.

Chapter 1: Introduction to CFD.

1.1 Introduction:

This chapter is intended as an introductory for Computational Fluid Dynamics CFD. In order to use CFD method, the following steps are required. First, the mathematical equations describing the fluid flow are known (usually a set of partial differential equations). In order to produce a numerical analogue of the equations, the discretization is used, and the computational domain is then divided into small grids or elements. Finally, since the equations are known, to solve these equations the initial conditions and the boundary conditions of the specific problem are used. The solution method can be direct or iterative.
In addition, certain control parameters are used to control the convergence, stability, and accuracy of the method.

Computational fluid dynamics is the solution of a system of partial differential equations (PDEs) to determine a numerical solution of a problem. Since the difficulty to solve the PDEs analytically for the flow physics, this allows numerical experiments to be performed without the need for full-blown experimental results.

Numerically, several different mathematical formulations are used to solve a system of PDEs.

1. Finite difference method (FDM)
2. Finite element method (FEM)
3. Finite volume method (FVM)

Currently the finite volume method is the method of choice for implementation within the majority of commercially available software packages. However, other methods have been shown to achieve accurate results. Finite volume methods (and all numerical methods) are used to create an approximation using discretization of the problem physics.

Recent advances in computational resources have made the use of computational fluid dynamics (CFD) to support industrial design activities more commonplace. While large and small organizations have adopted the technology. Especially for navel domain the CFD method has shown height efficiency.

1.1.1 Common Terminology and Abbreviations:

1.1.1.1 Abbreviations:

CFD: Computational Fluid Dynamics
DNS: Direct Numerical Simulations
FEM: Finite Element Method
FVM: Finite Volume Method
GPM: Gallons per minute
LES: Large Eddy Simulation
PDEs: Partial Differential Equations

1.1.1.2 Definition of Common Terms:

Automeshing : The ability of a software package to construct a mesh independently of user interaction.
Bias: Stretching the length of a mesh in one or more directions.
Grid or Mesh: Computational grid used to construct cells for a CFD solver.
Kolmogorov Scale: The turbulent scale where all eddies are considered isentropic and the eddy energy is dissipated through viscous effects.
Navier Stokes Equations: System of partial differential equations governing the behavior of a fluid or gas.

1.1.1.3 Definition of Common Mathematical Symbols:

Note: The symbols included in this list are indicative of the symbols used in this chapter.
There are several notations that differ between fields of study and among authors of various reference texts [9].

$\frac{D}{Dt}$: The material derivative can be defined as the operator $\frac{\partial}{\partial t} + v \,.\, \nabla$
μ: Dynamic viscosity [Pa/m²]
μ_t: Turbulent viscosity
ν :Kinematic viscosity
Ω: Representation of a mathematical domain or control volume
$\boldsymbol{\rho}$: Density of a material
Б: Stress tensor
τ_w :Wall shear stress
T: Deviatoric stress tensor
e :Specific energy density
f :Body forces per unit volume
k :von Karman constant
m :Mass of a material
P: Pressure
q :Heat vector
u :Velocity parallel to the wall (when referenced with law of the wall)
u^+ :Dimensionless velocity, velocity parallel to the wall as a function of y
u_r :Shear velocity
y :Distance from wall

1.2. Mathematics:

1.2.1 Lagrangian vs Eulerian Formulations:

In order to analyze the motion of the particles, there are two descriptions; the first is the Lagrangian formulations which involve tracking individual particles as a function of placement in the reference configuration and time.
The second is the Eulerian, in his description; the observations are made at a point in space.
Since that the motion of fluids is mysterious, it is impossible in some cases, to track individual material particles. Individual particles are not tracked; the user is aware of the necessary variables (such as velocity) in a given region or in the case of the finite volume method, within the control volume.

1.2.2 Navier Stokes Equations:

The Navier-Stokes equations are the result from the conservation of momentum coupled with conservation of mass, energy, and possible equations of state. In a non-reduced form, they create a complete mathematical model of the fluid. However, because of the complexity of the Navier-Stokes equations, including nonlinearity, they are not easily solved analytically. The complexity of these equations is the reason behind using a computational method to calculate a numerical solution [9].

1.2.2.1 Conservation of Mass:

Consider a finite control volume Ω in which lies the continuum under consideration. The material in this continuum has a mass m, and a density $\boldsymbol{\rho}$ within the control volume Ω. The mass within the control volume can be represented in terms of $\boldsymbol{\rho}$ in an integral form as:

$$m = \int_{\Omega} \rho d\Omega \qquad (1.1)$$

In the absence of mass sources and sinks, the mass in the control volume Ω is conserved; hence, the rate of change of mass within the control volume must be zero.

$$\frac{Dm}{Dt} = \frac{D}{Dt} \left(\int_{\Omega} \rho d\Omega \right) = 0 \qquad (1.2)$$

By applying Reynolds transport theorem, (1.2) can be represented as:

$$\int_{\Omega} \left(\frac{\partial \rho}{\partial t} + \nabla . (\rho\, v) \right) d\Omega = 0 \qquad (1.3)$$

This equation must hold for any arbitrary control volume. This can only occur if the integrand is equal to zero. Thus this can be simplified to;

$$\frac{\partial \rho}{\partial t} + \nabla . (\rho\, v) = 0 \qquad (1.4)$$

(1.4) is called the continuity equation (in an Eulerian description) and is representative of the conservation of mass. This applies to both compressible and incompressible fluids. A description of the meaning of these terms can be seen in (1.5).

$$\underset{\substack{Accumulation\ of\ mass \\ in\ a\ fixed\ Element}}{\frac{\partial \rho}{\partial t}} + \underset{\substack{Net\ Flow\ Rate \\ out\ of\ Element}}{\nabla . (\rho\, v)} = 0 \qquad (1.5)$$

If the fluid is incompressible, (1.4) can be reduced to:

$$\nabla . v = 0 \qquad (1.6)$$

1.2.2.2 Conservation of Momentum:

It can proceed with the derivation of the conservation of momentum in a similar fashion as the conservation of mass. This can be shown by stating that the time rate of change of momentum within a control volume Ω is affected by external body forces and internal forces created by stress within the continuum. The equation for conservation of momentum can be shown to be.

$$\rho \frac{Dv}{Dt} = \nabla . \sigma + f \qquad (1.7)$$

Where σ is the stress tensor and *f* is the total body forces applied per unit volume.

1.2.2.3 Conservation of Energy:

Like the conservation of mass, the conservation of energy can be developed over a control volume using basic laws. The conservation of energy equation is:

$$\rho \frac{De}{Dt} + \nabla . q - \sigma . \nabla v = 0 \qquad (1.8)$$

Where e is the specific energy density and q is the heat vector. The details of the specific energy density and the heat vector result from constitutive theory and thermodynamic relations.

1.2.2.4 Navier Stokes Equations:

The Navier Stokes equations are a system of equations that describe the conservation of mass, the conservation of momentum, and the conservation of energy. These are shown in (1.9). These still require a constitutive theory, an equation of state, and a description of the heat vector (generally Fourier heat conduction) [9].

$$\begin{cases} \dfrac{\partial \rho}{\partial t} + \nabla . (\rho v) = 0 \\ \rho \dfrac{Dv}{Dt} = \nabla . \sigma + f \\ \rho \dfrac{De}{Dt} + \nabla . q - \sigma . \nabla v = 0 \end{cases} \qquad (1.9)$$

1.2.2.5 General Form of Navier Stokes Equation of Motion:

The most general form of the Navier Stokes equation of motion results from the conservation of momentum in (1.7). It is convenient to regard the stress tensor σ as the sum of the isotropic part, having the same form as the stress tensor of a fluid at rest and a remaining non-isotropic part T. The non-isotropic part T may be called the deviatoric stress tensor, and has the distinctive property of being due entirely to the existence of the motion of the fluid [9]. Decomposing the stress tensor σ into its two components we obtain:

$$\sigma = -pI + T \qquad (1.10)$$

Substituting this definition of the stress tensor into the momentum equation in (1.7) we obtain:

$$\rho \frac{Dv}{Dt} = -\nabla p + \nabla . T + f \qquad (1.11)$$

Where p is a scalar quantity, being the static fluid pressure. (1.11) is the general form of the Navier-Stokes equation. However, this model is incomplete without an equation of state and an energy equation (if the fluid is considered incompressible), and a constitutive theory for the deviatoric stress tensor.

1.2.2.6 Incompressible Newtonian Navier Stokes Equation of Motion:

The incompressible Newtonian Navier-Stokes equations are a special subset of the Navier-Stokes equations that are used in many cases. Fluids in which the shearing stress is linearly related to the rate of shearing strain are designated as Newtonian fluids. This result can be seen in (1.12).

$$\tau \propto \frac{\partial u}{\partial y} \qquad (1.12)$$

This assumption is common for fluids such as water, oil, gasoline, and air. The relationship is continued by a linear relationship to the dynamic viscosity μ of a fluid. Values of the dynamic viscosity depend both on the temperature of the fluid and the fluid itself [1].

$$\tau = \mu \frac{\partial u}{\partial y} \qquad (1.13)$$

For an incompressible Newtonian fluid it can make the following assumptions:

- Density is constant, and it can apply the continuity equation $\nabla . v = 0$ shown in (1.6).
- The fluid is isotropic (i.e., material properties are the same regardless of orientation).
- The stress tensor is linear in the strain rates and is related through viscosity as shown in (1.13). This leads to the following for the deviatoric stress tensor T expressed in Einstein tensor notation:

$$Tij = \mu \left(\frac{\partial ui}{\partial xj} + \frac{\partial uj}{\partial xi} \right) \qquad (1.14)$$

If we replace the deviatoric stress tensor in the general Navier-Stokes equation in (1.11) with the deviatoric stress tensor in (1.14), the equation becomes:

$$\rho \frac{Dv}{Dt} = -\nabla p + \mu(\nabla(\nabla . v) + \nabla^2 v) + f \qquad (1.15)$$

However, from continuity (1.6) we know that $\nabla .v = 0$; therefore, we are left with:

$$\rho \frac{Dv}{Dt} = -\nabla p + \mu \nabla^2 v + f \qquad (1.16)$$

If we expand the material derivative with respect to velocity, we are left with the common form of the incompressible Navier-Stokes equations. In (1.17) the different terms are labeled with respect to their physical meaning.

$$\overbrace{\rho\left(\underbrace{\frac{\partial v}{\partial t}}_{\substack{Unsteady\\ acceleration}} + \underbrace{v.\nabla v}_{\substack{Convective\\ acceleration}}\right)}^{Inertia\ (per\ volume)} = \overbrace{\underbrace{-\nabla p}_{\substack{pressure\\ gradient}} + \underbrace{\mu\nabla^2 v}_{Viscosity} + \underbrace{f}_{\substack{other\ body\\ forces}}}^{Divergence\ of\ stress} \qquad (1.17)$$

It should be noted that despite the rather short form of (1.17), this is a representation of three distinct non-linear PDEs (for 3D Cartesian coordinates). Many assumptions must be made to obtain an incompressible fluid, and simplifications have been made. Even in their reduced form, the incompressible fluids case is still not trivial to solve. (1.17) can be expressed in many different coordinate systems. The most common is in Cartesian form. This system is shown below in (1.18).

$$\begin{aligned}
\rho\left(\frac{\partial u}{\partial t} + u\frac{\partial u}{\partial x} + v\frac{\partial u}{\partial y} + w\frac{\partial u}{\partial z}\right) &= -\frac{\partial p}{\partial x} + \mu\left(\frac{\partial^2 u}{\partial x^2} + \frac{\partial^2 u}{\partial y^2} + \frac{\partial^2 u}{\partial z^2}\right) + \rho g x \\
\rho\left(\frac{\partial v}{\partial t} + u\frac{\partial v}{\partial x} + v\frac{\partial v}{\partial y} + w\frac{\partial v}{\partial z}\right) &= -\frac{\partial p}{\partial y} + \mu\left(\frac{\partial^2 v}{\partial x^2} + \frac{\partial^2 v}{\partial y^2} + \frac{\partial^2 v}{\partial z^2}\right) + \rho g y \qquad (1.18) \\
\rho\left(\frac{\partial w}{\partial t} + u\frac{\partial w}{\partial x} + v\frac{\partial w}{\partial y} + w\frac{\partial w}{\partial z}\right) &= -\frac{\partial p}{\partial z} + \mu\left(\frac{\partial^2 u}{\partial x^2} + \frac{\partial^2 u}{\partial y^2} + \frac{\partial^2 u}{\partial z^2}\right) + \rho g z
\end{aligned}$$

Along with the continuity equation in (1.6), the three equations in (1.18) create a complete mathematical system governing incompressible flow. The solution of these equations is not trivial or obvious. While the incompressible cases can be reduced to more specific cases that can be solved analytically, it is evident that a generalized solution method is needed to solve complex flow profiles. For CFD this method is called the finite volume method.

1.3 Boundary Conditions:

Since the boundary conditions and the initial conditions are specified, the governing equation of fluid motion may result in a solution. The form of the boundary conditions that is required by any partial differential equation depends on the equation itself and the way that it has been discretized. Common boundary conditions are classified either in terms of the numerical values that have to be set or in terms of the physical type of the boundary condition. For steady state problems there are three types of spatial boundary conditions that can be specified [9]:

I. Dirichlet boundary condition: $\phi = f_1(x, y, z)$ (1.19)

The values of the variable ϕ on the boundary are known constants f_1. This allows a simple substitution to be made to fix the boundary value. For example, if *u* is the flow velocity, its value may be fixed at the boundary of the domain. For instance, for no-slip and no-penetration conditions on the solid walls, the fluid velocity is the same as the velocity of the wall.

II. Neuman boundary condition: f (x y z) $\frac{\partial \phi}{\partial n} = f_2(x\ y\ z)$ (1.20)

The derivatives of the variable ϕ on the boundary are known f_2, and this gives an extra equation, which can be used to find the value at the boundary. For example, if the velocity does not change downstream of the flow, we can assume that the derivative of *u* is zero at that boundary.

III. Mixed type boundary condition: $a\phi + b\frac{\partial \phi}{\partial n} = f_3\,(x\ y\ z)$ (2.21)

In addition, there are the physical boundary conditions which are commonly observed in the fluid problems [9]:

(A) Solid walls: Many boundaries within a fluid flow domain will be solid walls, and these can be either stationary or moving walls. If the flow is laminar then the velocity components can be set to be the velocity of the wall. When the flow is turbulent, however, the situation is more complex.

(B) Inlets: At an inlet, fluid enters the domain and, therefore, its fluid velocity or pressure, or the mass flow rate may be known. Also, the fluid may have certain characteristics, such as the turbulence characterizes which needs to be specified.

(C) Symmetry boundaries: When the flow is symmetrical about some plane there is no flow through the boundary and the derivatives of the variables normal to the boundary are zero.

(D) Cyclic or periodic boundaries: These boundaries come in pairs and are used to specify that the flow has the same values of the variables at equivalent positions on both of the boundaries.

(E) Pressure Boundary Conditions: The ability to specify a pressure condition at one or more boundaries of a computational region is an important and useful computational tool.
Pressure boundaries represent such things as confined reservoirs of fluid, ambient laboratory conditions and applied pressures arising from mechanical devices. Generally, a pressure condition cannot be used at a boundary where velocities are also specified, because velocities are influenced by pressure gradients. The only exception is when pressures are necessary to specify the fluid properties, e.g., density crossing a boundary through an equation of state.

(F) Outflow Boundary Conditions: In many simulations there is a need to have fluid flow out of one or more boundaries of the computational region. At such "outflow" boundaries there arises the question of what constitutes a good boundary condition.
In compressible flows, when the flow speed at the outflow boundary is supersonic, it makes little difference how the boundary conditions are specified since flow disturbances cannot propagate upstream. In low speed and incompressible flows, however, disturbances introduced at an outflow boundary can have an effect on the entire computational region.

(G) Opening Boundary Conditions: If the fluid flow crosses the boundary surface in either direction an opening boundary condition needs to be utilized. All of the fluid might flow out of the domain, or into the domain, or a combination of the two might happen.

(H) Free Surfaces and Interfaces: If the fluid has a free surface, then the surface tension forces need to be considered. This requires utilization of the Laplace's equation which specifies the surface tension-induced jump in the normal stress $p\ s$ across the interface:

$$p\ s = \sigma\ k \quad (1.22)$$

Where; σ represents the liquid-air surface tension and κ the total curvature of the interface. A boundary condition is required at the contact line, the line at which the solid, liquid and gas phases meet. It is this boundary condition which introduces into the model information regarding the wettability of the solid surface.

1.4 Overview of Solution Methods:

In order to solve the governing equations (mass, momentum, energy) of the fluid motion, first their numerical analogue must be generated. This is done by a process referred to as discretization.
There are various techniques for numerical discretization. The most commonly used techniques:

1.4.1 Finite Difference Method:

The finite difference method (FDM) was among the first methods applied to the approximation of PDEs.. The concept of the FD method is to approximate the solution of each point and its derivatives. This is done through the expansion of the dependent variable about a point through Taylor series. For an example let's consider the simple PDE of:

$$\frac{\partial \emptyset}{\partial x} = 0 \qquad (1.23)$$

To solve the PDE (1.23), we must have an approximation of the first derivative of ϕ. This can be done through Taylor series expansion about a grid point x_i by:

$$\emptyset(x) = \emptyset(xi) + \Delta x \left(\frac{\partial \emptyset}{\partial x}\right) i + \frac{\Delta x^2}{2} \left(\frac{\partial^2 \emptyset}{\partial x^2}\right) i + \cdots \qquad (1.24)$$

By neglecting terms higher than first order in (1.20) we can solve for the first derivative of ϕ:

$$\frac{\partial \emptyset}{\partial x} = \frac{\emptyset(xi + \Delta x) - \emptyset(xi)}{\Delta x} + 0(xi) \qquad (1.25)$$

Where $0(\Delta x)$ is an indication of the truncation error. The same procedure can be applied to derive more accurate derivatives as well as higher order derivations if (1.23) had called for them.

A finite difference approximation then provides an algebraic system at each grid point node (regardless of space dimension). This equation can be linear or non-linear depending on the PDE being solved. For the example shown in (1.23), only linear terms would be necessary. This system of equations can be written in matrix form as:

$$A\,\phi = Q \qquad (1.26)$$

The equation (1.26) can then be solved for the unknowns in ϕ to obtain a solution for the PDE (1.23). this is done through application of known boundary conditions and employing a matrix solving scheme to obtain a solution.

1.4.2 Finite Element Method (FEM):

The finite element method was originally employed solely to perform structural analysis. The original FEM codes arose from the need for deformation and stress prediction within the confines of the theory of linear elasticity. From this limited initial scope, FEM codes have grown alongside increasing computational power. In the early 90's the finite element method began to be applied to the solution of the Navier-Stokes equations. The finite element method has a very rigorous mathematical foundation and research into its potential applications with regards to fluids applications continues [9].

1.4.3 Finite Volume Method (FVM):

The finite volume method utilizes the integral form of the conservation laws (Navier-Stokes equations). This is done by separating a computational domain into a series of finite arbitrary control volumes. Two types of cell schemes are generally considered:
1. Cell-centered scheme flow quantities are stored at the center of each cell.
2. Cell-vertex scheme flow quantities are stored at the grid point of the cells.
The finite volume method is carried out directly in physical space, i.e., there is no change of coordinate systems or use of a jacobian of transformation. This can be both advantageous and disadvantageous, depending upon the situation.
Let's consider the incompressible continuity equation as a representation of how the FVM works. From (1.6) we know:

$$\nabla . v = 0 \qquad (1.27)$$

Represent the continuity equation of an incompressible flow. Converting (1.27) into an integral form over a control volume:

$$\int_{Vi} \nabla . v \, dV = 0 \qquad (1.28)$$

And applying the divergence theorem, we obtain (where η is a unit normal):

$$\oint_{Si} v . \eta \, ds = 0 \qquad (1.29)$$

Now we have obtained a boundary integral describing the continuity of an arbitrary control volume *Vi*. To precede further the finite volume method approximations of this surface integral would be required on a cell-by-cell basis. This is done by using suitable quadrature formula. Approximations are introduced for volume integrals as well; these would occur in equations other than (1.29) as well. As a result, a system of algebraic equations is obtained for each control volume, in which the centroids to its neighbors also appear.

1.4.4 Spectral Methods:

Another method of generating a numerical analog of a differential equation is by using Fourier series or series of Chebyshev polynomials to approximate the unknown functions.
Such methods are called the Spectral method. Fourier series or series of Chebyshev polynomials are valid throughout the entire computational domain. This is the main difference between the spectral method and the FDM and FEM, in which the approximations are local. Once the unknowns are replaced with the truncated series, certain constraints are used to

generate algebraic equations for the coefficients of the Fourier or Chebyshev series. Either weighted residual technique or a technique based on forcing the approximate function to coincide with the exact solution at several grid points is used as the constraint. For a detailed discussion of this technique refer to Gottlieb and Orzag.

1.4.5 General approach – convergence:

The iterative process is repeated until the change in the variable from one to the next iteration becomes so small that the solution can be considered converged.
At convergence, all discrete conservation equations (momentum, energy, etc.) are obeyed in all cells to a specified tolerance, the solution no longer changes with additional iterations and mass, momentum, energy and scalar balances are obtained.
Residuals measure imbalance (or error) in conservation equations, and the absolute residual at point *P* is defined as:

$$Rp=\left|a_p\emptyset_p-\sum_{nb}a_{nb}\emptyset_{nb}-b\right| \quad (2.30)$$

1.4.6 Convergence – continued:

Residuals are usually scaled relative to the local value of the property *f* in order to obtain a relative error:

$$R_{P.scaled}=\frac{\left|a_p\emptyset_p-\sum_{nb}a_{nb}\emptyset_{nb}-b\right|}{\left|a_p\emptyset_p\right|} \qquad (2.31).$$

They can also be normalized, by dividing them by the maximum residual that was found at any time during the iterative process.
An overall measure of the residual in the domain is:

$$R^{\emptyset}=\frac{\sum_{all\ cells}\left|a_p\emptyset_p-\sum_{nb}a_{nb}\emptyset_{nb}-b\right|}{\sum_{all\ cells}\left|a_p\emptyset_p\right|} \qquad (2.32)$$

It is common to require the scaled residuals to be on the order of 1E-3 to 1E-4 or less for convergence.

1.4.7Monitor residuals:

If the residuals have met the specified convergence criterion but are still decreasing, the solution may not yet be converged. And if the residuals never meet the convergence criterion, but are no longer decreasing and other solution monitors do not change either, the solution is converged.
The residuals are not the solution. Low residuals do not automatically mean a correct solution, and high residuals do not automatically mean a wrong solution.

Final residuals are often higher with higher order discretization schemes than with first order discretization. That does not mean that the first order solution is better. The residuals can be monitored graphically also.

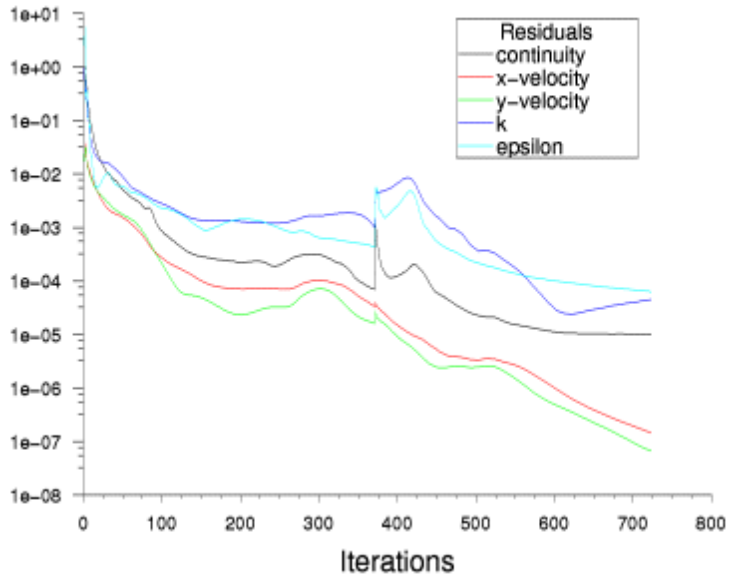

Figure 1.1: Monitor Residual of the simulation.

Other convergence monitors:

For models whose purpose is to calculate a force on an object, the predicted force itself should be monitored for convergence. E.g. for an airfoil, one should monitor the predicted drag coefficient.

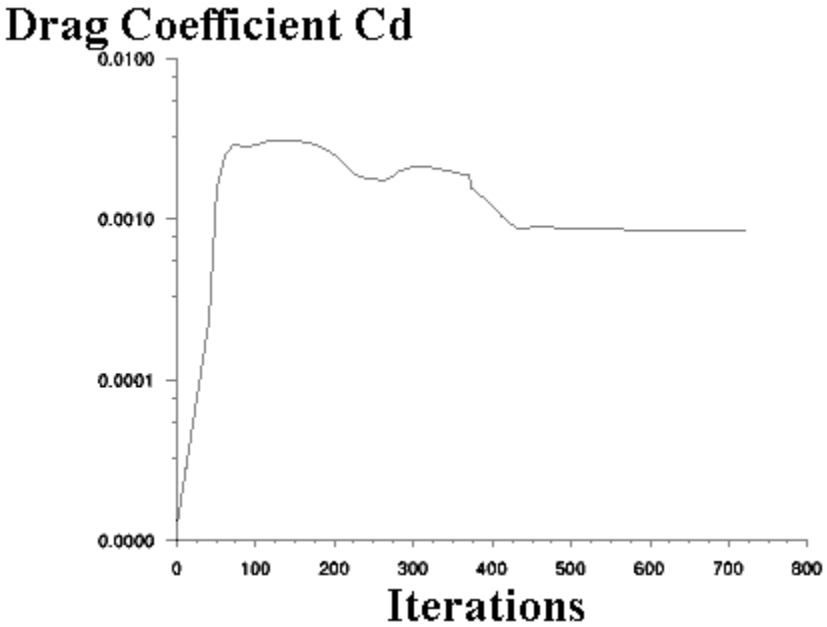

Figure n°1.2: Forces solution.

Overall mass balance should be satisfied. When modeling rotating equipment such as turbofans or mixing impellers, the predicted torque should be monitored.
For heat transfer problems, the temperature at important locations can be monitored.
One can automatically generate flow field plots every 50 iterations or so to visually review the flow field and ensure that it is no longer changing.

1.4.8 Numerical schemes, finding face values:

Face values of ϕ and $\frac{\partial \phi}{\partial x}$ are found by making assumptions about variation of ϕ between cell centers. The Number of different schemes can be devised:
– First-order upwind scheme.
– Central differencing scheme.
– Power-law scheme.
– Second-order upwind scheme.
– QUICK scheme.

1.4.8.1 First order upwind scheme:

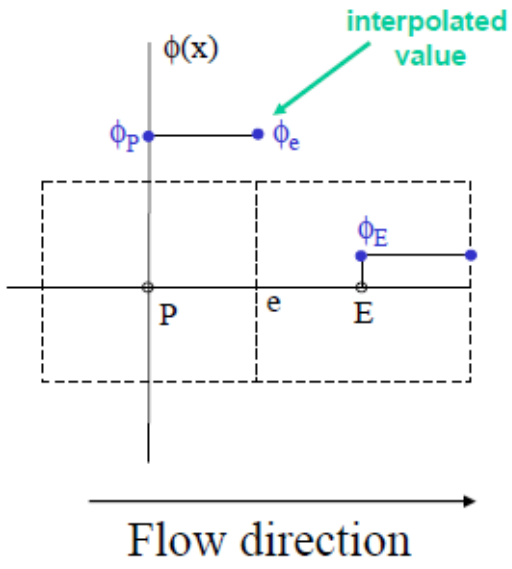

.

We assume that the value of *f* at the face is the same as the cell centered value in the cell upstream of the face.

We assume that the value of *f* at the face is the same as the cell centered value in the cell upstream of the face.
The main advantages are that it is easy to implement and that it results in very stable calculations, but it also very diffusive.
Gradients in the flow field tend to be smeared out, as calculations, but it also very diffusive.
Gradients in the flow field tend to be smeared out, as we will show later. This is often the best scheme to start calculations with.

Figure n°1.3: First order upwind scheme.

1.4.8.*2 Central differencing scheme:*

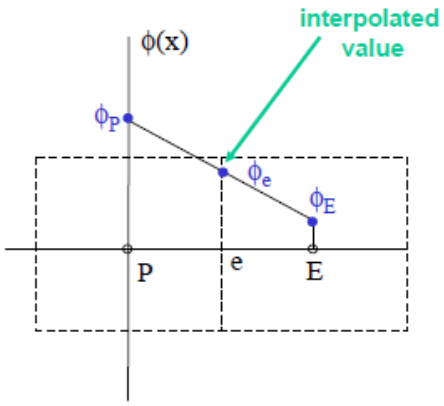

We determine the value of ϕ at the face by linear interpolation between the cells centered values.
This is more accurate than the first order upwind scheme, but it leads to oscillations in the solution or divergence if the local Peclet number is larger than 2. The Peclet number is the ratio between convective and diffusive transport:

$$P_e = \frac{\rho u L}{D} \qquad (1.33)$$

It is common to then switch to first order upwind in cells where Pe>2. Such an approach is called a hybrid scheme.

Figure n°1.4: First order upwind scheme.

1.4.8.3Power law scheme:

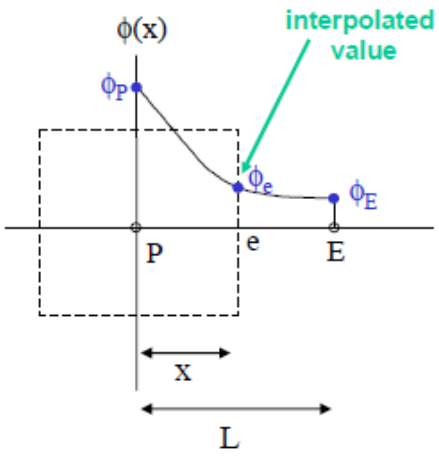

This is based on the analytical solution of the one-dimensional convection-diffusion equation.
The face value is determined from an exponential profile through the cell values. The exponential profile is approximated by the following power law equation:

$$\emptyset_e = \emptyset_p - \frac{(1-0.1P_e)^5}{P_e}(\emptyset_E - \emptyset_P) \qquad (1.34).$$

Pe is again the Peclet number.

For Pe>10, diffusion is ignored and first order upwind is used.

Figure n°1.5: Power law scheme.

1.4.8.4 Second-order upwind scheme:

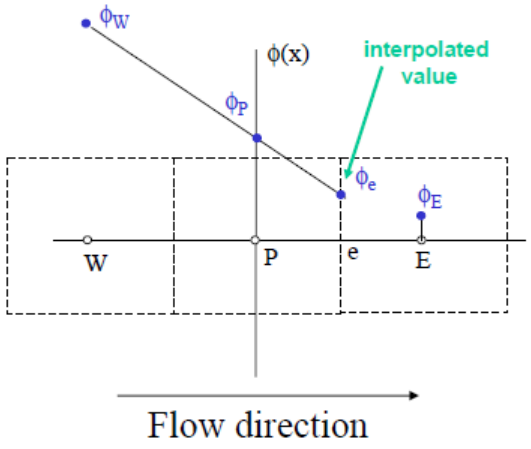

We determine the value of *f* from the cell values in the two cells upstream of the face.
This is more accurate than the first order upwind scheme, but in regions with strong gradients it can result in face values that are outside of the range of cell values. It is then necessary to apply limiters to the predicted face values.
There are many different ways to implement this, but second-order upwind with limiters is one of the more popular numerical schemes because of its combination of accuracy and stability.

Figure n°1.6: Second-order upwind scheme.

1.4.8.5 QUICK scheme:

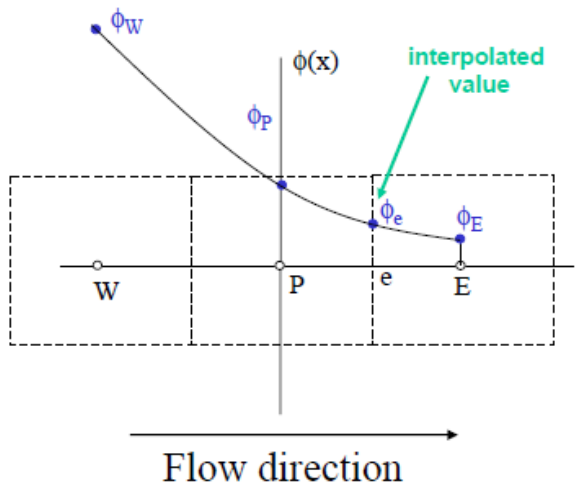

QUICK stands for Quadratic Upwind Interpolation for Convective Kinetics.
A quadratic curve is fitted through two upstream nodes and one downstream node.
This is a very accurate scheme, but in regions with strong gradients, overshoots and undershoots can occur. This can lead to stability problems in the calculation.

Figure n°1.7: QUICK scheme.

1.4.9 Solution accuracy:

Higher order schemes will be more accurate. They will also be less stable and will increase computational time. It is recommended to always start calculations with first order upwind and after 100 iterations or so to switch over to second order upwind. This provides a good combination of stability and accuracy.
The central differencing scheme should only be used for transient calculations involving the large eddy simulation (LES) turbulence models in combination with grids that are fine enough that the Peclet number is always less than one. It is recommended to only use the power law or QUICK schemes if it is known that those are somehow especially suitable for the particular problem being studied.

1.5. Mesh classification:

One of the more important things in CFD analysis is the mesh generation; the direct results have been the expansion of available mesh elements and mesh connectivity (how cells are connected to one another). The easiest classifications of meshes are based upon the connectivity of a mesh or on the type of elements present.

1.5.1Connectivity-Based Classification:

The most basic form of mesh classification is based upon the connectivity of the mesh: structured or unstructured.

1.5.1.1Structured Meshes:

A structured mesh is characterized by regular connectivity that can be expressed as a two or three dimensional array. This restricts the element choices to quadrilaterals in 2D or hexahedra in 3D. The above example mesh is a structured mesh, as we could store the mesh connectivity in a 40 by 12 array. The regularity of the connectivity allows us to conserve

space since neighborhood relationships are defined by the storage arrangement. Additional classification can be made upon whether the mesh is conformal or not.

1.5.1.2Unstructured Meshes

An unstructured mesh is characterized by irregular connectivity is not readily expressed as a two or three dimensional array in computer memory. This allows for any possible element that a solver might be able to use. Compared to structured meshes, the storage requirements for an unstructured mesh can be substantially larger since the neighborhood connectivity must be explicitly stored.

1.5.1.3 Hybrid Meshes:

A hybrid mesh is a mesh that contains structured portions and unstructured portions. Note that this definition requires knowledge of how the mesh is stored (and used). There is disagreement as to the correct application of the terms "hybrid" and "mixed." The term "mixed" is usually applied to meshes that contain elements associated with structured meshes and elements associated with unstructured meshes (presumably stored in an unstructured fashion).

1.5.2 Element-Based Classification

Meshes can also be classified based upon the dimension and type of elements present. Depending upon the analysis type and solver requirements, meshes generated could be 2-dimensional (2D) or 3-dimensional (3D). Common elements in 2D are triangles or rectangles, and common elements in 3D are tetrahedral or bricks. As noted above, some connectivity choices limit the types of element present, so there is some overlap between connectivity-based and element-based classification.

For a 2D mesh, all mesh nodes lie in a given plane. In most cases, 2D mesh nodes lie in the XY plane, but can also be confined to another Cartesian or user defined plane. Most popular 2D mesh elements are quadrilaterals (also known as quads) and triangles (tries), shown below.

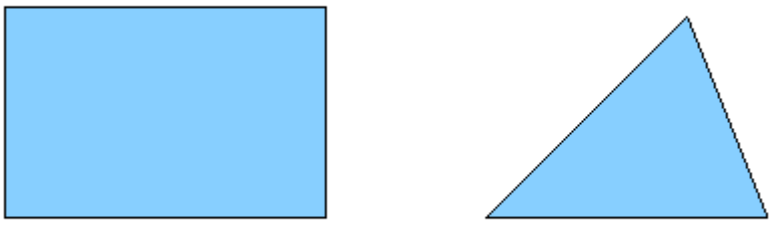

Figure n°1.8:2D mesh elements are quadrilaterals and triangles.

3D mesh nodes are not constrained to lie in a single plane. Most popular 3D mesh elements are hexahedra (also known as hexes or hex elements), tetrahedral (tets), square pyramids (pyramids) and extruded triangles (wedges or triangular prisms), shown below. It is worth noting that all these elements are bounded by faces belonging to the above mentioned 2D

elements. Some of the current solvers also support polyhedral elements, which can be bounded by any number and types of faces.

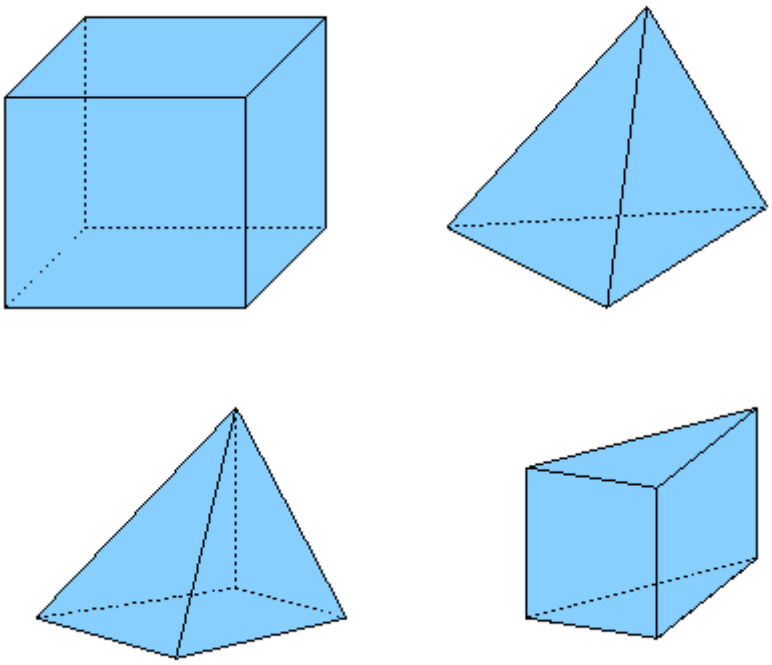

Figure 1.9: Most popular 3D mesh elements hexahedra, tetrahedral, square pyramids and extruded triangles.

Since all 3D elements are bounded by 2D elements, it is obvious that 3D meshes have exposed 2D elements at boundaries. Most of the meshing packages and solvers prefer to club exposed elements together in what is known as a surface mesh (for the purposes of applying boundary conditions, rendering meshed domains and visualizing results). A surface mesh does not have to be 2D, since volume meshes may conform to domains with non-planar boundaries. Many meshing algorithms start by meshing bounding surfaces of a domain before filling the interior with mesh nodes (such algorithms are also known as boundary to interior algorithms). For such algorithms, generation of good quality surface meshes is of prime importance, and much research has been done in the field of efficient and good quality surface mesh generation. Since surface meshes are geometrically somewhere between 2D and 3D meshes, they are also sometimes known as 2.5D meshes.

1.6 Introduction to Turbulence:

1.6.1 Turbulence definition:

The dictionary definition of turbulence is: "The haphazard secondary motion caused by eddies within a moving fluid".
For the engineering terminology, the turbulence is the spatial and time-varying components of a flow field. Below it's shown some example for the turbulence.

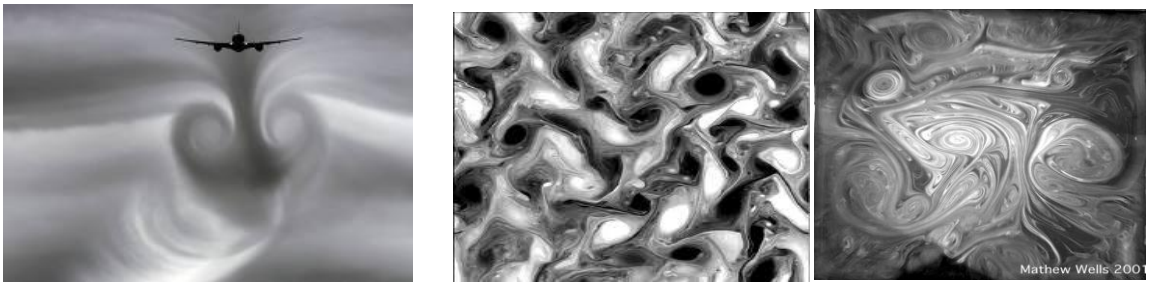

(a) Vortex Structures Behind Passenger Aircraft *(b) Atmospheric Turbulence on the Sun* *(c) Chemical Reactions Turbulence at a Molecular Level.*

Figure n°1.10: Examples of Turbulence

Turbulence can be characterized by the following properties; Irregular, Diffuse, Rotational, Dissipative, Chaotic and Cascading energies which are divided into three; Integral, Taylor microscales, Kolmogorov scales [9].

Given the time and spatial variation of flow fields caused by turbulence it can be stated that turbulent flows are not deterministic, rather they must be studied using statistical methods. Further, by definition, the solution of a time-dependent, nonlinear equation set is dependent on the initial conditions and the time-dependent boundary conditions (i.e., the solution can display chaotic behavior) [9].

1.6.2 Handle Turbulence by CFD:

The Navier-Stokes equations are almost perfect; all it has to do is modify them to include a mean and time-varying component.

$$\rho[\frac{\partial(Ui+ui)}{\partial t}+(Uj+uj)\frac{\partial(Ui+ui)}{\partial xj}=-\frac{\partial(P+p)}{\partial xi}+\frac{\left(Tij^{(v)}+\tau ij^{(v)}\right)}{\partial xj} \qquad (1.35)$$

In order to solve this equation in CFD, the computational domain should construct with enough grid points. The number of points required to resolve this is proportional to the Reynolds number raised to the 1.35 power, in all three Euclidean directions.

$$N^3 \geq Re^{9/4} \qquad (1.36)$$

This massive grid then has to be analyzed with a time-step small enough that a fluid particle moves less than the grid spacing for a time-step:

$$C=\frac{u'\delta t}{h}<1 \qquad (1.37)$$

The analysis must then go through enough steps that all length scales (through the largest) are resolved in the flow field, Note that this very easily becomes millions of steps. While this analysis is performing, every boundary condition must be exactly matched in time and space.

The engineer role:

The engineer first has to start by jumping through several math hoops to create the Reynolds stress equations:

$$\frac{\partial(uiuk)}{\partial t} + Uj\ \frac{\partial(uiuk)}{\partial xj} = -\left(\frac{p}{\rho}\left[\frac{\partial ui}{\partial uk} + \frac{\partial ui}{\partial uk}\right]\right) + \frac{\partial}{\partial xj}\{-[(puk)\delta ij + (pui)\delta kj] - (uiukuj) + 2\nu\,[(sijuk) + (sijuk)]\} - \left[(uiuj)\frac{\partial Uk}{\partial xj} + (ukuj)\frac{\partial Ui}{\partial xj}\right] - 2\nu\,\left[\left(sij\frac{\partial uk}{\partial xj}\right) + \left(skj + \frac{\partial ui}{\partial xj}\right)\right] \qquad (1.38)$$

The RHS terms are commonly referred to as:

- Pressure-strain rate
- Turbulence transport
- Production
- Dissipation

The inspection of the equations will show that there are more unknowns than variables. Thus a methodology needs to be derived that allows an approximate solution of the equations. To derive the methodology, it's customary to simplify the equations by introducing a new term for the turbulent kinetic energy:

$$\text{k}=\frac{1}{2}\,(ui\ ui) = \frac{1}{2}(q^2) = \frac{1}{2}\,[u^2{}_1 + u^2{}_2 + u^2{}_3 \qquad (1.39)$$

Inserting k into (1.35) produces:

$$\left[\frac{\partial}{\partial t} + Uj\ \frac{\partial}{\partial xi}\right]k = \frac{\partial}{\partial xj}\left\{-\frac{1}{2}\,(pui)\delta ij - \frac{1}{2}(q^2uj) + \nu\ \frac{\partial}{\partial xj}\ k\right\} - (uiuj)\frac{\partial U}{\partial xj} - \nu\left(\frac{\partial ui}{\partial xj}\ \frac{\partial ui}{\partial xj}\right) \qquad (1.40)$$

In this case on the RHS we have a rate of change of turbulent kinetic energy due to time-dependence of the mean (first term) and for the rate of change of turbulent kinetic energy due to convection by the mean flow (second term). On the LHS we have, in order:

- Transport of kinetic energy due to pressure fluctuations, turbulence and viscous stresses.
- Rate of production of turbulent kinetic energy from the mean flow.
- Rate of dissipation of turbulent kinetic energy due to viscous stresses, also referred to as the Reynolds stresses.

It should develop a method to predict the Reynolds stress. To this end, in 1887 Boussinesq introduced the concept of eddy viscosity.

$$-\rho u'_i u'_j = \mu_t \left(\frac{\partial Ui}{\partial xi} + \frac{\partial Ui}{\partial xj}\right) - \frac{2}{3}\rho k \delta_{ij} \qquad (1.41)$$

In this case we need to predict μ_t and k. There are a variety of methods to predict these variables, including one equation, two equation and Reynolds stress transport models. Below is a brief description of each model type.

- One equation models - One equation turbulence models solve one turbulent transport equation, typically for turbulent kinetic energy. One equation models are typically used for aerodynamic calculations, and are most suitable where the flow remains attached to the surface and any separation present is mild.
- Two equation models - Two equation models are the most common types of turbulence models. The models operate by solving for two transported variables. Most of the models separate into two distinct categories:

- $k-\varepsilon$»models:$k-\varepsilon$" models solve for the turbulent kinetic energy (k) and the turbulent dissipation rate (ε).
  $k-\omega$»models:$k-\omega$» models solve for the turbulent kinetic energy (k) and the specific dissipation rate (ω).

For the two equation models, the first term represents the turbulent energy contained in the flow and second term considers the scale (time or length) associated with the turbulence.

- Reynolds stress models - Reynolds stress models solve a system of 7 equations to calculate all Reynolds stresses. Only 6 stresses need to be solved for since the stress matrix is symmetric, and a seventh equation is solved to determine the specific dissipation. The model is known as a second-order closure model. While the Reynolds stresses are modeled, the model does not perform well for wall-bounded turbulent flows. This is because:

- Ad hoc wall reaction terms are required in most pressure-strain models to mask deficient predictions for the logarithmic region of the boundary layer.
- Near-wall models typically that depend on the unit normal to the wall must be introduced. This makes it virtually impossible to systematically integrate second-order closures in complex geometry.

What's this wall?

Recall, the first rule of fluid dynamics is that the velocity is zero at the wall. Further, basic fluid dynamics tells us that there will be some velocity profile between the zero wall value and the bulk flow velocity of the fluid. Finally, consider, without walls there would be no turbulence. The shear stresses induced in the fluid decelerating near the wall induces rotational energy in the flow. Rotational energy leads to vortices, vortices lead to 3-dimensional vertical structures, 3-dimensional vertical structures are turbulence. Therefore, the shear stresses at the wall must be considered.

1.7 The Law of the Wall:

In 1930, based on experimental evidence, Theodore von Karman proposed the Law of the Wall. The Law of the Wall states that the average velocity of a turbulent flow is proportional to the distance from that point to the wall. In general the Law of the Wall is only valid for the

first 20% of the flow height from the wall. In most cases the law takes a general logarithmic formulation, where the velocity at a distance from the wall is given as:

$$u^+ = \frac{1}{k}\, ln\, y^+ C^+ \qquad (1.42)$$

Where:

$$y^+ = \frac{y u_r}{v} \qquad (1.43)$$

And

$$u_r = \sqrt{\frac{\tau_w}{\rho}} \qquad (1.44)$$

And

$$u^+ = \frac{u}{u_r} \qquad (1.45)$$

Further, in implementation the model is modified to account for the velocity profile in the viscous sublayer, y+ <= 5. In this region u+ is taken as y+. The figure below shows the velocity profiles inherent with the Law of the Wall modeling method. As can be seen from the figure, neither the viscous sublayer or logarithmic approximations fully capture the transition velocity profile in the region 5 < y+ < 30.

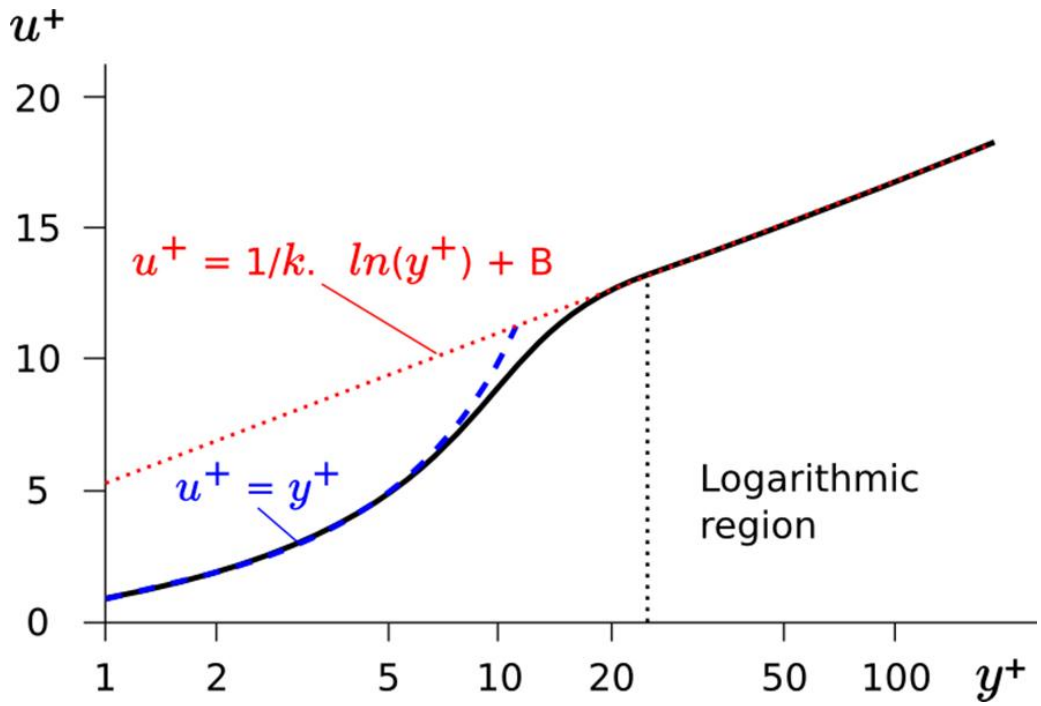

Figure n°1.11: The Law of the Wall.

Other mean flow quantities such a temperature, production of turbulent kinetic energy and/or species concentration can then be predicted, based on this assumed velocity profile. How some of these quantities are calculated dependent on the turbulence model selection. It should be noted that when the Law of the Wall is explicitly used in the solution (i.e., there is minimal to no attempt at near wall velocity profile resolution) these assumed profiles, and their associated quantities, will influence the calculated wall values.

Depending on the near wall mesh resolution, in practice there are typically three methods used for implementation of the Law of the Wall:

- High-y+ - The high y+ model assumes that the centroid of the near wall cell lies in the logarithmic region (y+ > 30).
- Low-y+ - The low y+ model assumes that the mesh is resolved to the viscous sublayer. In this case, wall laws are not used. While theoretically this occurs at y+ < 5, in practice the mesh normal to the wall should be resolved enough to produce solution y+ values less than 1.
- All-y+ - The all y+ model attempts to mimic the behavior of both the high and low y+ models to allow for relatively coarse grids with flows that stagnate, or have a greatly reduced friction velocity. Additionally, most of these models contain a functional blending treatment to better represent the velocity between the viscous sublayer and the logarithmic regions.

Chapter 2: Ship resistance

2.1- Introduction :

Prior to the mid-nineteenth century, comparatively little was known about the laws governing the resistance of ships and the power that was required to give a particular speed. Brown (1983) gives an account of the problems of that time and depicts the role of William Froude, who can be justly considered as the father of ship resistance studies [1].

The analysis procedure William Froude (1955) recognized that ship models of geometrically similar form would create similar wave systems, albeit at different speeds. Furthermore, he showed that the smaller models had to be run at slower speeds than the larger models in order to obtain the same wave pattern. His work showed that for a similarity of wave pattern between two geometrically similar models of different size the ratio of the speeds of the models was governed by the relationship shown below [1]:

$$\frac{V_1}{V_2} = \sqrt{\frac{L_1}{L_2}} \qquad (2.1)$$

By studying the comparison of the specific resistance curves of models and ships Froude noted that they exhibited a similarity of form although the model curve was always greater than that for the ship (Figure 2.1) [1].

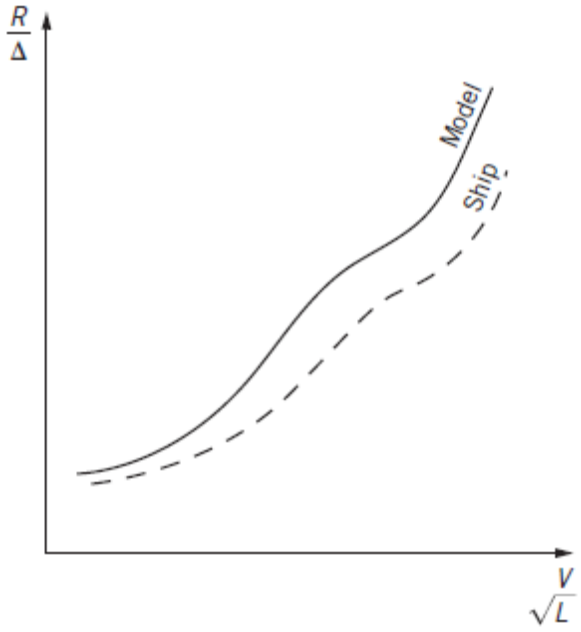

Figure n° 2.1 Comparison of a ship and its model's specific resistance curves.

This leads Froude to the conclusion that two components of resistance were influencing the performance of the vessel and that one of these, the wave-making component R_w , scaled with $V / \sqrt{L}$ and the other did not. This second component, which is due to viscous effects, derives principally from the flow of the water around the hull but also is influenced by the air flow and weather acting on the above-water surfaces. This second component was termed the frictional resistance R_F.

After this experience, Froude get conclusion that the two sources of resistance might be separated and treated independently. In this approach, Froude suggested that the viscous resistance could be calculated from frictional data whilst that wave-making resistance R_w could be deduced from the measured total resistance R_T and the calculated frictional resistance R_F as follows[1]:

$$R_w = R_T - R_F \qquad (2.2)$$

In order to provide the data for calculating the value of the frictional component Froude performed his famous experiments at the Admiralty owned model tank at Torquay. These experiments entailed towing a series of planks ranging from 10 to 50 ft in length, having a series of surface. Although the results of these experiments suffered from errors due to temperature differences, slight bending of the longer planks and laminar flow on some of the shorter planks, Froude was able to derive an empirical formula which would act as a basis for the calculation of the frictional resistance component R_F in Equation (2.2). The relationship Froude derived took the form [1]:

$$RF = f S V^n \qquad (2.3)$$

In which the index *n* had the constant value of 1.825 for normal ship surfaces of the time and the coefficient *f* varied with both length and roughness, decreasing with length but increasing with roughness. In Equation (2.3), *S* is the wetted surface area.
As a consequence of this work Froude's basic procedure for calculating the resistance of a ship is as follows [1]:

1. Measure the total resistance of the geometrically similar model R_{TM} in the towing tank at a series of speeds embracing the design $V / \sqrt{L}$ of the full size vessel.
2. From this measured total resistance subtract the calculated frictional resistance values for the model R_{FM} in order to derive the model wave making resistance R_{WM}.
3. Calculate the full-size frictional resistance R_{FS} and add these to the full-size wave making resistance R_{WS}, scaled from the model value, to obtain the total full-size resistance R_{TS}.

$$R_{TS} = R_{WM}\left[\frac{\Delta_s}{\Delta_M}\right] + R_{FS} \qquad (2.4)$$

The scaling Froude's law, Equation (2.1), states that the wave making resistance coefficients for the model and ship are the same when they are moving at the same $V / \sqrt{L}$ value, however, the dimensionless Froude number can be derived from it to give:

$$F_n = \frac{V}{\sqrt{(gL)}} \qquad (2.5)$$

The using of dimensional analysis it can readily be show today that the resistance of a body moving on the surface, or at an interface of a medium, can be given by the equation below:

$$\frac{R}{\rho V^2 L^2} = \emptyset\left\{\frac{VL\rho}{\mu}, \frac{V}{\sqrt{gL}}, \frac{V}{a}, \frac{\sigma}{g\rho L^2}\frac{p_0 - p_V}{\rho V^2}\right\} \qquad (2.6)$$

In this equation the left-hand side term is the resistance coefficient *C*R whilst on the right hand side of the equation:

The 1st term is the Reynolds number *R*n, the 2nd term is the Froude number *F*n (Equation (2.5)), the 3rd term is the Mach number *M*a, the 4th term is the Weber number *W*e, and the 5th term is the Cavitation number σ0.

For the purposes of ship propulsion the 3rd and 4th terms are not generally significant and can, therefore, be neglected [1]. Hence Equation (2.6) reduces to the following for all practical ship purposes:

$$C_R = \emptyset\{R_n, F_n, \sigma_0\} \qquad (2.7)$$

In which:
ρ is the density of the water, μ is the dynamic viscosity of the water, p0 is the free stream undisturbed pressure, pv is the water vapor pressure.

2.2. Components of calm water resistance:

As a ship moves through calm water with lower speed, that is where the ship's weight balances the displacement up thrust without the significant contribution of hydrodynamic lift forces there are many factors that combine to form the total resistance force acting on the hull, the components of calm water resistance can be broken down into the contributions shown in Figure 1.2[1].

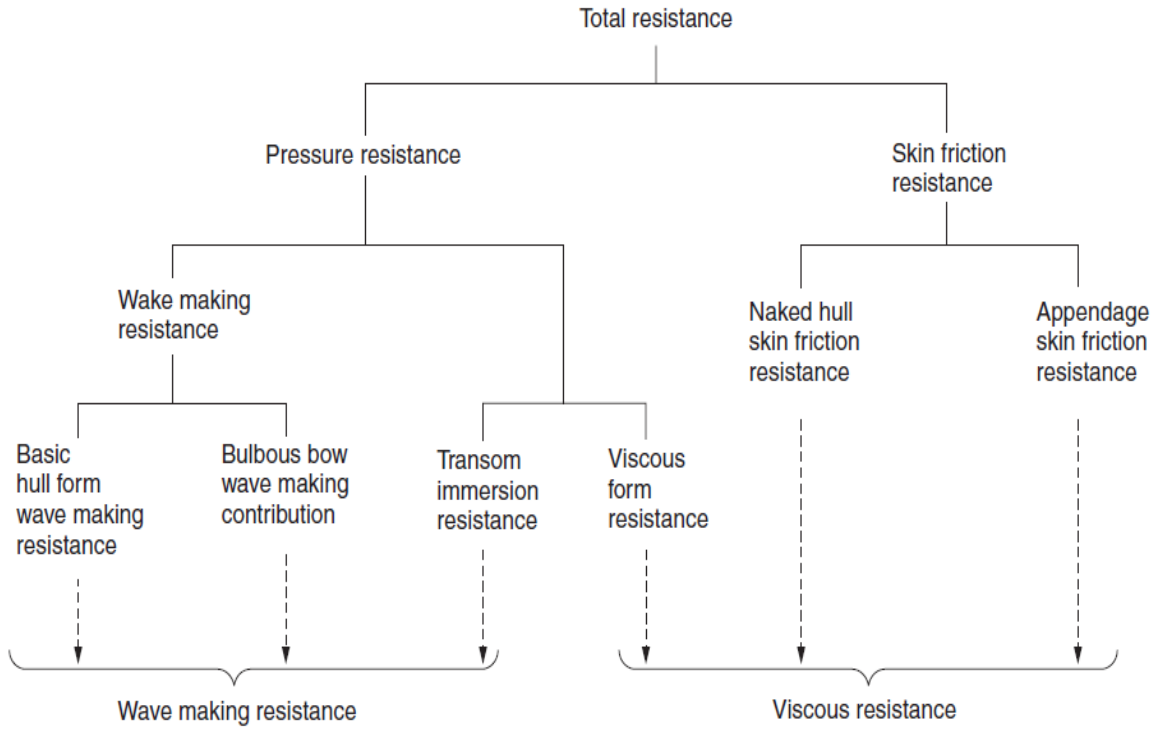

Figure n°2.2: Component of ship resistance.

From the figure 2.2, it is seen that the total resistance can be decomposed into two primary components, pressure and skin friction resistance, and these can then divided into more discrete components. There are also others resistances as the air resistance and added resistance due to rough weather; these are, detailed in Sections below.

Each of the components shown in Figure 2.2 can be studied separately provided that it is remembered that each will have an interaction on the others and, therefore, as far as the ship is concerned, need to be considered in an integrated way.

From the reference [2], in mathematical terms, total resistance can be written as:

$$R_T = R_V + R_W + R_{AA}$$

Where: R_T = total hull resistance

R_V = viscous (friction) resistance

R_W = wave making resistance

R_{AA} = resistance caused by calm air

Other factors affecting total hull resistance will also be presented. Figure 2.3 shows how the magnitude of each component of resistance varies with ship speed.

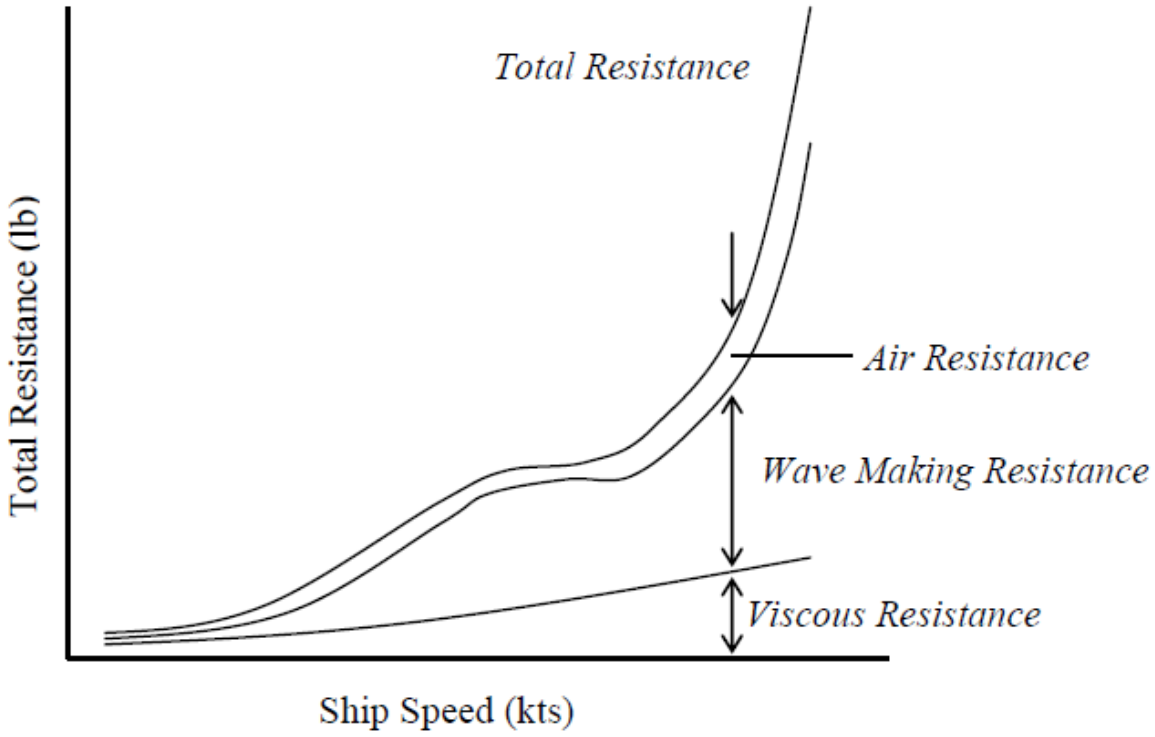

Figure 2.3: Component of Hull Resistance.

2.2.1 Naked hull skin friction resistance:

As discussed in the previous sections, the original data upon which to calculate the skin friction component of resistance was that provided by Froude in his plank experiments. This data was subject to error and in 1932 Schoenherr re-evaluated Froude's original data in association with other work in the light of the Prandtl–von Karman theory.

From the experiments carried out by Osborne Reynolds on water flow through pipes, the existence of two different flow regimes is suggested, each with a different associated friction resistance law. The results of which were presented to the Royal Society in 1883.Reynolds found that these different flow conditions varied depending on the ratio of the product of

local fluid velocity and the diameter of the pipe to the fluid kinematic viscosity[3], commonly referred to as Reynolds number.
However, at low Reynolds numbers the flow was considered laminar (i.e. Flowing in layers) and leads to lower resistance, and at high Reynolds numbers the flow was regarded as turbulent (i.e. a random eddying motion) and leads to increase the resistance.
Modern empirical skin friction formulations assume skin friction to be a function of Reynolds number to the base of length [3].

Later analytical and experimental investigations carried out by Blasius, Prandtl and Von Karman attempted to theoretically calculate the resistance coefficient of flat plates with respect to Reynolds number.
The Blasius's formulation determined the resistance of a flat plate in the laminar flow region with respect to Reynolds number, the results found by Blasius's formulation are close to these found by Froude at low Reynolds numbers. The resistance equation derived by Blasius (Laminar) is as follows:

$$C_F = \frac{R_F}{\frac{1}{2}\,\rho.S.V^2} = 1.327\,(Re)^{-\frac{1}{2}} \quad Re < 5\times 10^5 \qquad (2.8)$$

Prandtl and Von Karman's formulation however, determined the resistance of a flat plate in the turbulent flow based on a *1/7* [th] power law boundary layer velocity distribution, this formulation found good agreement with Froude's finding at the high Reynolds numbers, the turbulent resistance equations derived by Blasius, Prandtl and Von Karman is as follows[3].

$$C_F = \frac{R_F}{\frac{1}{2}\,\rho.S.V^2} = 0.072\,(Re)^{-\frac{1}{5}} \quad 5\times 10^5 < Re < 1\times 10^7 \qquad (2.9)$$

These formulas (2.8 and 2.9) give good approximations of the resistance coeffficients for flat plates with either laminar or turbulent flow conditions. However, Prandtl indetified that the reynolds numbers occurring in practical applications generally exceeded the range of validity of 1/7 [th] power law equation (2.9) and sort to derive a resistance formula that would be valid at much higher reynolds numbers, Prandtl later derived a skin friction formula based on the universal logarithmic buondary layer velocity profile, which could be extrapolated up to arbitrary large Reynolds numbers. The form of this skin friction equation is shown below[3]:

$$\frac{1}{\sqrt{C_F}} = A + B\log_{10}(Re.C_F) \qquad (2.10)$$

The constants A and B in equation (2.10) were determined by fitting the equation to available experimental test data. Following the publication of this formula, schoenherr re-plotted all the available experimental flat plate data to obtain the constants A and B to give Equation (2.11).this formula is still frequently used today in calculating skin friction of ship hulls [3].

$$\frac{1}{\sqrt{C_F}} = 4.13\,.\log_{10}(Re.C_F) \qquad (2.11)$$

The formulas given above have a good approximation for flows in either the laminar or the turbulent flow regions, but do not account for transition between the two.
The transition between the two different flow phenomena is not a simple one since it does not occur simultaneously over the whole plate, see Figure 2.4.

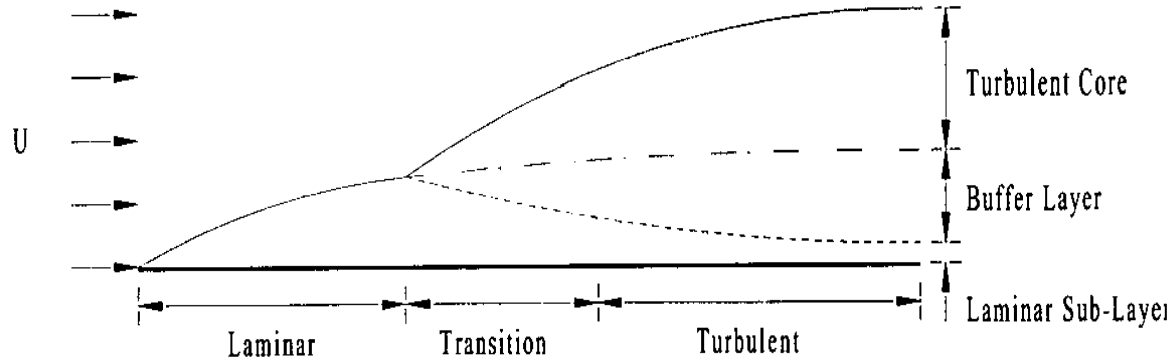

Figure 2.4: Flat plate boundary layer transition.

It's seen from the figure above that the transition on flat plate occurs when the local Reynolds number reaches a critical value. As the velocity, and hence the Reynolds number increase, the point of transition along the plate surface moves forwards the leading edge so that the local Reynolds number remains equal to the critical. The local Reynolds number is defined with respect to the distance from the leading edge of the plate to the point of transition [3].
Therefore, fore any flat plate flow there will be two regions with different resistance characteristics due to small region of laminar flow followed by a turbulent region.
The formulation of a skin friction line, applicable to smooth surfaces, of the following form:

$$\frac{0.242}{\sqrt{C_F}} = \log(R_n \,.\, C_F) \qquad (2.12)$$

This equation, known as the Schoenherr line, was adopted by the American Towing Tank Conference (ATTC) in 1947 and in order to make the relationship applicable to the hull surfaces of new ships an additional allowance of 0.0004 was added to the smooth surface values of C_F given by Equation (2.12). By 1950 there was a variety of friction lines for smooth turbulent flows in existence and all, with the exception of Froude's work, were based on Reynolds number. Phillips-Birt (1970) provides an interesting comparison of these friction formulations for a Reynolds number of 3.87×10^9 which are applicable to ships of the length of the former trans-Atlantic liner *Queen Mary* and are rather less than that for the large supertankers: in either case lying way beyond the range of direct experimental results [1].
The comparison is shown in Table 2.1.

Friction line	C_F
Gerbers	0.00134
Prandtl–Schlichting	0.00137
Kemph–Karham	0.00103
Telfer	0.00143
Lackenby	0.00140
Froude	0.00168
Schoenherr	0.00133
Schoenherr +0.0004	0.00173

Table 2.1: Comparison of C_F values for different friction lines for a Reynolds number Rn = 3.87 $\times 10^9$ (taken from Phillips-Birt(1970)).

It is seen that close agreement is seen to exist between most of the results except for the Froude and Schoenherr modified line. These last two, whilst giving comparable results, include a correlation allowance in their formulation. Indeed the magnitude of the correlation allowance is striking between the two Schoenherr formulations: the allowance is some 30 per cent of the basic value.

In the general application of the Schoenherr line some difficulty was experienced in the correlation of large and small model test data and wide disparities in the correlation factor *C*A were found to exist upon the introduction of all welded hulls. These shortcomings were recognized by the 1957 International Towing Tank Conference (ITTC) and a modified line was accepted. The 1957 ITTC line is expressed as [1].

$$C_F = \frac{0.075}{(\log_{10} Rn - 2.0)^2} \qquad (2.13)$$

The comparison between the ATTC friction line and ITTC 57 is shown in figure below:

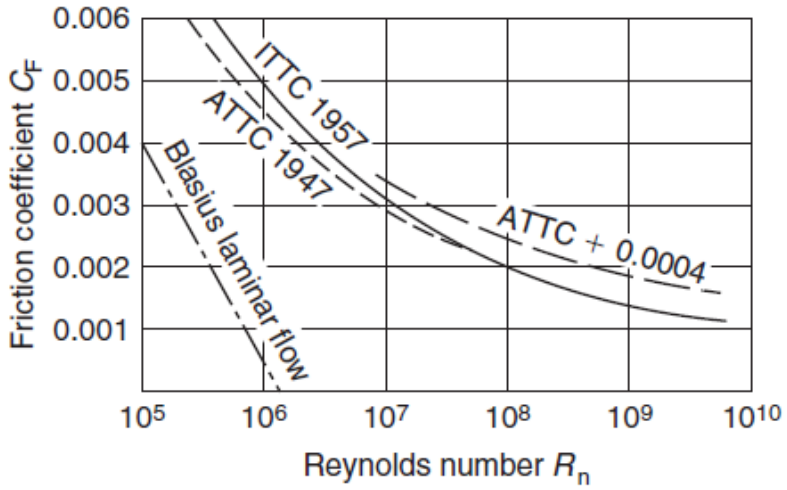

Figure n°2.5: Comparison of ITTC 57 and ATTC 47 friction lines.

The frictional resistance R_F derived from the use of either the ITTC or ATTC lines should be viewed as an instrument of the calculation process rather than producing a definitive

magnitude of the skin friction associated with a particular ship. As a consequence when using a Froude analysis based on these, or indeed any friction line data, it is necessary to introduce a correlation allowance into the calculation procedure. This allowance is denoted by *C*A and is defined as [1]:

$$C_A = C_{T(measured)} - C_{T(estimated)} \quad (2.14)$$

In this equation, as in the previous equation, the resistance coefficients *C*T , *C*F , *C*W and *C*A are non-dimensional forms of the total, frictional, wave making and correlation resistances, and are derived from the basic resistance summation $R_T = R_W + R_V$ by dividing this equation throughout by $\frac{1}{2}\ \rho\ Vs^2.S, \frac{1}{2}\ \rho\ Vs^2.L^2\ or\ \frac{1}{2}\ \rho\ Vs^2.\nabla^{2/3}$, according to convenience.

2.2.2 *Appendage skin friction:*

Appendage Resistance is the Resistance caused by all the underwater appendages such as the propeller, propeller shaft, struts, rudder, bilge keels, pit sword, sea chests and so on. The appendage resistance can be dividing to two components mentioned below.

The appendages introduce a skin friction resistance above that of the naked hull resistance, Where at model scale the flow over the appendages it would normally be laminar, except if it is artificially stimulated, which in itself may introduce a flow modeling problem, whereas at the ship scale the flow over the appendages is turbulent.

In addition, many of the hull appendages are working wholly within the boundary layer of the hull, and since the model is run at Froude identity and not Reynolds identity this again presents a problem. As a consequence the prediction of appendage resistance needs care if significant errors are to be avoided [1].

In addition to the skin friction component of appendage resistance, if the appendages are located on the vessel close to the surface then they will also contribute to the wave making component since a lifting body close to a free surface, due to the pressure distribution around the body, will create a disturbance on the free surface[1].

As a consequence of the two components of appendage resistance, the total appendage resistance can be expressed as the sum of the skin friction and surface disturbance effects as follows:

$$\boldsymbol{R_{APP} = R_{APP(F)} + R_{APP(w)}} \quad (\mathbf{2.15})$$

Where $R_{APP\ (F)}$ and $R_{APP\ (W)}$ are the frictional and wave making components, respectively, of the appendages.

In most cases of practical interest to the merchant marine $R_{APP\ (W)} \cong 0$ and can be neglected: this is not the case, however, for some naval applications [1]. In Naval ships appendages can sometimes account for approximately 2-14% of the total resistance.

2.2.3 *Viscous form resistance:*

The total drag on a body immersed in a fluid and travelling at a particular speed is the sum of the skin friction components, which is due the shearing stresses taken over the surface of the body(a force acting tangent to the hull), and the form drag, which is due to the normal forces acting on the body.

As the fluid flows around the body, there is a pressure distribution normal to the body. In the forward section of the hull there is a component of pressure resisting motion, and in the aft section of the body there is a component of pressure assisting motion.

In an inviscid fluid the flow along any streamline is governed by Bernoulli's equation and the flow around an arbitrary body is predictable in terms of the changes between pressure and velocity over the surface [1] (see figure 2.5).

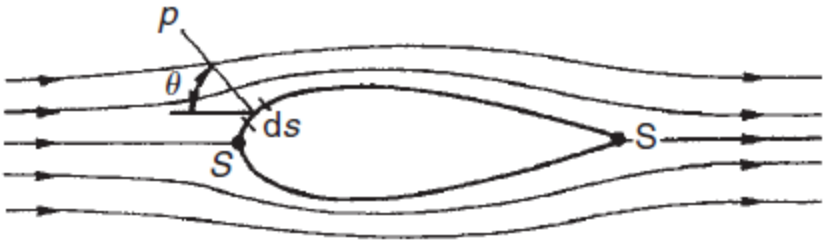

Figure n° 2.5: Body in inviscid fluid flow.

From this case shown in the figure above it leads that the net axial force in the direction of motion being equal to zero. That's mean that:

$$\oint p \cos\theta \, ds = 0 \qquad (2.16)$$

When moving in a real fluid, a boundary layer is created over the surface of the body which, in the case of a ship, will be turbulent and is also likely to separate at some point in the after body. As known that the water is not an ideal fluid and therefore some differences in the flow around a body exist. See figure below.

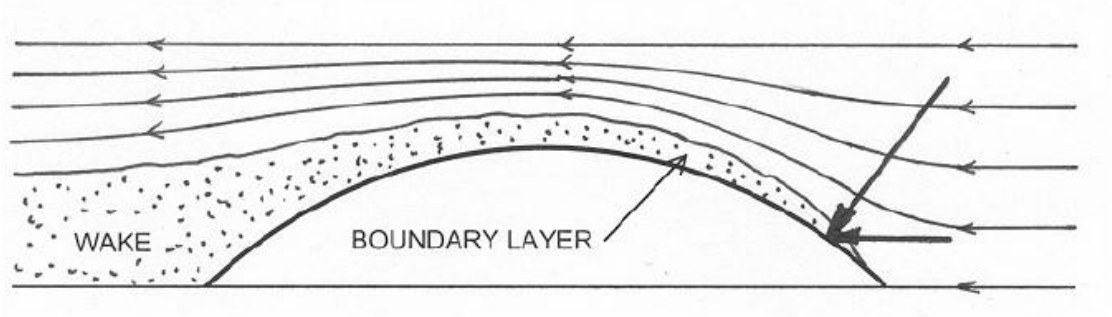

Figure n°2.6: Flow around a body submerged in water.

From the figure 2.6 it seen that the turbulent boundary layer has developed along the hull producing a wake. It seen also that the hull pressure forces act normal to the surface in the forward part of the body; however, in the aft portion of the hull the boundary layer reduces the forward acting component of pressure, that's due to the pressure acting on the hull.
This increase in resistance due to pressure is called "viscous pressure drag" or "form drag", and is sometimes also referred to as the normal component of viscous resistance [2].

As it's mentioned in the previous paragraph, the presence of the boundary layer and its growth along the surface of the hull modifies the pressure distribution acting on the body from that of the potential or inviscid case.

As a consequence, the left-hand side of Equation (2.16) can no longer equal zero and the viscous form drag R_{VF} is defined for the three-dimensional case of a ship hull as [1]:

$$R_{VF} = \sum_{k=1}^{n} p_k \cos\theta_k \delta S_k \qquad (2.17)$$

In which the hull has been split into n elemental areas δS_k and the contribution of each normal pressure p_k acting on the area is summed in the direction of motion see (Figure 2.7).

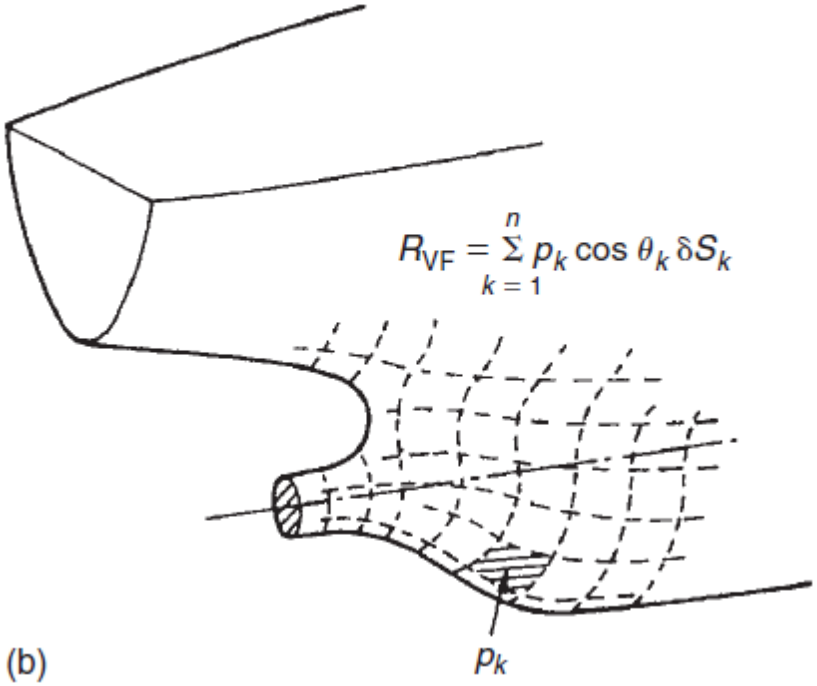

Figure n° 2.7 Pressure acting on shell plate of the ship.

The equation (2.17) is an extremely complex equation to solve since it relies on the solution of the boundary layer over the vessel.

2.2.4 Viscous resistance:

As it's mentioned in the previous section (figure 2.2), the viscous resistance is principally the sum of the form resistance, the naked hull skin friction and the appendage resistance. It's known that calculation by analytical means of the viscous form resistance is extremely complex matter, and it was not possible with any degree of accuracy at the present time for many hulls with a complex shape.

In order to provide a better empirical foundation for the viscous resistance, Hughes (1954) divided an approach which incorporated the viscous form resistance and the naked hull skin friction.

To form a basis for this approach Hughes undertook a series of resistance tests using planks and pontoons for a range of Reynolds numbers up to a value of 3×10^8 . From the results of this experimental study Hughes established that the frictional resistance coefficient C_F could be expressed as a unique inverse function of aspect ratio AR and, furthermore, that this

function was independent of Reynolds number. The function derived from this work had the form [1]:

$$C_f = C_f|AR = \infty \,.\, f\left(\frac{1}{AR}\right) \qquad (2.18)$$

In which the term $C_f = C_f|AR = \infty$ is the frictional coefficient relating to a two-dimensional surface; that is, one having an infinite aspect ratio.
This function permitted Hughes to construct a two-dimensional friction line defining the frictional resistance of turbulent flow over a plane smooth surface. This took the form:

$$C_f|_{AR=\infty} = \frac{0.066}{[\log_{10} Rn - 2.03]^2} \qquad (2.19)$$

The equation (2.19) is quite similar to the ITTC 1957 line expressed by Equation (2.13).There is a difference which is that the ITTC and ATTC lines contain some three-dimensional effects, whereas Equation (2.19) is defined as a two-dimensional line.

Hughes proposed the calculation of the total resistance of a ship using the basic relationship:

$$C_T = C_V + C_W \qquad (2.20)$$

It's known from previously section that$C_V = C_f|AR = \infty + C_{FORM}$, thereby giving the total resistance as:

$$C_T = C_f|AR = \infty + C_{FORM} + C_W \qquad (2.21)$$

In which C_{FORM} is a form resistance coefficient which takes into account the viscous pressure resistance of the ship. In this approach the basic skin friction resistance coefficient can be determined from Equation (2.19). To determine the form resistance the ship model can be run at a very slow speed when the wave making component is very small and can be neglected; when this occurs, that is to the left of point *A* in Figure 2.8 , then the resistance curve defines the sum of the skin friction and form resistance components[1].

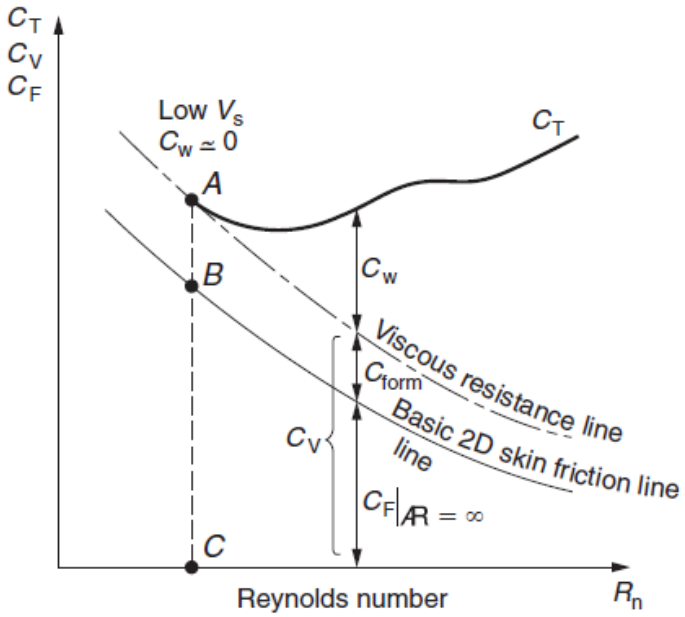

Figure n°2.8: Hughes model of ship resistance.

At the point *A*, when the wave making resistance is negligible, the ratio

$$\frac{AC}{BC} = \frac{viscous\ resistance}{skin\ friction\ resistance} = \frac{skin\ friction\ resistnace + viscous\ form\ resistance}{skin\ friction\ resistance}$$
$$= 1 + \frac{viscous\ form\ resistance}{skin\ friction\ resistance}$$

$$and\ if\ k = \frac{viscous\ form\ resistance}{skin\ friction\ resistance}$$
$$then\ \frac{AC}{BC} = (1 + k) \qquad (2.22)$$

In Equation (2.22), (1 + *k)* is termed the form factor and is assumed constant for both the ship and its model. Indeed the form factor is generally supposed to be independent of speed and scale in the resistance extrapolation method. In practical cases the determination of (1+*k*) is normally carried out using a variant of the Prohashka method by a plot of C_T against Fn^4 and extrapolating the curve to *F*n = 0 [1](see Figure 2.9).

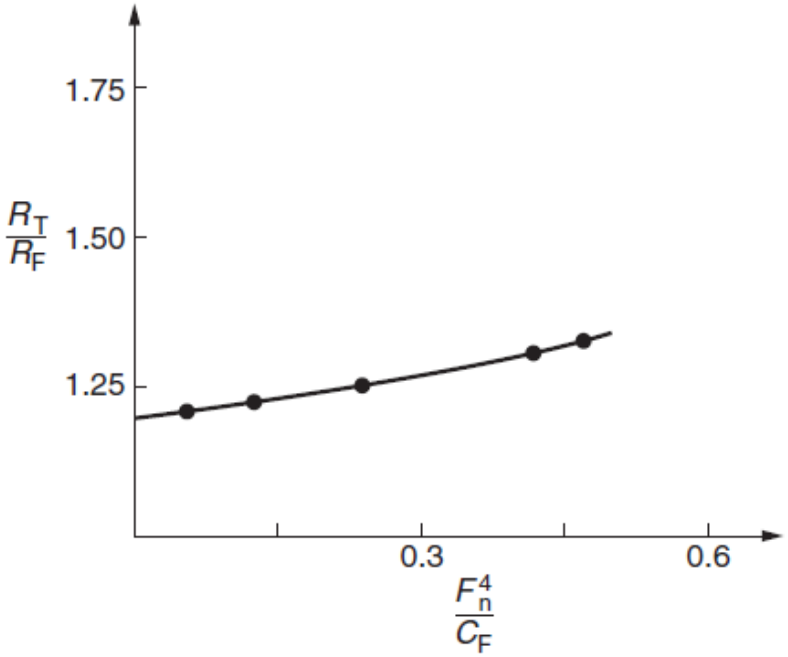

Figure n°2.9: Determination of (1 + k) using Prohaska method.

From this figure the form factor (1 + *k)* is deduced from the relationship

$$1+k = lim_{F_n \to 0}(\frac{R}{R_F}) \qquad (2.23)$$

This derivation of the form factor can be used in the resistance extrapolation only if scale-independent pressure resistance is absent.
Refer to [1] the form factor (1 + *k*) is treated as a constant with varying Froude number the fundamental question remains as to whether it is valid to assume that the (1 + *k*) value, determined at vanishing Froude number, is valid at high speed. This is of particular concern at speeds beyond the main resistance hump where the flow configuration around the hull is

likely to be very different from that when *F*n = 0, and therefore a Froude number dependency can be expected for (1 +*k)*.

Comparison of (a) extrapolation using Hughes approach and (b) extrapolation using Froude approach is shown in figure 2.10.

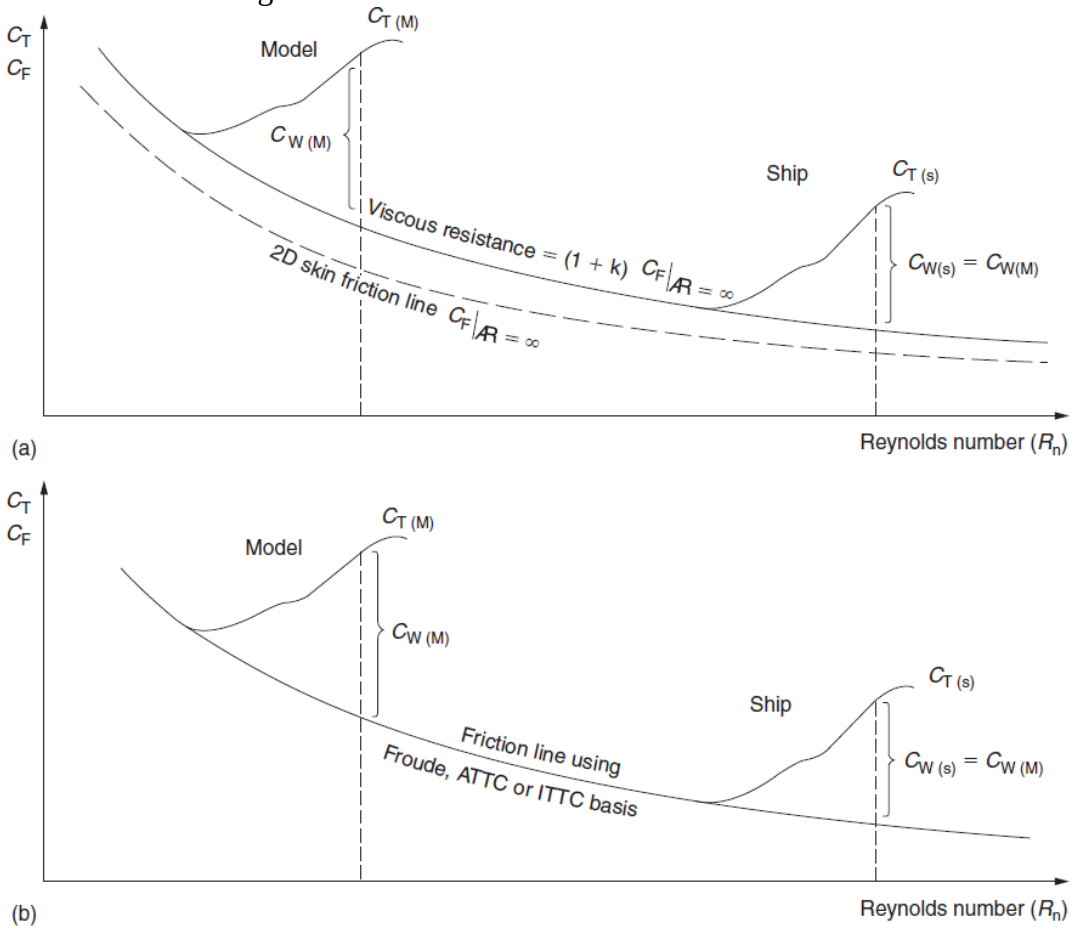

Figure n°2.10: Comparison of extrapolation approaches: (a) extrapolation using Hughes approach and (b) extrapolation using Froude approach.

From the figure 2.10(a), it is seen that the two-dimensional skin friction line, Equation (2.19), is used as a basis and the viscous resistance is estimated by scaling the basic friction line by the form factor (1 + *k)*. However, the Froude approaches (Figure 2.10(b)), is essentially the same, except that the frictional resistance is based on one of the Froude equation (ATTC or ITTC) friction lines without a factor (1+*k)*.

In practice both the Froude and Hughes approaches are used in model testing; the latter, however, is most frequently used in association with the ITTC 1957 friction formulation rather than Equation (2.19). Research is being expended in the development of form parameters which will reflect the hull surface contours in a more equable way [1].

2.2.5 Wave making resistance R_W:

Every Body or ship moving over a liquid is accompanied by at least three pressure disturbances on each side, and these are area rather than point disturbances. They produce not one but several trains waves. In fact the body as a whole sets up an unusual traveling undulation, presently to be described, which is not wave in the ordinary sense of the term because it moves along with the body and is non-repeating [4].

If it's consider that a moving ship in 2- dimensional form, the liquid surface around the ship is accompanied by more than three pressure changes along the length of the ship.
Where it's appear two regions of +Δp, one is at the bow and the second at the stern, and one region of –Δp located at mid length. The –Δp region amidships usually has variations in magnitude which serve as pressure disturbances in themselves. In addition there are some other pressure disturbances below the surface waterline area. (See figure 2.11).

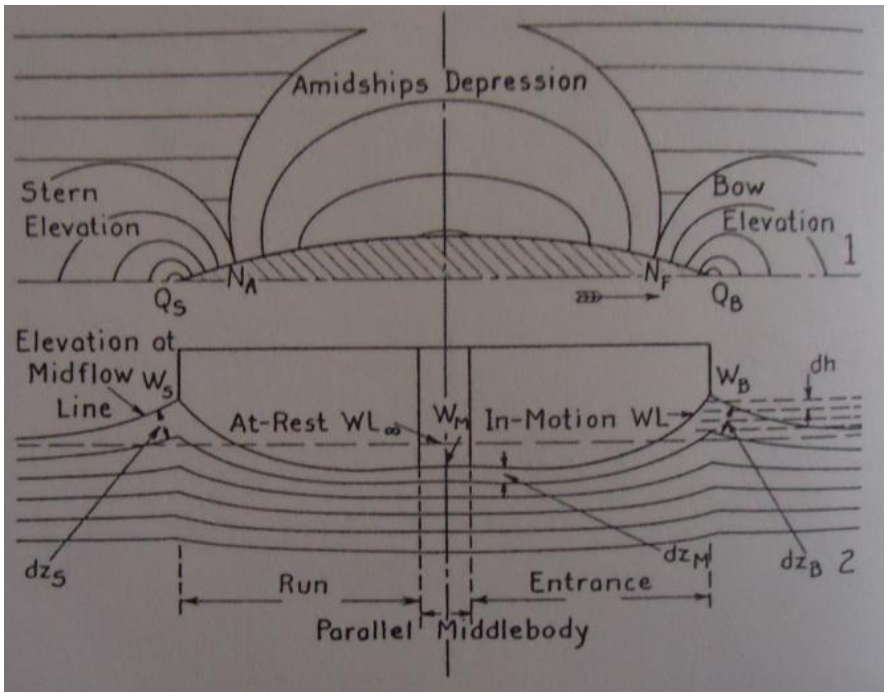

Figure 2.11: Bernoulli contour system around a simple ship form.

The surface of the liquid is free to respond to the pressure changes around the simple lenticular ship moving forward with a velocity, subject only the action of gravity and inertia [4]. From the figure (2.11) it's seen that there is a rise of the liquid surface begins at a point rather well forward of the bow, due to the +Δp developed forward. The rise continues as it approaches the bow, where it reaches the height W_B. the region of –Δp along the side, beginning behind the forward shoulder, causes the water surface to drop below the water line , and after that there is the region of +Δp at the stern of the ship.

Lord Kelvin in 1904 studied the problem of the wave pattern caused by a moving pressure point. He showed that the resulting system of waves comprises a divergent set of waves together with a transverse system which are approximately normal to the direction of motion of the moving point. Figure 2.12 shows the system of waves so formed. The pattern of waves

is bounded by two straight lines which in deep water are at an angle ϕ to the direction of motion of the point; whereϕ is given by equation below [1].

$$\emptyset = sin^{-1}\left(\frac{1}{3}\right) = 19.471 \qquad (1.24)$$

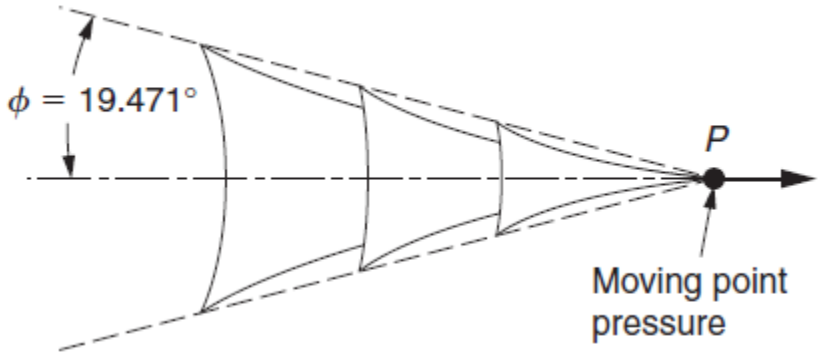

Figure n° 2.12: Wave pattern induced by a moving-point pressure in calm water.

Since that the interference between the divergent and transverse systems gives waves their characteristic shape. And due to the same velocity of the systems and ship, the wave length λ between successive crests is:

$$\lambda = \frac{2\pi}{g}V^2 \qquad (2.25)$$

Due to the constant energy in the wave, the height of the wave systems formed decreases fairly rapidly. More energy is absorbed by the transverse system than by the divergent system, and its increases with increasing speed.

Since that the real form ship cannot be represented adequately by a single moving point as analyzed by Kelvin, in order to present a ship is to place a moving pressure field near to the both bow and stern in order to simulate the wave system, see figure (2.13).

In this model the bow pressure field create crest near the bow, from observation this occurs at about λ /4 from the bow whilst the suction field will introduce a wave trough at the stern: both of these wave systems have a wavelength λ =2 π V² / g [1].

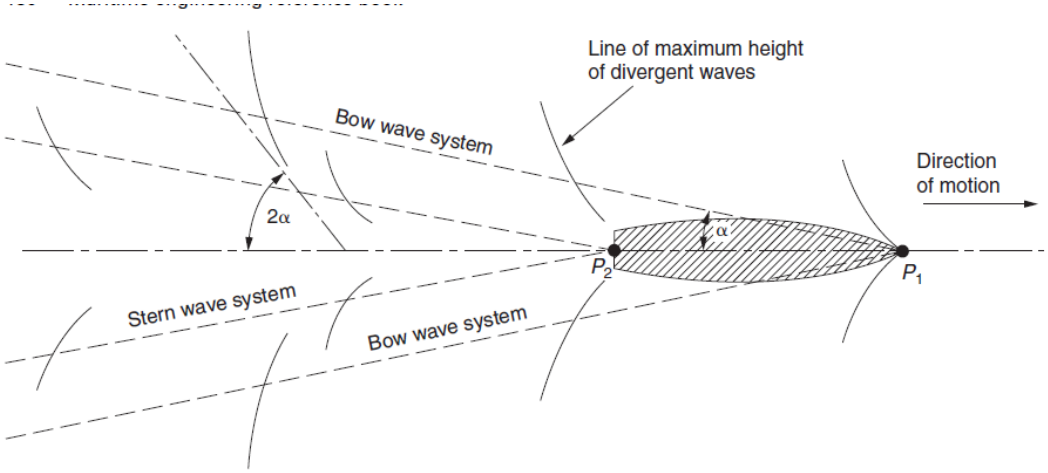

Figure n°2.13: Simple ship wave pattern representation by two pressure points.

The divergent component of the wave system derived from the bow and the stern generally do not exhibit any strong interference characteristics. This is not the case, however, with the transverse wave systems created by the vessel, since these can show a strong interference behavior. Consequently, if the bow and stern wave systems interact such that they are in phase a reinforcement of the transverse wave patterns occurs at the stern and large waves are formed in that region. For such a reinforcement to take place, Figure 2.14(a) , the distance between the first crest at the bow and the stern must be an odd number of half-wavelengths as follows[1]:

$$L - \frac{\lambda}{4} = k\frac{\lambda}{2} \quad \begin{cases} where\ k = 1,3,5 \ldots, (2j+1) \\ with\ j = 0,1,2,3 \end{cases}$$

Form which

$$\frac{4}{2k+1} = \frac{\lambda}{L} = \frac{2\pi V^2}{gL} = 2\pi(Fn)^2 \qquad (1.26)$$

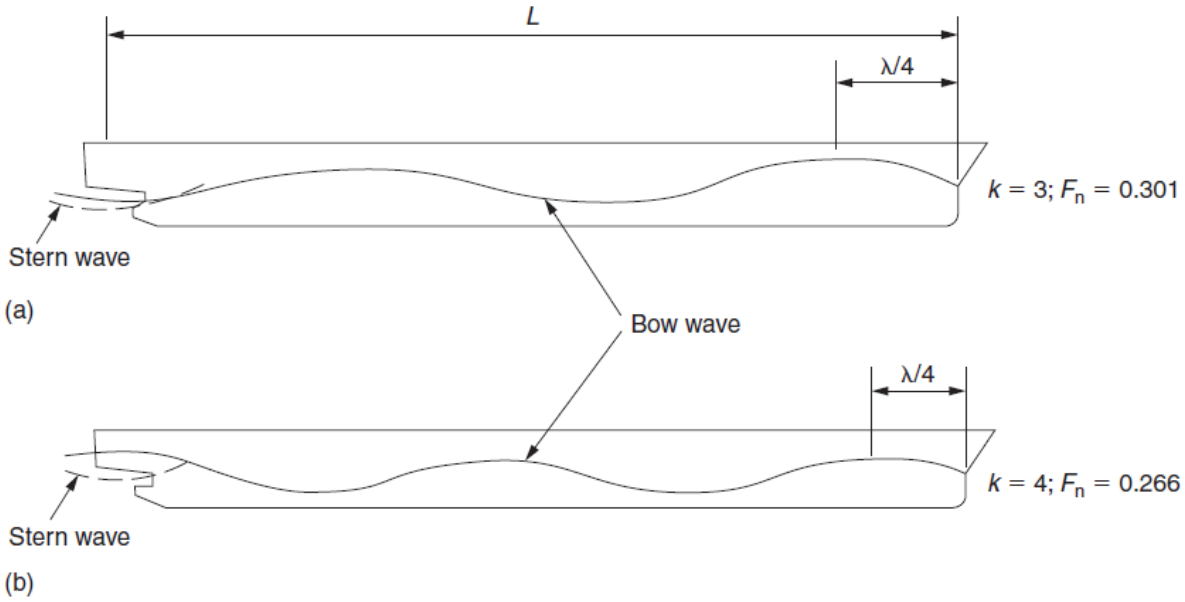

Figure n°1.14: Wave reinforcement and cancellation at stern: (a) wave reinforcement at stern and (b) wave cancellation at stern.

That is:

$$F_n = \sqrt{\frac{2}{\pi(2k+1)}} \qquad (2.27)$$

For the converse case when the bow and stern wave systems cancel each other, and hence produce a minimum wave making resistance condition, the distance $L = \lambda / 4$ must be an even number of half wave lengths (Figure 2.14(b)):

$$L - \frac{\lambda}{4} = k\frac{\lambda}{2} \quad \begin{cases} where\ k = 2,4,6 \ldots, 2j \\ with\ j = 0,1,2,3 \end{cases}$$

Hence:

$$F_n = \sqrt{\frac{2}{\pi(2k+1)}} \qquad (2.28)$$

As before, but with *k* even in this case.

From the Equation (2.27), this particular model of wave action identifies the Froude numbers at which reinforcement (humps) and cancellation (hollows) occur in the wave making resistance. The results are shown in Table 2.2

K	F_n	*Description*
1	0.461	1st hump in R_w curve
2	0.357	1st hollow in R_w curve
3	0.301	2nd hump in R_w curve
4	0.266	2nd hollow in R_w curve
5	0.241	3rd hump in R_w curve
⋮	⋮	⋮

Table n° 2.2: Froude numbers corresponding to maxima and minima in the wave making resistance component.

In order to see the variation of the wave making resistance related to the various number of k, the wave making resistance is plotted on function of speed. See figure 2.15.

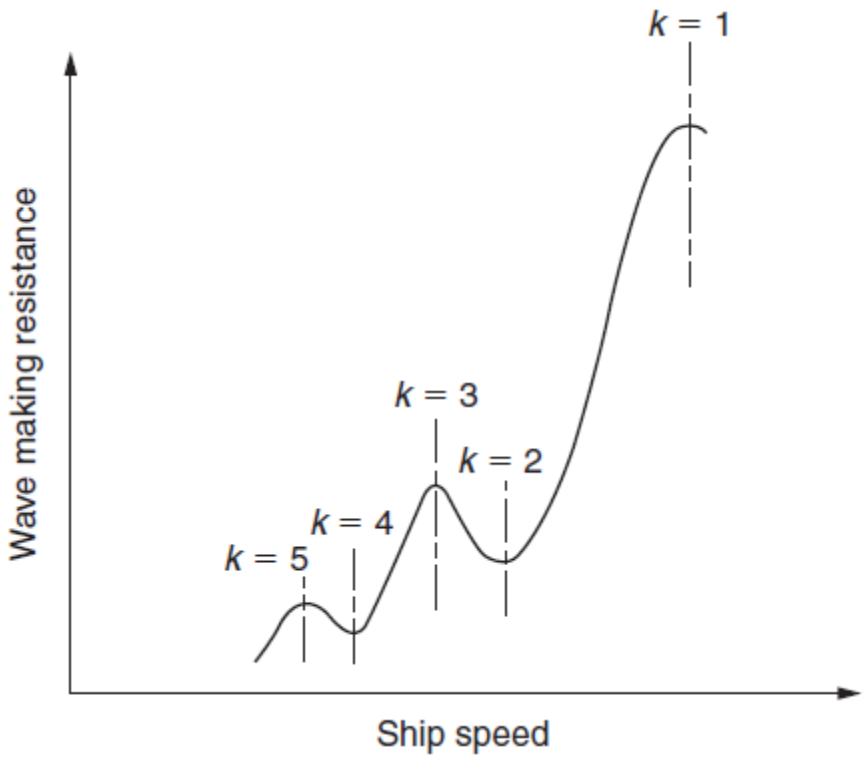

Figure n° 2.15: Wave making resistance as function of speed.

It seen from the curve of the wave making resistance that the 'humps' occur, that's because the wave profiles and hence the wave making resistance are at their greatest, in these conditions, whilst the converse is true in the case of the 'hollows'.
The Figure 2.16 shows the schematic wave profiles associated with the various values of *k.*

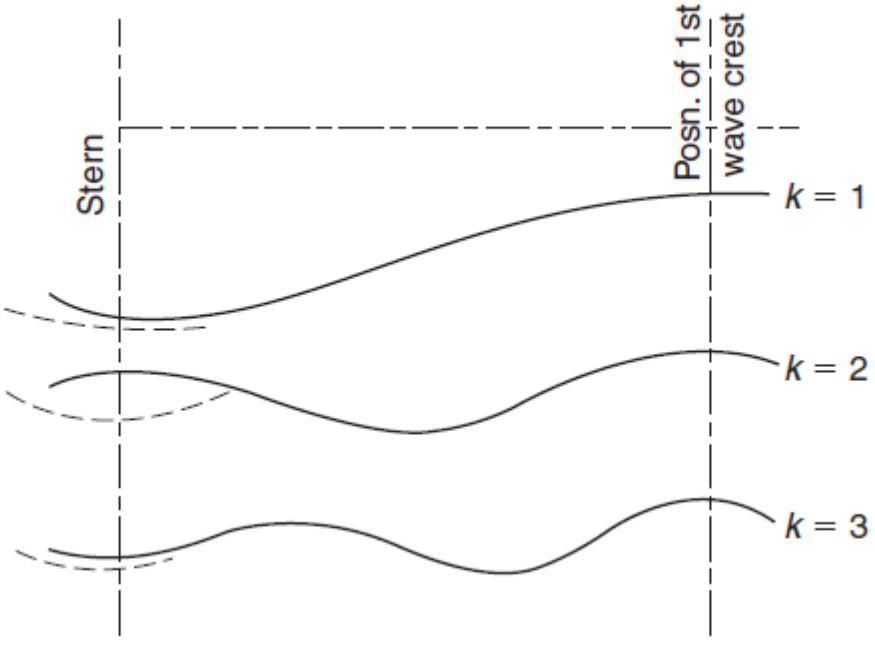

Figure 2.16 Form of wave making resistance curve* associated with the various values of *k.

It seen in the figure above that the first hump associated with k=1 is the most pronounced hump and occurs at the highest speed; refer to [1] this hump termed 'main hump'.
The second hump, k = 3, is called the ‘prismatic hump’ since it is influenced considerably by the prismatic coefficient of the particular hull form.

The derivation of Figure 2.16 and Table 2.2 relies on the assumptions made in its formulation; for example, a single pressure and suction field, bow wave crest at λ /4; stern trough exactly at the stern, etc. Clearly, there is some latitude in all of these assumptions, and therefore the values of *Fn* at which the humps and hollows occur vary. In the case of warships the distance between the first crest of the bow wave and the trough of the stern wave has been shown to approximate well to 0.9 L , and therefore this could be used to rederive Equation (2.27), and thereby derive slightly differing values of Froude numbers corresponding to the ‘ humps ’ and ‘ hollows ’ . Table2.3 shows these differences and it is clear that the greatest effect is formed at low values of *k.* Figures 2.16, 2.15 for this and the other reasons cited is not unique but is shown here to provide awareness and guidance on wave making resistance variations[1].

k	*1*	*2*	*3*	*4*	*5*
$L - \lambda/4$ basis	0.46	0.36	0.30	0.27	0.24
$0.9L$ basis	0.54	0.38	0.31	0.27	0.24

Table n° 2.3: Effect of difference in calculation basis on prediction of hump and hollow Froude numbers.

In order to make a better approximation to the wave form of the ship, it can consider that the ship is solid body further than two point sources. As an example Wigley initially used a simple parallel body with two pointed ends and showed that the resulting wave pattern along the body could be approximated by the sum of five separate disturbances of the surface (see Figure 2.7)[1].

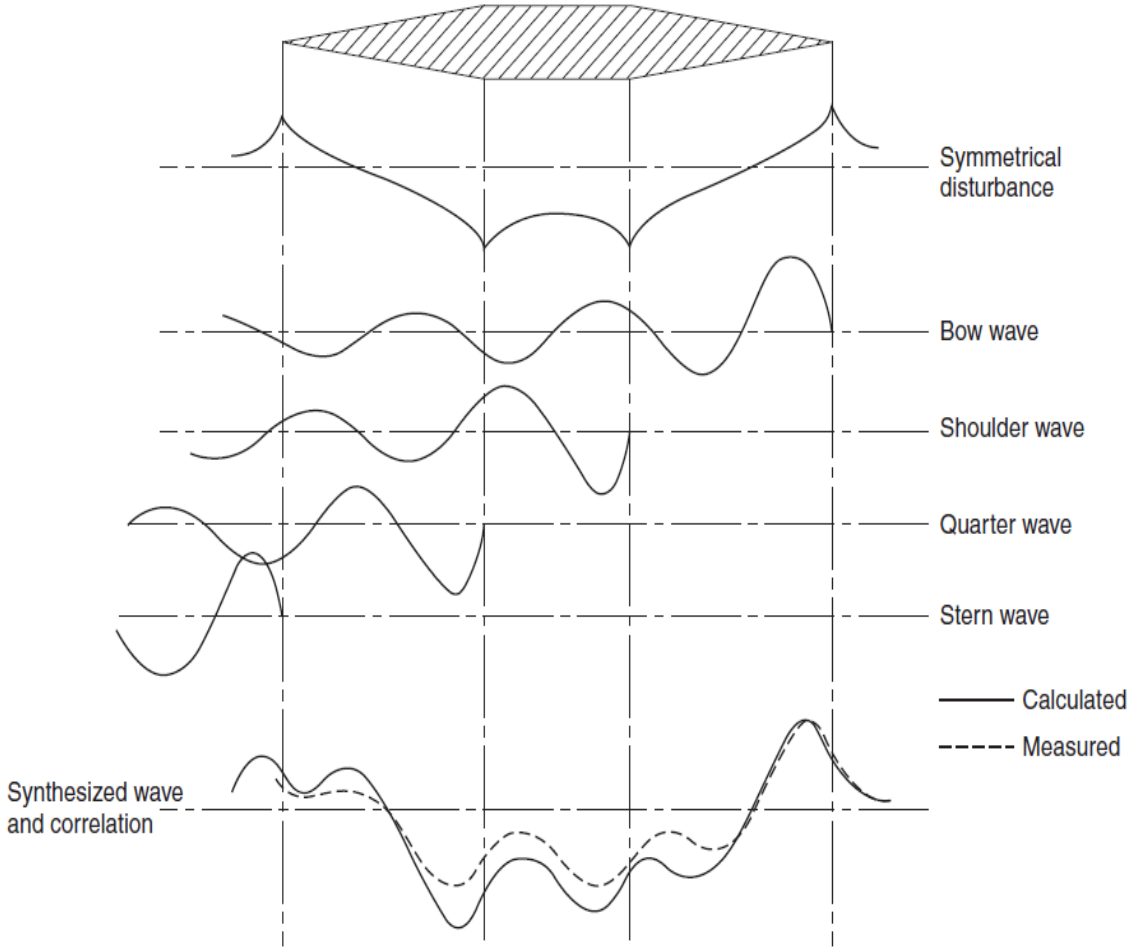

Figure n°2.17: Components of wave systems for a simple body.

From this figure it is seen that a symmetrical disturbance corresponds to the application of Bernoulli's theorem with peaks at the bow and stern and a hollow, albeit with cusps at the start and finish of the parallel middle body, between them. Two wave forms starting with a crest are formed by the action of the bow and stern whilst a further two wave forms commencing with a trough originates from the shoulders of the parallel middle body [1].

In the bottom of figure 2.17, it's shown the sum of wave's profiles, since the wave length λ varies with speed so it's clear to understand that the whole profile of the resultant wave form will change with speed length ratio.

The previous analysis was extended by Wigley for a more realistic hull form; the figure 2.18 shows the results of wave form.

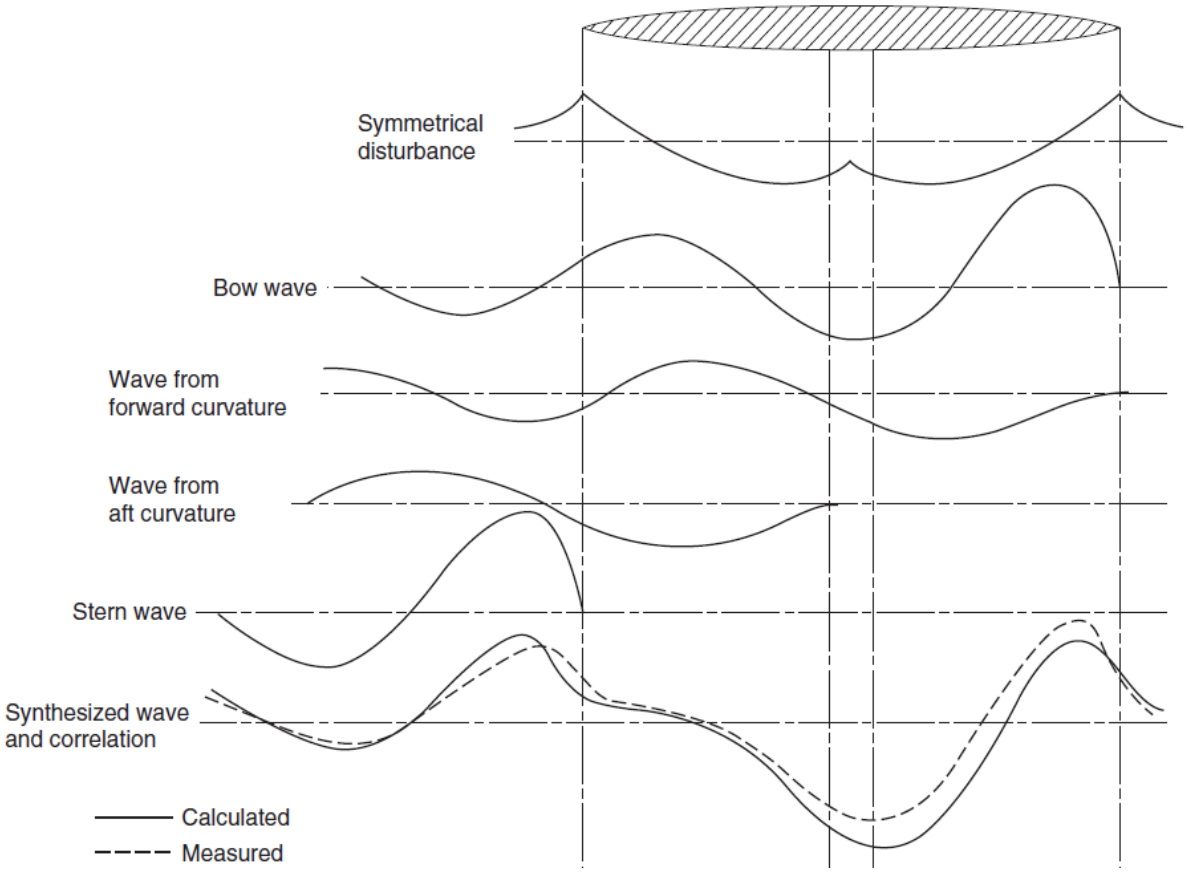

Figure n° 2.18 Wave components for a body with convex ends and a parallel middle body.

The take into consideration of this type leads to design a hull form with a minimum wave making resistance. The basis of these theories is developed by Kelvin and his work on pressure source.

2.2.6 The contribution of the bulbous bow:

Bulbous bows are today commonplace in the design of ships. Their origin is to be found before the turn of the century, but the first application appears to have been in 1912 by the US Navy. The general use in merchant applications appears to have waited until the late 1950s and early 1960s [1].The basic theoretical work on their effectiveness was carried out by Wigley (1936) in which he showed that if the bulb was nearly spherical in form, then the acceleration of the flow over the surface induces a low-pressure region which can extend towards the water surface. This low-pressure region hen reacts with the bow pressure wave to cancel or reduce the effect of the bow wave [1].
Therefore the main effect of bulbous bow is to reduce in the majority cases the effective power required to propel the ship, (see figure 2.19).

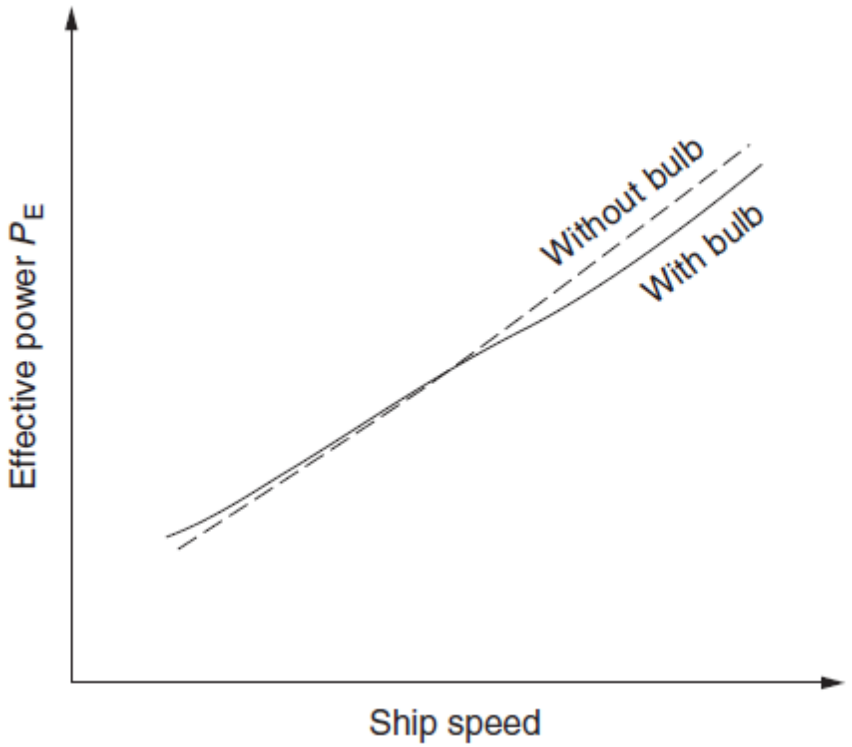

Figure n° 2.19: Influence of a bulbous bow of the effective power requirement.

The figure above it can be seen that the presence of the bulb is beneficial at the highest speeds and disadvantage at low speeds. This is because the balance between of the wave reduction effect and frictional resistance. The details for the bulbous bow effect are shown in the next chapter.

2.2.7 Transom immersion resistance:

It does generally occur when the transom of the ship is immersed, in this case the flow separation taking place, as the flow form under the transom passes out beyond the hull.
The vertices behind the transom lead to a pressure loss behind the hull which is considered important to take it on consideration in some analysis.
Refer to [1] the magnitude of this resistance is generally small, and is neglect when the stern is dry. Transom immersion resistance is largely a pressure resistance that is scale independent see figure 2.20.

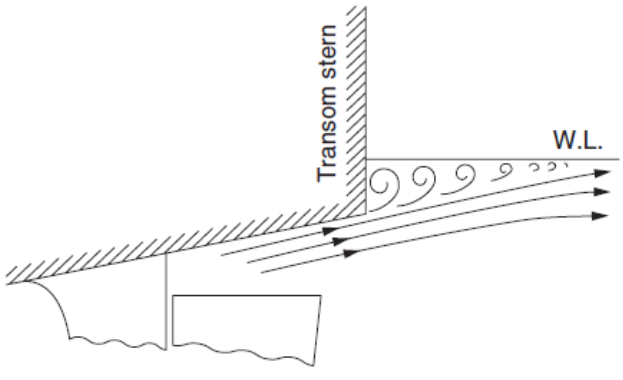

Figure n° 2.20 Flow around an immersed transom stern.

2.3 Methods of resistance evaluation:

To evaluate the power required to tow the ship, is important to calculate the ship resistance, so the designers create a several methods to calculate the ship resistance starting by the traditional methods until to advanced method, the choose of the method is depends on the available and the accuracy desired. The methods used to calculate the ship resistances are shown in the figure below.

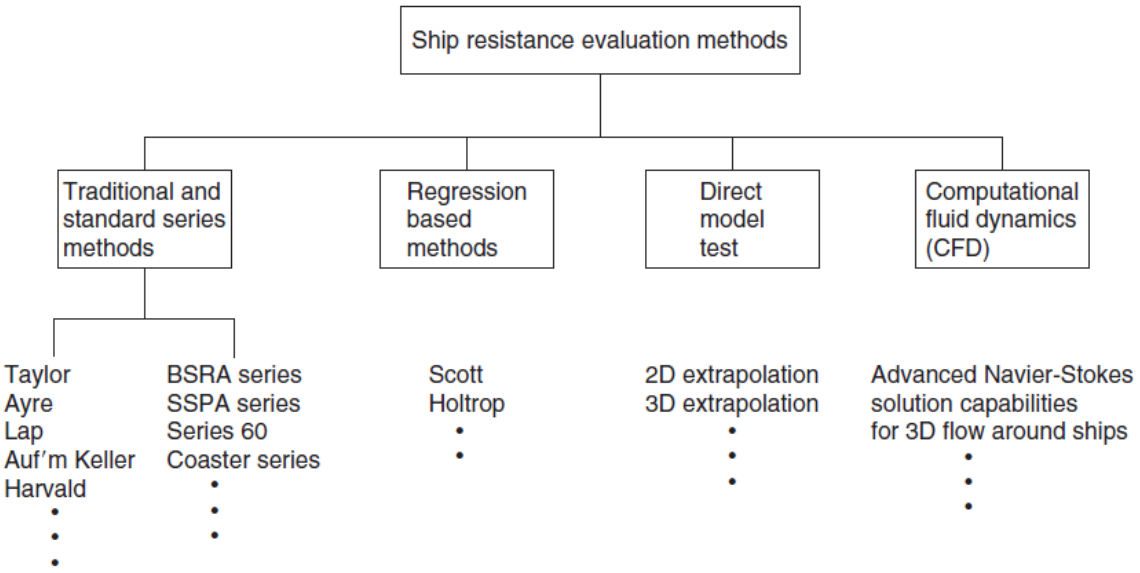

Figure n°2.21: Ship resistance evaluation methods and examples.

In this chapter it's focused on the computational fluid dynamic method which is used to calculate the ship resistance in this project.

2.3.1*Computational fluid dynamics method:*

(a) Wave resistance computations:

The wave resistance problem considers the steady motion of the ship, in ideal fluid where the viscosity effect is neglect. The ship create a wave at the freely surfaces, this phenomena considered popular problem in computational fluid dynamics.

In the wave resistance problem, it's considering that a ship moving with constant speed V in water of constant depth and width. For inviscid and irrotational flow is equivalent to a ship being fixed in an inflow of constant speed. In order to simplify the problem, some simplifications are generally assumed:

Water is incompressible, irrotational, and inviscid, Surface tension is negligible, there are no breaking waves, the hull has no knuckles which cross streamlines and the appendages and propellers are not included in the model. (The inclusion of a propeller makes little sense as long as viscous effects are not also included.)[1].

The governing field equation is Laplace's equation. A unique description of the problem requires further conditions on all boundaries of the modeled fluid domain [1]:

● Hull condition: water does not penetrate the ship's surface.

●Transom stern condition: It's for the ship with a transom stern, the flow is assumed separated and the transom stern is dry, so the atmospheric pressure is enforced at the edge of the transom stern. Assuming that the flow is in the longitudinal direction the condition is usually considered linearized. For fast ships which have a very large transom stern, several researchers report problems. For submerged transom sterns at low speed, the potential flow model is inapplicable and only field methods are capable of an appropriate analysis [1].

● Kinematic condition: water does not penetrate the water surface.

● Dynamic condition: there is atmospheric pressure at the water surface. Beneath an air cushion, this condition modifies to the air cushion pressure. The inclusion of an air cushion in wave resistance computations has been reported in various applications. However, these computations require the user to specify the distribution of the pressure, especially the gradual decline of the pressure at the ends of the cushion. In reality, this is a difficult task as the dynamics of the air cushion and the flexible skirts make the problem more complicated. Subsequently, the computations must be expected to be less accurate than for conventional displacement hulls [1].

● Radiation condition: waves created by the ship do not propagate ahead. (This condition is not valid for shallow water cases when the flow becomes unsteady and solution waves are pulsed ahead. for subcritical speeds with depth Froude number $F_{nh} \leq 1$, this poses no problem.)[1]

● Decay condition: the flow is undisturbed far away from the ship.

● Open-boundary condition: waves generated by the ship pass unreflected any artificial boundary of the computational domain.

● Equilibrium: the ship is in equilibrium, i.e. trim and sinkage are changed in such a way that the dynamical vertical force and the trim moment are counteracted.

● Bottom condition (shallow-water case): no water flows through the sea bottom.

● Side-wall condition (canal case): no water flows through the side walls.

(b) Viscous flow computations

RANS solvers are state of the art for viscous ship flows. A computational prediction of the total calm water resistance using RANS solvers to replace model tests would be desirable, but so far the accuracy of the RANS predictions is largely perceived as still insufficient. Nevertheless, RANS solvers are widely applied to analyze:

● The flow around aftbodies of ships.
● The flow around appendages.

The first research applications for RANS solutions with wave making for ships appeared in the late 1980s. By the late 1990s various research groups also presented results for ships free to trim and sink. However, most computations for actual ship design projects in practice still neglected all free-surface effects (double-bodyfl ow). Most computations, especially those for practical design applications, were limited to Reynolds numbers corresponding to model tests. Sometimes, potential flow computations were used as preprocessors to determine trim and sinkage and the wave elevation, before RANS computations started with fixed boundaries.

Various applications to ship design and research applications are found in the literature. Representative for the state of the art for ship design applications are surveys by leading companies in the field such as Flowtech (Larsson (1997, 1998), or HSVA (Bertram and Jensen (1994)), Bertram (1998)). The state of the art in research is documented in validation workshops like the Tokyo 1994 workshop and the Gothenborg 2000 workshop.

RANS computations require considerable skill and experience in grid generation and should therefore as a rule be executed by experts usually found in special consulting companies or modern towing tanks. Comprehensive reviews of developments in theoretical and numerical modelling of resistance are given in ITTC (2002a, 2005a)

Chapter 03: Design of Bulbous bow:

3-1 Introduction:

From the previous chapter it's appearing that the bulbous bow improve the efficiency of the hull, but it must respect the good design for the bulb, so the parameters geometry of the bulbous has an influence on the ship powering.

Therefore the design data are derived from a statistical of routine test results of the Hamburg and the Berlin Model Basins, HSVA and VWS, respectively, supplemented by results of additional test to fill the gaps. So the bulb efficiency is related to the bulb parameters which are the volume, the length, the section area, and also some parameters of the hull have an effect on the bulbous properties. These parameters of the bulbous lead to bulb to have a different shape (design).
This chapter explains the deferent kind of bulb and the effect of each parameter on its efficiency further on the ship resistance.

3-2 Bulb forms and parameters:

The bulbs shapes are difficult to define with a finite number of geometry, but it's possible to use a few parameters. With the shape of the cross section of the bulb A_{BT} at the forward perpendicular (FP), it can obtain three bulb types, see figure 3.1.

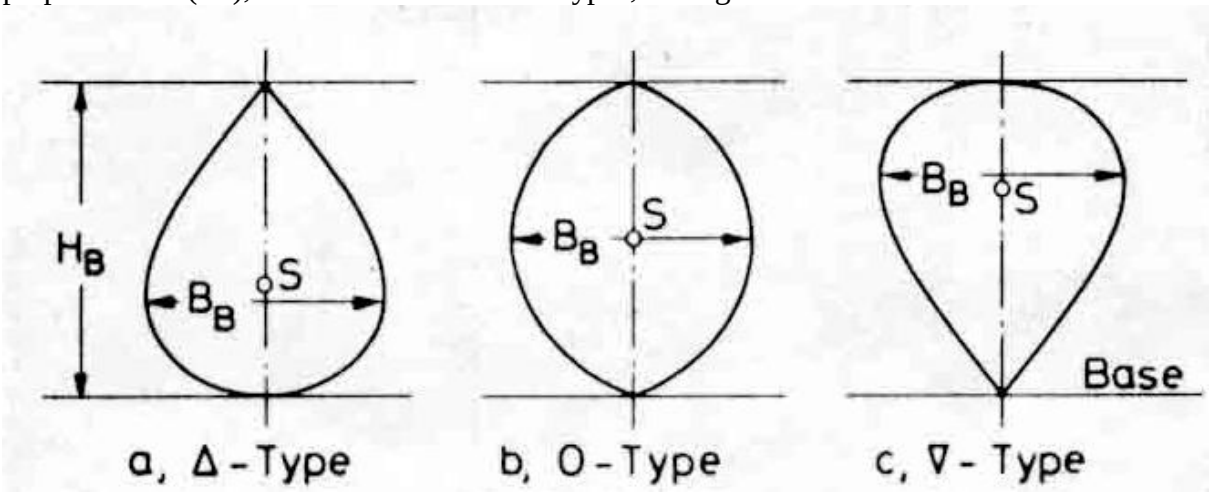

Figure n°3.1: Bulb types.

From the figure it seen that there are three types of the bulb shape. The figure 3.1 (a), shows the delta shape of sectional area of the bulb, the volume bulb concentrates on the low part (Taylor bulb). The figure 3.1(b) shows the O-Type of the bulb shape, it has a center area and volume in the middle (cylindrical bulbs). Figure 3.1(c) shows the nabla-type, it has a center area and volume in the upper part on the bulb, and near to the free surface, because of its favorable seakeeping properties this type is the most common bulb [5].

In addition there are six parameters, the three linear and three nonlinear geometric bulb quantities that are reduced to the bulb which are shown in figure (3.2).

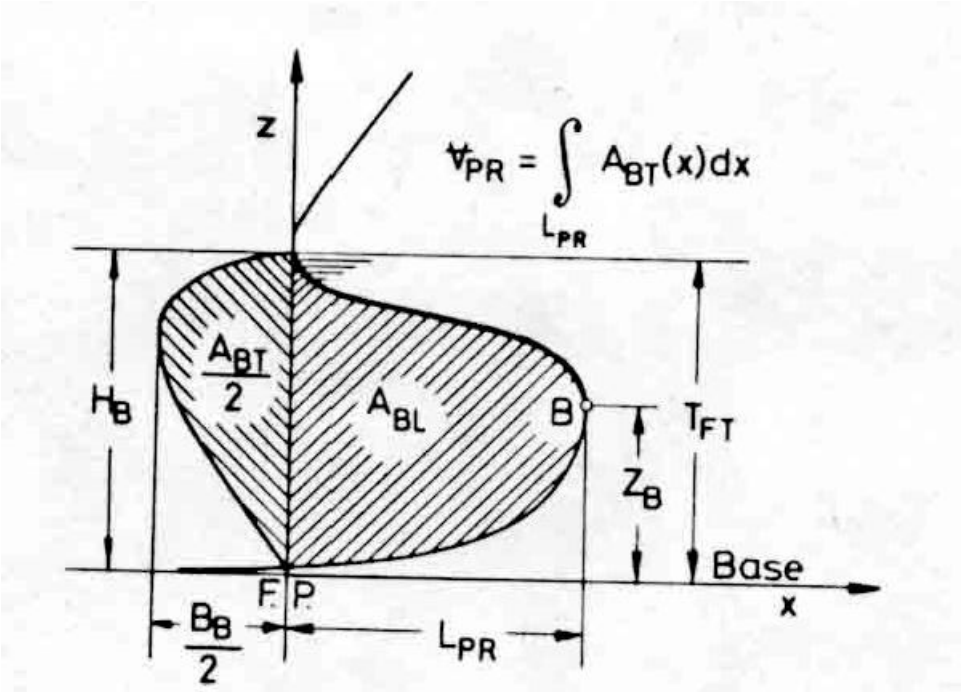

Figure n° 3.2: Linear and nonlinear bulb quantities.

The three linear bulb parameters are:

1- The breadth parameter, that is, the maximum breadth B_B of bulb area A_{BT} at the FP divided by the beam B_{MS} of the ship:

$$C_{BB} = B_B / B_{MS} \qquad (3.1)$$

2- The length parameter, that is, the protruding length L_{PR} normalized by the L_{PP} of the ship:

$$C_{LPR} = L_{PR} / L_{PP} \qquad (3.2)$$

3- The depth parameter, that is, the height Z_B of the foremost point of the bulb over the base divided by the draft T_{FP} at the FP.

$$C_{ZB} = Z_B / T_{FP} \qquad (3.3)$$

The three nonlinear bulb parameters are:

1- The cross section parameter, that is, the cross sectional area A_{BT} of the bulbous bow at the FP divided by the mindship section area A_{MS} of the ship.

$$C_{ABT} = A_{BT} / A_{MS} \qquad (3.4)$$

2- The lateral parameter, that is, the area of ram bow A_{BL} in the longitudinal plane normalized by $A_{MS.}$

$$C_{ABL} = A_{BL} / A_{MS} \qquad (3.5)$$

3- The volumetric parameter, that is, the volume V_{PR} of the protruding part of the bulb divided by the volume of displacement V_{WL} of the ship.

$$C_{VPR} = V_{PR} / V_{WL} \qquad (3.6)$$

The volume V_{PR} is the nominal bulb volume. The total or effective bulb volume V_{Btot} is the sum of V_{PR} and the fairing volume V_F, which results from the fairing of the bulb into the ship hull.
Finally a distinction is possible between an additive and an implicit bulb. An additive bulb increases the displacement volume V_{WL} of the ship by the effective bulb volume V_{Btot}. The sectional area curve of the original hull remains unchanged [5].
On the other hand, the effective volume V_{Btot} of an implicit bulb is part of the displacement volume V_{WL} of the main hull that is shifted from unfavorable region and concentrated in the vicinity of the forward perpendicular. By this process, the sectional area curve of the original ship is changed [5].

3-3Influence of a bulbous bow on the properties of a ship:

Before discussing the influence of the bulbous bow on the ship's resistance, it should mention that the bulb has also an influence on thrust deduction and wake fraction. Both are increased by an additive as well as by an implicit bulb. See figure (3.3).

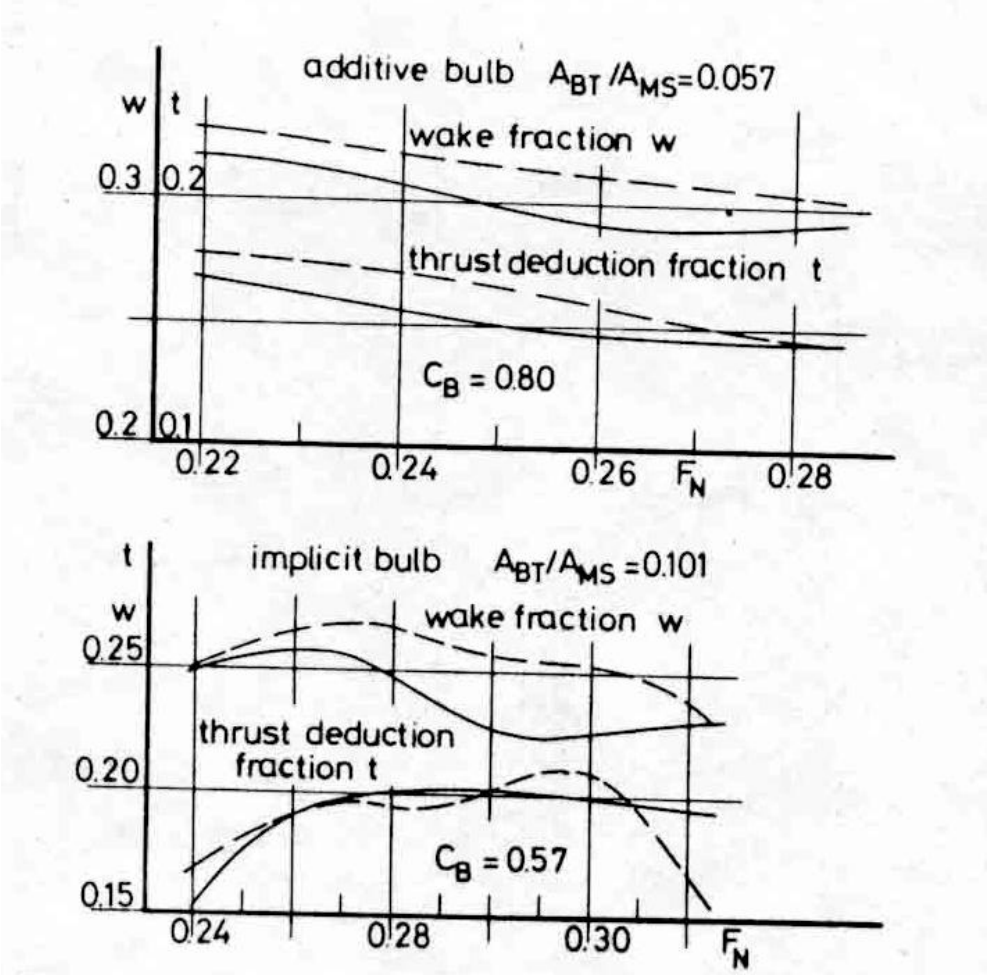

Figure n° 3.3: Influence of a bulbous bow on thrust deduction and wake fraction (---- with,_ _ without).

In addition the bulb has also an influence on the wake distributions in the propeller plane. The figure 3.4 represents the comparison of a radial distribution of axial wake components of ships with and without a bulb.

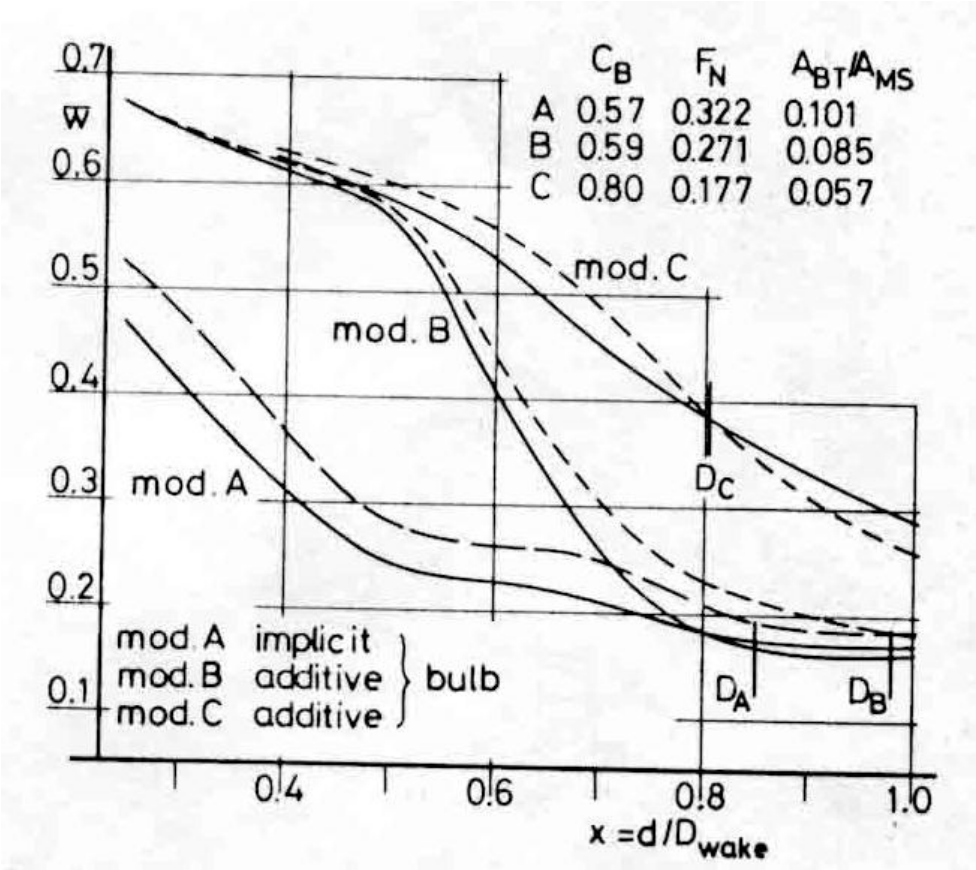

Figure n°3.4: Influence of a bulbous bow on the radial distribution of circumferential average nominal axial wake component (---- with,_ _ without).

3-4 Resistance and bulb effect:

As it's mentioned in the previous chapter that the bulb has a big influence on the ship resistance components, for better understanding this influence, the hydrodynamic phenomenon should be discussed, for this purpose the following subdivision of total resistance is used:

$$R_T = R_V + R_{WF} + R_{WB} = R_F + R_{VR} + R_{WF} + R_{WB} \quad (3.7)$$

Which, R_V is the viscous resistance, R_F is the frictional resistance, R_{VR} is the viscous residual resistance, R_{WF} is the wave making resistance, R_{WB} is the wave breaking resistance.
The contribution of the wave making resistance R_W to the total ship resistance is different for the ships; it depends on the form and speed, its reduction can be by the addition of the bulb.

In addition, the additional of the bulb surface always increase the frictional resistance R_F, but in the reanalysis of test data based on Froude's method, presented here, this point is of no account.

The bulb problem is a pure interference problem of the free wave systems of the ship and the bulb. Depending on phase difference and amplitudes, a total mutual cancellation of both interference wave systems may occur. The position of the bulb body causes the phase

difference, while its volume is related to the amplitude. The wave resistance is evaluated by analysis of the free wave patterns measured in model experiments [5].

The wave breaking resistance R_{WB} depends directly on the rising and development of free as well as local waves in the vicinity of forebody and is a question of typical spray phenomenon. R_{WB} includes all parts of the energy loss by the breaking of too-steep bow waves, this wave system consist mainly of the two back waves of bow and stern which are generated by deflection of the momentum. The deflection rate of the flow is a degree of the steepness of the back waves, of which only the bow wave is of a practical importance in bulb design [5].

The bulb effect can be discerned by taking the difference of the corresponding resistance components of the ship without (index 0) and with bulb (index w):

$$\Delta R_T = R_{T0} - R_{Tw} = \Delta R_V + \Delta R_{WF} + \Delta R_{WB} \qquad (3.8)$$

The difference of the wave resistance:

$$\Delta R_{WF} = R_{WF0} - R_{WFw} = \Delta R_{WI} + \Delta R_{Wb} \qquad (3.9)$$

It's the interference effect, which is equal to the sum of the interference resistance and the wave resistance of the bulb body alone.
The difference between the wave breaking resistances:

$$\Delta R_{WB} = R_{WB0} - R_{WBw} \qquad (3.10)$$

It's the breaking effect, which is the main contribution to the total bulb effect for full slow ships. Its contribution is the bigger the bulb, the better the deflection of the flow in the vicinity of the bow region. This means for the bulb form an optimal distributed bulb volume in the longitudinal direction to minimize gradients of the hull surface in the region of rising bow waves [5].

The difference between the viscous resistance parts:

$$\Delta R_V = R_{V0} - R_{Vw} = (R_{F0} - R_{Fw}) + (R_{VR0} - R_{VRw}) \qquad (3.11)$$

It's considering as the secondary effect of the bulb and in general cases is neglected.

3-5 influence of bulb parameters on bulb effect:

At constant Froude number F_N, the bulb effect is a function of all six bulb parameters:

$$\Delta R = f(C_{VPR}, C_{ABT}, C_{ABL}, C_{LPR}, C_{BB}, C_{ZB}) \qquad (3.12)$$

This multidimensional relationship is very complicate, because some parameters cannot vary independently, so the only way to know the relationship is the experimental test, unfortunately the systematic model experiment is too expansive.

The interference effect depends on the volumetric parameter $C_{VPR} = V_{PR} / V_{WL}$ in a quadratic manner. Also the breaking effect shows a similar dependence. Therefore with increasing bulb volume, both affect increase up to a maximum with a subsequent decrease.

For a constant bulb volume and depth, the length parameter $C_{LPR} = L_{PR} / L_{PP}$ has a great influence on the interference effect. The influence of the length parameter on the breaking effect can be caught intuitively by its mode of action. With increasing C_{LPR}, this effect increases at first and after a maximum decreases monotonically to zero, due to the fact that the deflection of momentum in the vicinity of the bow is hardly altered by a very long cylindrical bul. Because the lateral parameter is strongly related to the length parameter, its influence on the bulb effect is similar [5]. See figure 3.5.

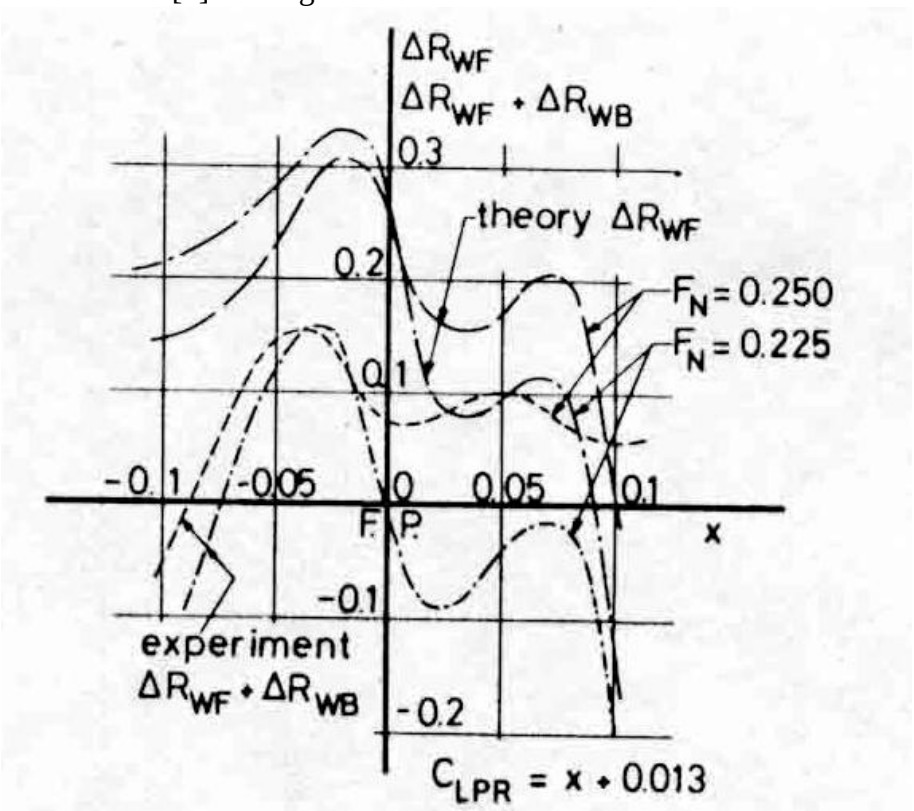

Figure n° 3.5: Dependence of interference and primary bulb effect on the length parameter $C_{LPR} = L_{PR}/L_{PP}$, Comparison of theory and experiment with an elementary ship of the form.

The dependence of the interference effect on the depth parameter $C_{ZB} = Z_B / T_{FP}$ is described simply by linear theory because the term Z_B of a spherical bulb coincides with the center of the sphere. If such a bulb of constant volume and longitudinal position is moved from infinite depth up to the water surface, the interferential effect increases at first monotonically from zero to a maximum, decreases subsequently, and finally becomes negative due to an increase of the resistance of the emerging bulb body. The breaking effect behaves similarly, but it can become positive again, if $Z_B > T_{FP}$, as with the ∇-Type, in this case the behavior of a ship-bulb combination is similar to a longer main hull increased in length by L_{PR} [5].

In addition to the previously influence of the bulb on the ship resistance, there is also the influence of the ship parameters on bulb parameters, but in this project is not the case as we have already the initial bulbous. So the idea in this project is to change the bulb parameters by the systematic method according to the influence of these parameters on the ship resistance in order to get an optimal bulb shape leads to a minimum resistance of the ship.

Chapter 04: Numerical simulation of ship resistance for a motor yacht.

4-1 Introduction:

In this chapter the ship resistance will simulate using the Starccm+ software, in order to estimate the accuracy of the calculation further the quality of the mesh. The result obtained from the numerical simulation will compared with the one obtained from the experimental test which is already tested by the company AZIMUT-BENETTI in the towing tank. The comparison between the experimental and numerical results will be only for one velocity of the ship which is the cruising speed. The maximum deference required by the company is about of 5 %.
Once the ship resistance computation is done, the bulb shape will modify according to the theory seen in the previous chapter in order to obtain a minimum ship resistance. In this case the systematic method will use as guidance to modify the bulb parameters. the optimal bulb shape will compare with the initial bulb shape.

4-2 STARCCM+ Software:

STAR-CCM+ provides the world's most comprehensive engineering physics simulation inside a single integrated package. Much more than just a CFD solver, STAR-CCM+ is an entire engineering process for solving problems involving flow (of fluids or solids), heat transfer and stress. It provides a suite of integrated components that combine to produce a powerful package that can address a wide variety of modeling needs. These components include [6]:

3D-CAD Modeler:

3D-CAD is a feature-based parametric solid modeler within STAR-CCM+ that allows geometry to be built from scratch. The geometry created with 3D-CAD is stored as 3D-CAD models, which can subsequently be converting to geometry parts for integration with the meshing and simulation process [6].

CAD Embedding:

STAR-CCM+ simulations can be set up, run and post-processed from within popular CAD and PLM environments such as SolidWorks, CATIA V5, Pro/ENGINEER and NX. STAR-CCM+’s unique approach will get you from CAD model to an accurate CFD solution more quickly or more reliably [6].

Surface Preparation Tools:

At the heart of STAR-CCM+ is an automated process that links a powerful surface wrapper to CD-adapco’s unique meshing technology. The surface wrapper significantly reduces the number of hours spent on surface cleanup and, for problems that involve large assemblies of complex geometry parts, reduces the entire meshing process to hours instead of days.

Physics Models:

The STAR-CCM+'s physics modeling capabilities include are:

Solvers: Segregated**,** Coupled and Finite volume solid stress

Time: Steady state**,** Implicit and explicit unsteady**,** Harmonic balance

Turbulence : RANS**,** RSM**,** LES/DDES and Laminar-turbulent transition

Compressibility**:** Ideal Gas**,** Real Gas.

Heat transfer: Conjugate Heat Transfer (CHT)**,** Multiband and grey thermal surface to surface radiation**,** solar radiation and discrete ordinates radiation (DOM) including participating media

Multiphase: Lagrangian particle tracking**,** VOF (incompressible and compressible)**,** Cavitation & boiling**,** Eulerian multiphase**,** De-icing & De-fogging and Melting & solidification

Moving Mesh: Dynamic Fluid Body Interaction (DFBI or 6DOF)**,** Rigid body motion**,** Mesh morphing and Multiple reference frames (MRF).

Combustion & chemical reaction: Reaction kinetics**,** Eddy break up (EBU)**,** Presumed probability density function (PPDF)**,** Complex chemistry**,** Ignition and NOx modeling.

Distributed Resistance (Porous media): Anisotropic**,** Orthotropic**,** User defined and Porous baffles.

Turbulence Modeling:

In addition to its provision for inviscid and laminar flow, STAR-CCM+ has a comprehensive range of turbulence models:
• k-epsilon (Standard, V2F, Realizable, Two-layer)
• k-omega (Standard, SST and BSL)
• Reynolds Stress (RSM – linear and quadratic)
• Spalart-Allmaras Turbulence models
• Boundary-layer transition
• Large Eddy Simulation (LES)
• Detached Eddy Simulation (DES, in the new Delayed Detached Eddy Simulation or DDES formulation)

Post-processing:

STAR-CCM+ has a comprehensive suite of post-processing tools designed to enable you to obtain maximum value and understanding from your CFD simulation. This includes scalar and vector scenes, streamlines, scene animation, numerical reporting, data plotting, import and export of table data, and spectral analysis of acoustical data [6].

CAE Integration:

Several third-party analysis packages can be coupled with STAR-CCM+ to further extend the range of possible simulations you can do. Co-simulation is possible using Abaqus, GT-Power, WAVE and OLGA, and file-based coupling is possible for other tools such as Radtherm, NASTRAN and ANSYS [6].

4-3 Methodology:

In the simulation, the ship considers fixed and the flow moves around the ship, the ship is free to one translation movement (Heave), and one rotation movement (Pitch).

Governing Equations:

In the simulation the flow is considered Newtonian; therefore the flow field satisfies the conservation of mass, momentum, and energy. In order to simplify the problem for the marine problems that it is possible to consider that the fluid is incompressible, viscous, and isothermal, because of the low Mach number and near to the constant temperature [7]. This simplification leads the use of the Navier-Stokes equations. See chapter 1.
STAR-CCM+'s multiphase segregated flow model is used to separate the governing equations for both the water and air.

Multiphase Flow Formulation:

It's known from the previous chapter that there is a resistance caused by the water and one caused by the air even if that is negligible comparing to the water resistance, in this condition the ship should be run in the too kind of fluids the heavy fluid (water) and the light fluid (air). Therefore the ship runs near to the free surface, which is the interface of air and water, so in the simulation should be no interaction between the two fluids, for this reason STARCCM+ uses the property of the mixture fluid (two phases) which is the volume of fluid method (VOF).

Linear wave (Airy Wave Theory):

The propagation of waves on the surface of a potential flow and above a horizontal bottom is linear. The free surface elevation η of one wave component with wave height H is sinusoidal, as a function of horizontal position x and time t:

$$\eta(x,t) = a\cos(kx - \omega t) = \frac{H}{2}\cos(kx - \omega t)$$

Where:
Wave number $k = 2\pi/\lambda$, Angular frequency $\omega = 2\pi/T$, and phase Speed $c_p = \omega/k = \lambda/T$.
The airy characteristics are: Periodic wave in space and time, Propagation along x>0, Constant depth h, Steepness of waves is small $H/\lambda << o(1)$ [8].

External forces and moment:

In the towing test, the model has been towed along the shaft line, this external force on the model test generate a moment on y axis and a forces in x and y direction. These force and moment have an influence on the result of the resistance.

In order to compare the results obtained from numerical simulation and real test, these external forces and moment should be added to the numerical model. The Starccm+ software allows the addition of external forces and moments acting on the 6-DOF body.

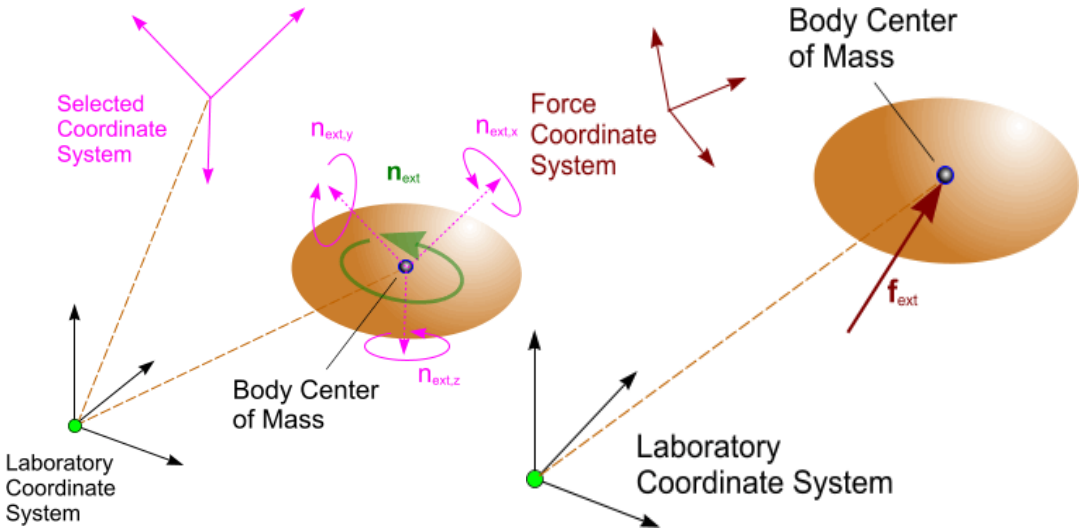

Figure n°4.1: External forces and moments acting on the ship model.

4-4 Computational Model:

Discretization of computational domain:

Since FVM method was selected as the numerical solver, a finite computational domain was determined. In the ship resistance simulation where the external flow, the domain defined by the principle dimensions of the ship model which listed in table 4.1.the hull model was delivered and provided by AZIMUT-BENETTI Company.

	Ship
WL	41.53 m
LPP	41.40 m
Beam	8.52 m
Design Draught	2.707 m
Design Speed	14 knots
Displacement	450 t

Table n° 4-1: Principle dimensions of the ship.

Figure n°4.2: Super Motor yacht.

The length of the ship is considered the main factor to determine the size of far field domain, and due to the symmetry of the ship, it's possible to simulate only half of the field in order to reduce the whole time computational and the result obtained should be multiplied by 2 to get a final result for whole model. See figure (4.3).

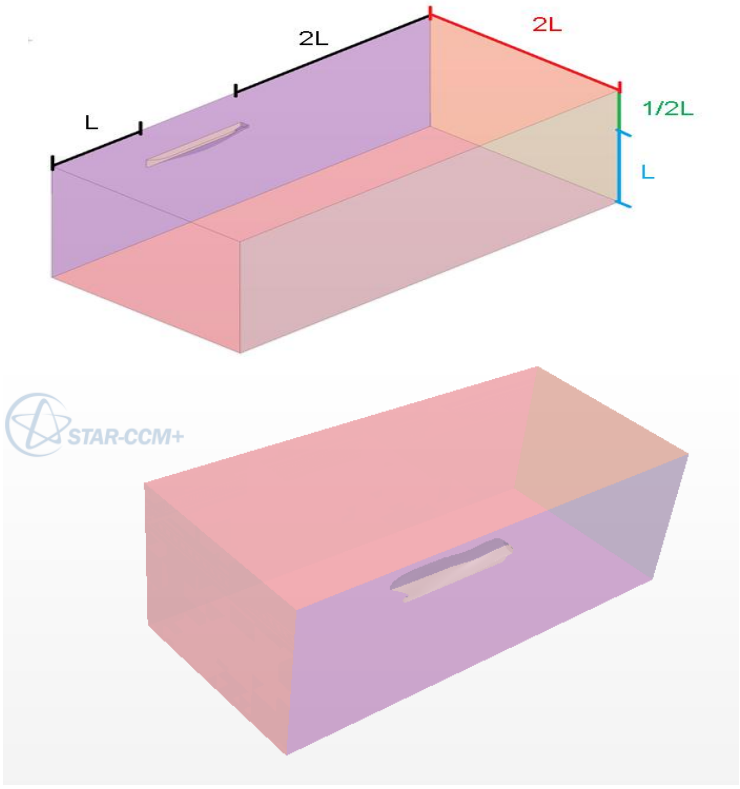

Figure n° 4.3: Dimensions of the computational domain.

Boundary conditions:

The computational domain defined before was defined by three type of boundaries. The first one is the velocity inlet, which is specifies a velocity on the front of the boundary; it's applied to the top part, side part, bottom part, and front part of the domain. The second boundary is pressure outlet specifies a hydrostatic pressure; it's applied to the after part of the domain. The third boundary is the Symmetry plan, which is applied to the symmetrical side.
The all boundaries conditions are shown in the figure 4.4:

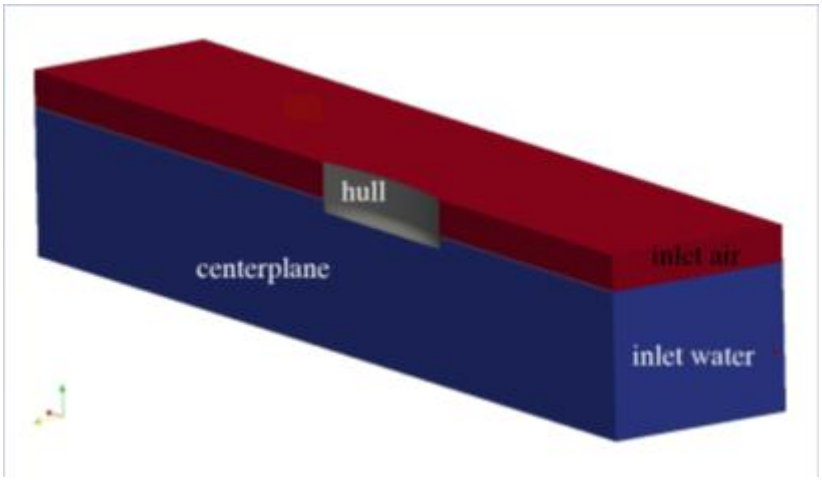

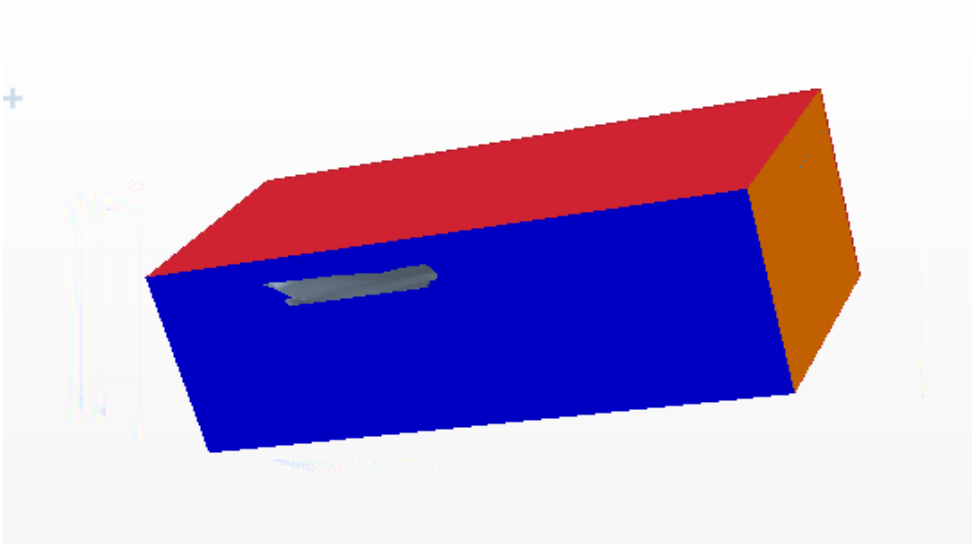

Figure n° 4.4: Boundary condition for the computational domain.

Grid generation:

Because the quality of the CFD analysis is mostly depends on the quality of generated mesh. The mesh (Grid) generation is the most important task and valid mesh generation is the most time consuming part in CFD analysis.

The automated meshing and surface mesh editing features in STAR-CCM+ were used to grid the numerical domain. The mesh model used is called a "Trimmer" mesh, which features hexagonal cells, and the prism layer mesher which is a mesh created around the surface mesh in order to accurately capture the viscous velocity gradient.

The grid of the domain is divided to two algorithms; the first one is the prism layer which is generated on the wall, where the first layer near to the wall is calculated by the formula below, in order to be capable to control the y+.

Using the friction coefficient correlation:

$$\frac{\overline{C_f}}{2} = \frac{0.036}{Re_L^{1/5}}$$

The definition of the friction coefficient is used to compute the wall shear stress:

$$\bar{C_f} = \frac{\tau_w}{\rho U^2/2} => \tau_w = \bar{C_f} * \rho U^2/2$$

The wall stress is used to compute u*:

$$u = \sqrt{\frac{\tau_w}{\rho}}$$

The y+ has been targeted, so:

$$y^+ = \frac{u^* y}{V} => y = \frac{V * y^+}{u^*}$$

The prism layer is shown in the figure below:

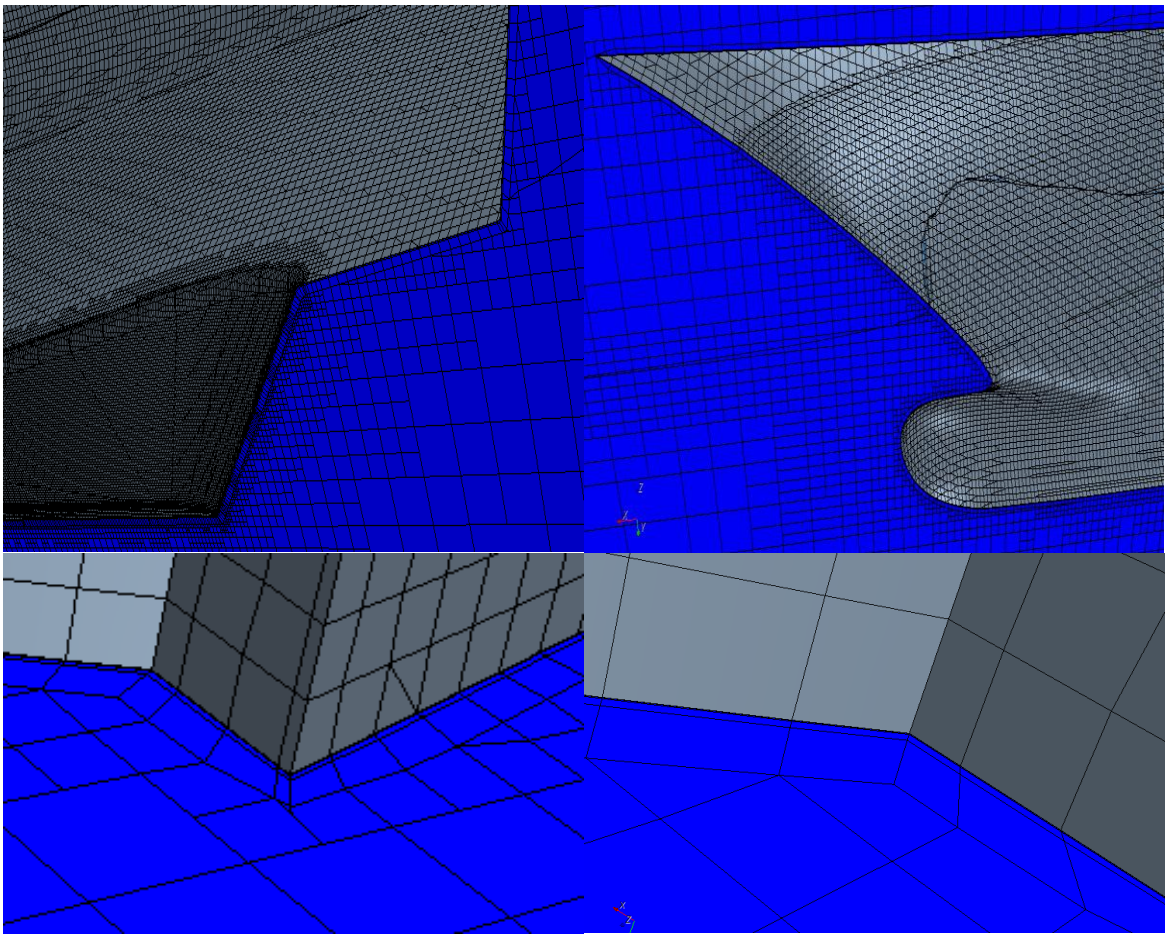

Figure n° 4.5: Prism layers near the hull.

The second part of the mesh domain is Cartesian grid, where the mesh is very fine near to the wall and starts to increase as the distance from the free surface and the ship increase. See figure below.

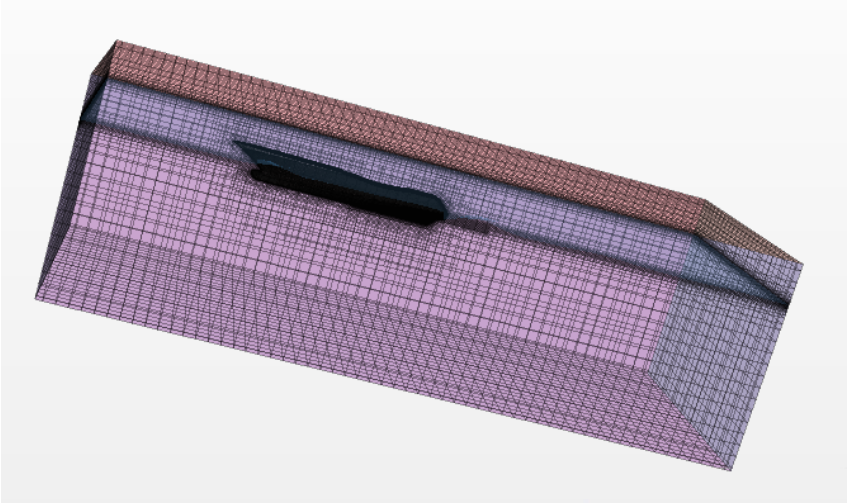

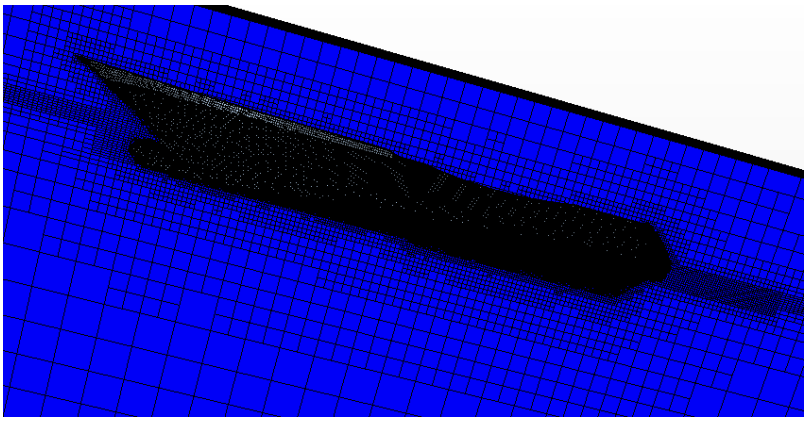

Figure n° 4.6: Mesh (Grid) of computational domain.

For these simulations the base size for the cells is 1.4 m, the cell characteristic length in the vicinity of the free surface is 0.35 m. the size of the cell increase as the distance from the hull increase starts with 1.4 m until reach the maximum size value which is 2.8m.
The prism layer has fore layers that increase in height further away from the surface mesh. The volume mesh for the viscous simulations is composed of about 1.6 million cells.

In addition, there are also the independents mesh which are the blocks (volume control) added on the hard (critical) part of the domain in order to get more refined mesh. Thus they were added on the bow and stern of the ship where there is a higher turbulent and separation flow and on the free surface where there is the wave elevation. See figure below.

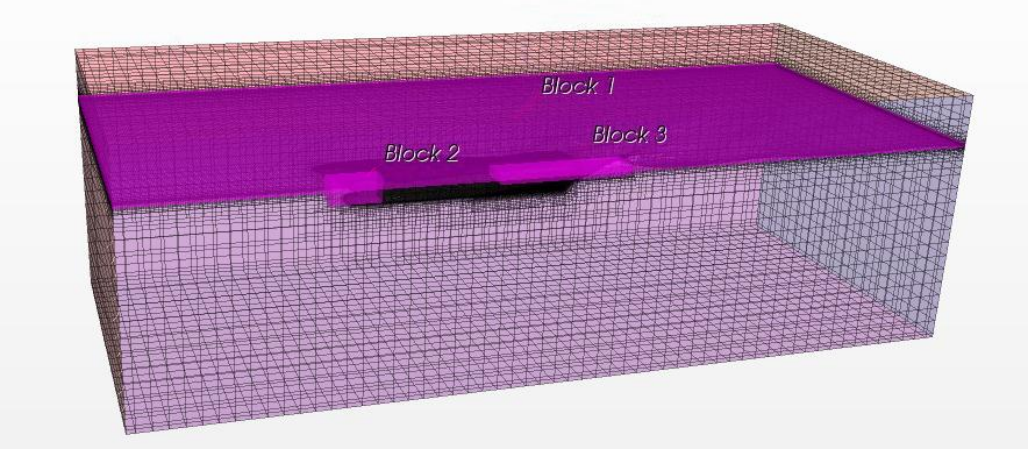

Figure n°4.7: Representation of the three mesh blocks.

In order to get a good mesh for the simulation several iterations have been tested, the table below shows the desired mesh of the control volumes.

Element	Cell Size [m]
Block 1	0.167
Block 2	0.167
Block 3	0.182

Table n° 4.2: Desired mes.

Rigid body motion:

In this simulation the six degrees of freedom (6-DOF) is used, in STAR-CCM+ the (6-DOF) allows the computational domain to move in any of the translational or rotational degrees of freedom. The solid body becomes able to react to both the natural forces (pressure, viscous and body forces) and to any user defined forces (external forces). Though the reaction to the forces on the body only is computed, the whole computational domain is moved to preserve the mesh. With this model, the domain moves with a body-centric local coordinate system while the flow remains moving relative to a global coordinate system.
This simulation has only two degrees of freedom enabled, translational heave and rotational pitch.

Temporal Discretization Solver:

The temporal discretization solver for this simulation is a first order implicit unsteady. With this model, solutions are found at each time step and marched through time. For these simulations, the number of the inner iterations between time steps is five.
The time step used for each of the simulations is governed by the Courant- Friedrichs-Lewy (CFL) number. The CFL number is defined in Equation below:

$$C = \frac{u\,\Delta t}{\Delta x}$$

Which; Δx is the grid sizing, U is the velocity, Δt is the time step, By limiting the time step size to give a CFL number of one or less, no more fluid enters a cell than is available in the upwind cell for each time step. Though simulations using a CFL number greater than one can give solutions, they are not time accurate.

Turbulence model:

There are several RANS turbulence models; each one is related to different problem. In this work the standard k-ε was selected.

4-5 Results:

4.5.1 Experimental results:

In order to check the ship resistance result obtained from the numerical simulation (STARCCM+), the result is compared with the one obtained from the towing tank.
The model was tested in Brodarski Institut- Zagreb. The results obtained for full scale ship resistance are shown in the table (4.3) and figure (4.8).

Figure n° 4.8: Model test in towing tank.

V (kn)	RT (kN)
8	13.4
9	18.3
10	24.4
11	31.8
12	40.5
13	50.9
14	63.9
15	83.5
16	114.1
17	155.6
18	204.1

Table n° 4.3: Results of towing tank test for full ship scale.

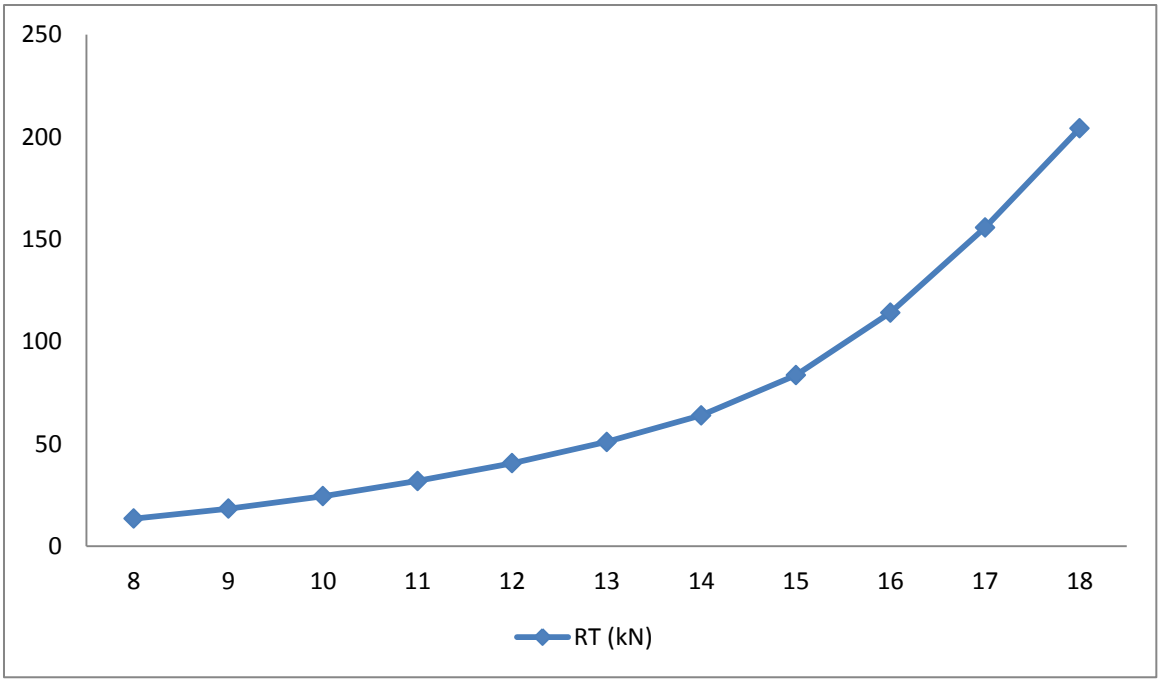

Figure n°: 4.9: The ship resistance curve as function of the velocity.

4.5.2 Result of ship resistance:

Assuming that the ship move in calm water, with a constant velocity (14kn), the result obtained from the numerical simulation can be exposed on the total Drag which will be compared with the experimental resistance.

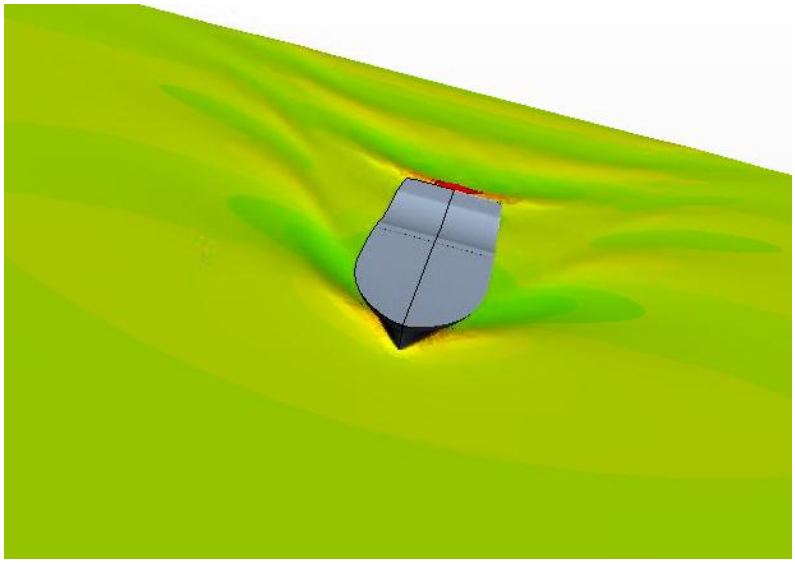

Figure n° 4.10: Model in STARCCM+.

Control of wall Y+:

In order to check the validity of the result obtained from the numerical simulation, it must control the wall Y+, as it's shown in the figure (4.11), the value of the wall Y+ respects the theory of the wall. See chapter 1.

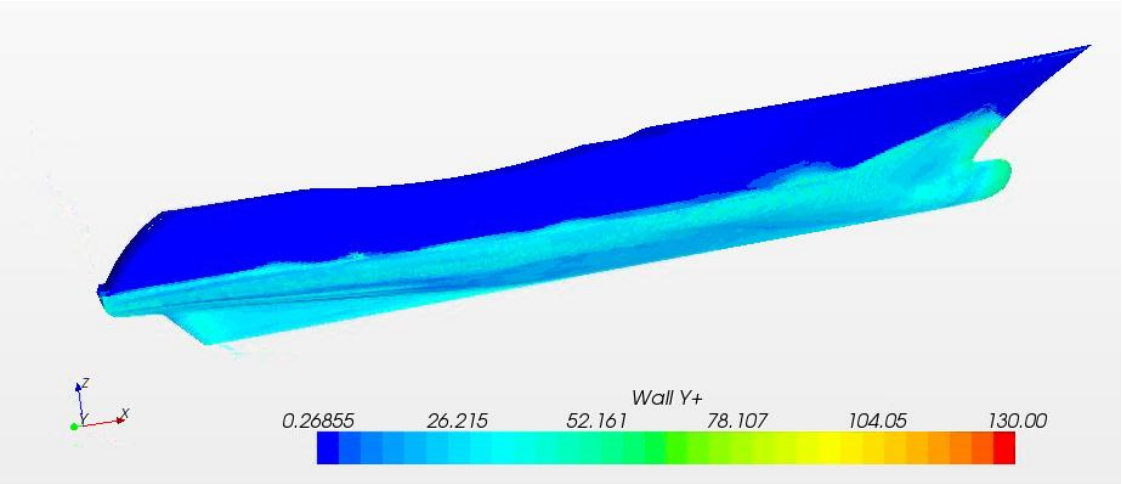

Figure n°4.11: The checking of the Value of wall Y+ on the hull.

Comparison of result:

The comparison between the towing tank test and the model tested in numerical simulation shown that the wave pattern generated by the both numerical and experimental model has the same shape, the same thing for the bow wave and stern wave. See figures below.

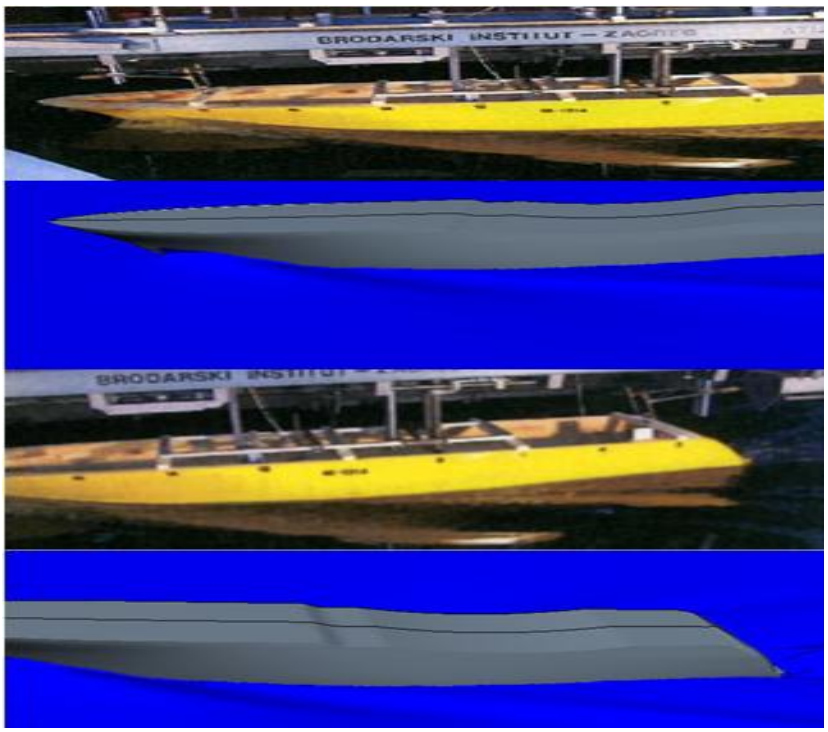

Figure n°4.12: Comparison of the waves generated by the ship moving between experimental and numerical test.

Comparison between experimental and numerical results:

The comparison between the values of the ship resistance obtained from the numerical simulation and from the experimental test is shown in the table below:

V (kn)	Numerical simulation(KN)	Experimental test(KN)	Deference
14	65.50	63.9	2.5%

It seen from the table above that the deference found is about of 2.5 %, which is accepted and confirmed by the company as they required about of 5%. This result proves the validity of the mesh. This mesh is desired to use for the next simulations.

4.5.3 Results of bulbous bow optimization:

Using the KRACHT theory mentioned in the chapter 3 which shown the influence of the bulbous parameters on ship resistance. The bulb geometry has been changed according to these parameters influence.

Using the software Rhinoceros to modify the bulbous shape, where the bulb is divided by transversal and longitudinal lines, and by using the control point property in Rhino, it's possible to modify the geometry of the bulb.
The longitudinal lines allowed the modification of the bulb geometry in longitudinal and vertical direction, and the transversal lines permitted to modify the volume of the bulbous bow. The figure below represents the control point on the bulb shape.

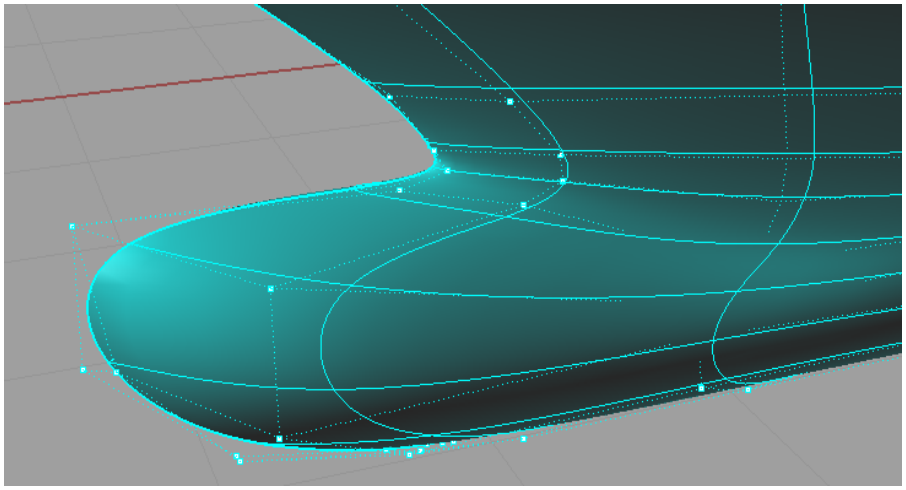

Figure n°4.13: Longitudinal and transversal curves defined the geometry of the bulb.

Since motor yachts are supposed to operate most of the time at cruise speed as mentioned before (*Fn = 0.35*.) It is obvious for the designer to optimize the bulb for this case.

As it's mentioned before that the systematic method is used in this project to modify the bulb geometry, the method is based on the modification of the bulb parameters then calculate the results for the ship resistance. This result will compare with the result obtained from the initial bulb shape in order to see the influence of the parameters on the bulb efficiency and on ship resistance in general. The all parameters of the bulb are detailed on the previous chapter.

The initial bulb dimensions are represented with the coefficients in the table below:

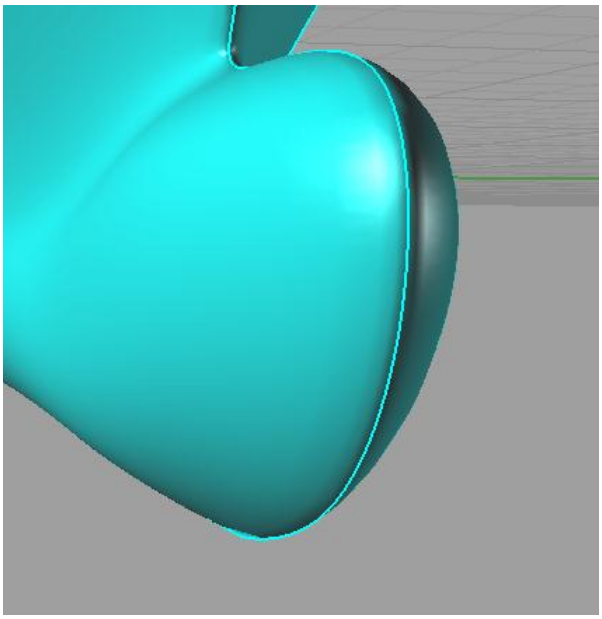

Initial bulb geometry coefficients	
C_{BB}	0.065
C_{LPR}	0.034
C_{ZB}	0.53
C_{VPR}	0.0027

Figure n°4.14: Initial bulb.

1- First bulb modification (Bulb Transversal Section modification):

In this simulation the bulb keep the same dimensions as the initial bulb (length and depth), the only one changed is the breadth parameter, which has been increased in order to increase the transversal section.

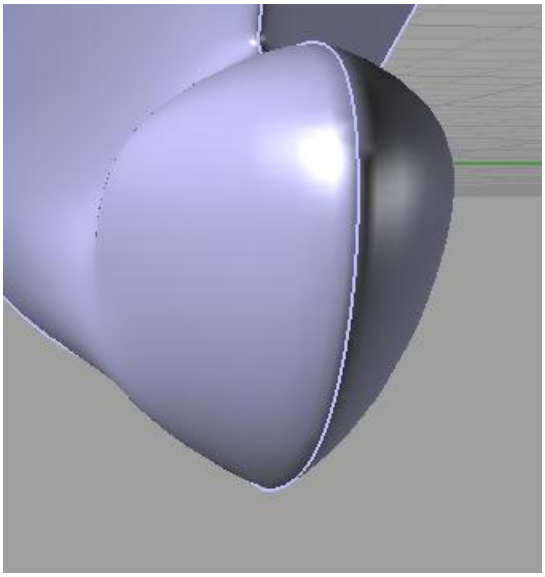

First bulb geometry coefficients	
C_{BB}	0.079
C_{LPR}	0.034
C_{ZB}	0.53
C_{VPR}	0.003

Figure n°4.15: The geometry of the first modification bulb.

The result obtained for the ship resistance from this simulation is shown in the table below:

V (kn)	Initial bulb resistance(KN)	Section bulb modification (KN)	Deference
14	65.50	65.73	0.4%

From the results it seen that there is no big difference between the resistances, which the deference is found about of 0.4 %. If we consider the error of calculation the value of the ship resistance doesn't change. From the comparison of the bulb parameters coefficient we see that the difference of the bulb volume between the initial bulb and the modify bulb is very small. Therefore we can deduce from this first test that the section modification doesn't have a big influence on the ship resistance (decrees ship resistance). Thus drive us to conclude that if we want to increase the transversal section further the volume according to the theory we have to increase the volume of the forward part of the bulb (forward the PPAV).

2- Second bulb modification (Bulb Depth parameter modification):

In this simulation, the bulb keep the same geometrics parameters (coefficients) as the initial bulb, the only parameter modified is depth parameter.

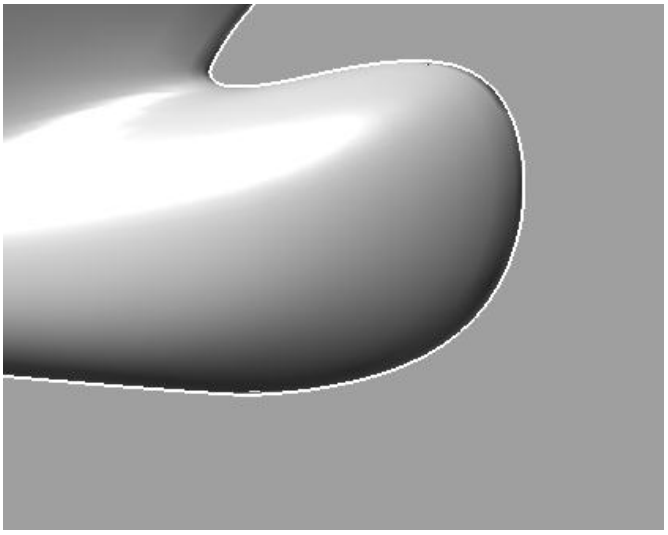

Second bulb geometry coefficients	
C_{BB}	0.065
C_{LPR}	0.034
C_{ZB}	0.64
C_{VPR}	0.0029

Figure n°4.16: The geometry of the second modification of the bulb.

The result obtained for the ship resistance from this bulb is shown in the table below:

V (kn)	Initial bulb resistance(KN)	Second bulb modification (KN)	Deference
14	65.50	67.74	2%

The resistance obtained from the modify bulb is more than the one obtained from the initial bulb. This result doesn't correspond to the KRACHT theory (Chapter 3) which is the increase of bulb depth decrease the ship resistance. Thus we conclude that the bulb depth has a link with the others geometries parameters of the bulb, if we want to increase the depth we should modify the others parameters. This will be check in the next simulations.

3- Third Modification (Bulb Length parameter):

In order to modify the bulb length, the KRACHT graph is used. See figure below.

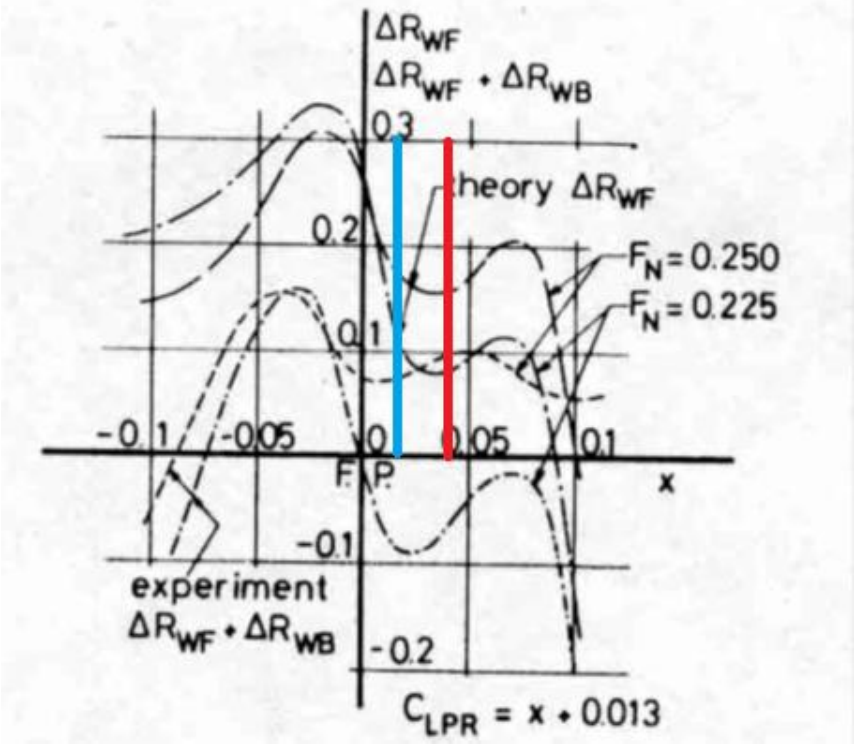

Figure n°4.17: Variation of the delta resistance as function of bulb's length coefficient.

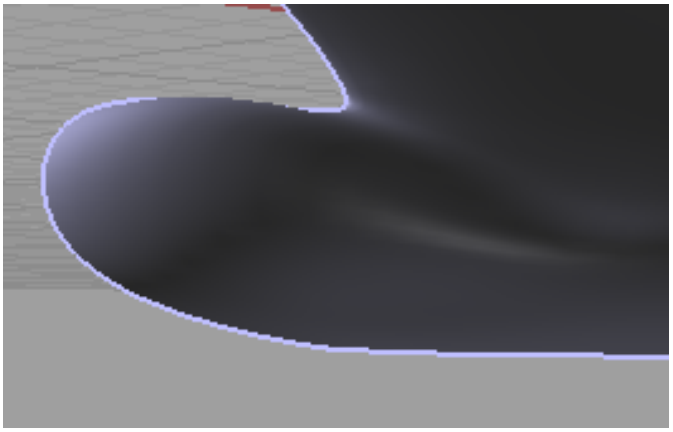

Third bulb geometry coefficients	
C_{BB}	0.79
C_{LPR}	0.055
C_{ZB}	0.64
C_{VPR}	0.0061

Figure n°4.18: The geometry of the third modify bulb.

The result obtained of the ship resistance from this simulation is shown in the table below:

V (kn)	Initial bulb resistance(KN)	Third bulb modification (KN)	Deference
14	65.50	66.90	2.2%

It seen from the table above that the increasing of bulb length increases the ship resistance which the difference has been found 2.2 %. In order to analyze this result, we have to get a look on the KRACHT graph in order to define which delta resistance correspond to the coefficient length chosen for this bulb. We can see in figure (4.17), that the delta resistance

correspond to the length coefficient of the initial bulb (blue line) is bigger than the value of length coefficient of the modify bulb (red line).
In addition, even that the bulb volume Increase according to the theory but the resistance doesn't decrease. Therefore we deduce that the bulb length has a big influence on the bulb efficiency.

4- Forth Bulb Modification (Length and Depth parameters):

In this test the length corresponds to the delta resistance less than delta resistance correspond to the initial bulb as the previous case, according to the theory the increase of the depth increase the resistance we increase the depth and we keep the same volume.

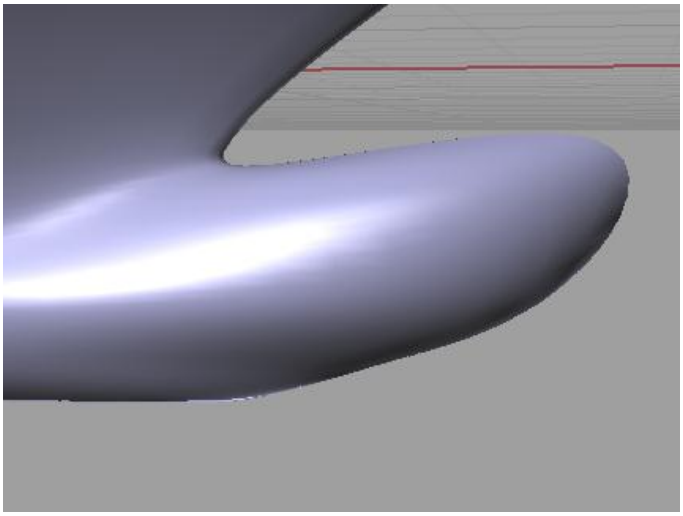

Forth bulb geometry coefficients	
C_{BB}	0.79
C_{LPR}	0.055
C_{ZB}	0.64
C_{VPR}	0.0061

Figure n°4.18: The geometry of the forth modified bulb.

V (kn)	Initial bulb resistance(KN)	forth bulb modification (KN)	Deference
14	65.5	67.24	2%

From the result obtained we deduce that even the depth increased according to the theory, but the resistance still increased. We conclude that the influence of the bulb length is bigger than the bulb depth. We will focus the next modification on the bulb length first then the volume and depth of the bulb.

5- Fifth Modification (Length coefficient Clrp =0.063 and Depth):

In order to check the influence of the volume parameter, we choose the bulb length correspond to the same delta resistance as the initial bulb. The volume bulb in forward part is small comparing to the initial bulb.

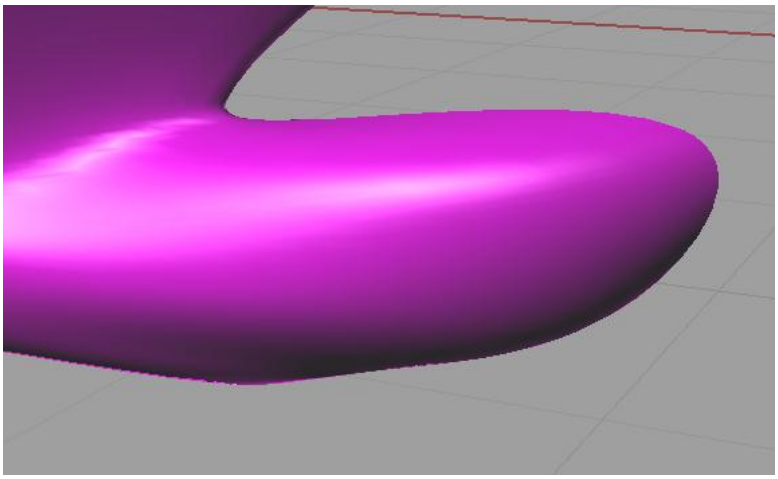

Fifth bulb geometry coefficients	
C_{BB}	0.065
C_{LPR}	0.063
C_{ZB}	0.65
C_{VPR}	0.0068

Figure n°4.19: The geometry of the fifth modified bulb.

V (kn)	Initial bulb resistance(KN)	Fifth bulb modification (KN)	Deference
14	65.5	66.61	1.7%

We conclude from the result obtained that even the length is correspond to the same delta resistance and the depth is the same as the initial bulb, but the resistance increase, therefore we conclude that the forward volume of the bulb has a big influence on the resistance and its existence is important. The next test will be with the same geometrical characteristics of the bulb with increasing the volume of the forward part of the bulb.

6- Sixth Modification (Length Clrp =0.063 + Depth+ Volume):

In this simulation the bulb keeps the same geometrical characteristics as the previous case; nevertheless the volume of the forward part of the bulb has been increased.

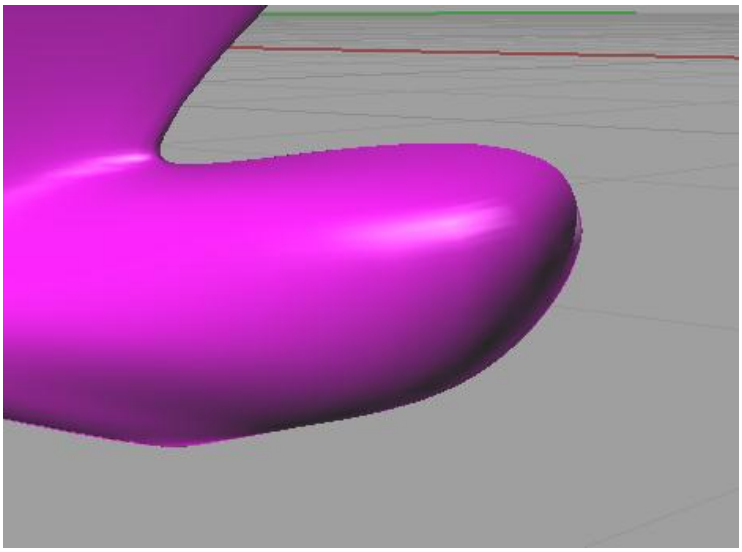

Sixth bulb geometry coefficients	
C_{BB}	0.065
C_{LPR}	0.063
C_{ZB}	0.65
C_{VPR}	0.0076

Figure n°4.20: The geometry of the sixth modified bulb.

V (kn)	Initial bulb resistance(KN)	sixth bulb modification (KN)	Deference
14	65.5	61.82	- 5.5 %

From the result we can see that the increasing of the volume at the same length and depth as the previous simulation the resistance decreases with 5.5%. From this we conclude that the result prove KRACHT theory.

7- Seventh Modification (Length Clpr=0.083 + Depth + Volume):

In order to get an optimized bulb; the bulb geometry in this test has been modified according to the KRACHT theory, where the length chosen corresponds to the maximum delta resistance and the volume and depth are increased in order to get more bulb efficiency.

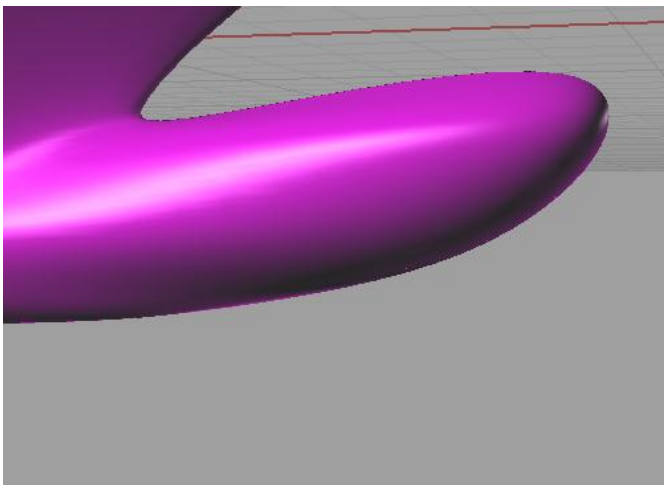

Seventh bulb geometry coefficients	
C_{BB}	0.065
C_{LPR}	0.063
C_{ZB}	0.70
C_{VPR}	0.012

Figure n°4.21: The geometry of the seventh modified bulb.

V (kn)	Initial bulb resistance(KN)	seventh bulb modification (KN)	Reduction
14	65.5	61.74	5.7 %

The result found is correspond to the KRACHT theory, where all the parameters increased by particular reference to the bulb length.

Conclusion:

We conclude from these simulations for different bulbs geometries that, first the review to the results obtained correspond for the each bulb modification geometry drives us to conclude that each parameter of the bulb geometry has an influence on the bulb efficiency, and each parameter has a degree effect on the bulb efficiency. The higher degree effect corresponds to the length parameter.

Second, there is a link between the all geometries parameters of the bulb; sometimes we cannot modify only one parameter. Therefore in order to get an optimal bulb we should modify all the bulb parameters.

4.6: Comparison between the optimum hull and the initial hull:

The characteristics geometry of the bulbs is shown in the tables below:

Seventh bulb geometry coefficients	
C_{BB}	0.065
C_{LPR}	0.063
C_{ZB}	0.70
C_{VPR}	0.012

Initial bulb geometry coefficients	
C_{BB}	0.065
C_{LPR}	0.034
C_{ZB}	0.53
C_{VPR}	0.0027

The results obtained from the optimization of the bulbous bow for about of 42 meters motor yacht are shown in figures 22, 23 and 24. This optimization leads to a substantial 5 to 6% reduction in total resistance relative to the non-optimized bulbous bow.

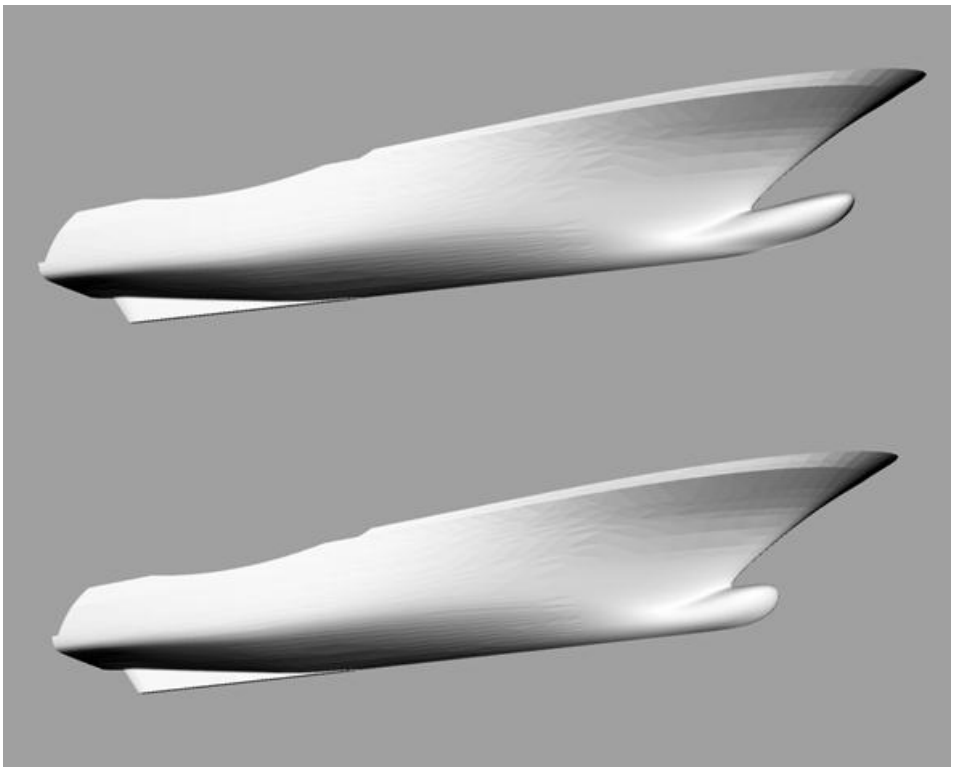

Figure n°4.22: Rendered view of the bulbous bow before (bottom) and after (top) optimization.

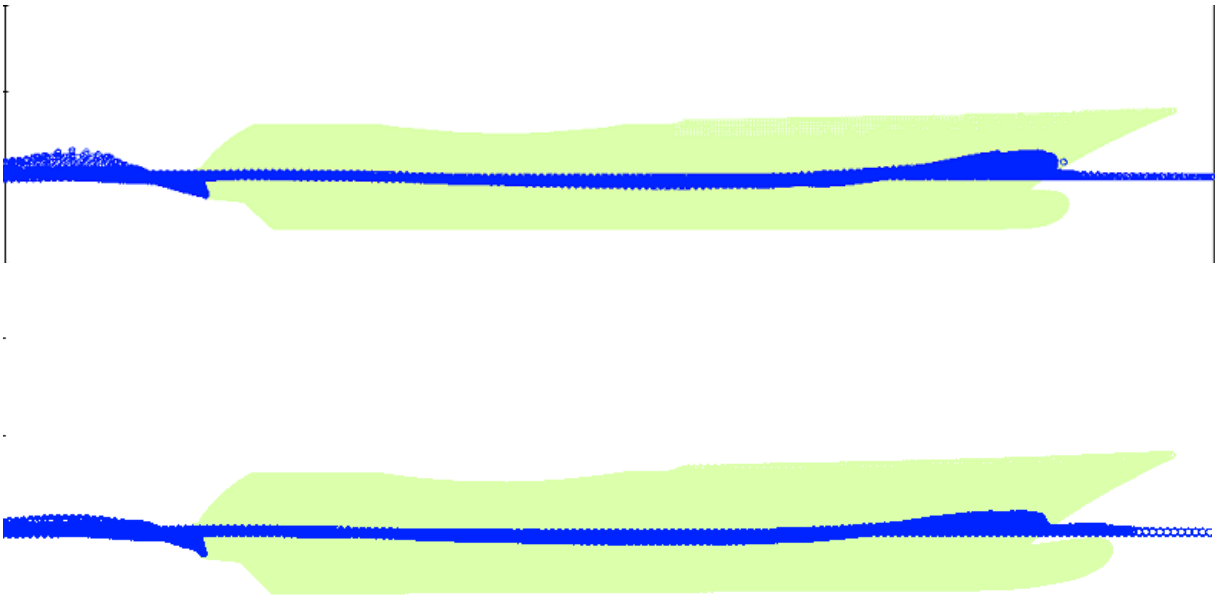

Figire n° 4. 23: Wave profiles along the optimized bulbous bow (bottom) and the bulbous bow before optimization (top).

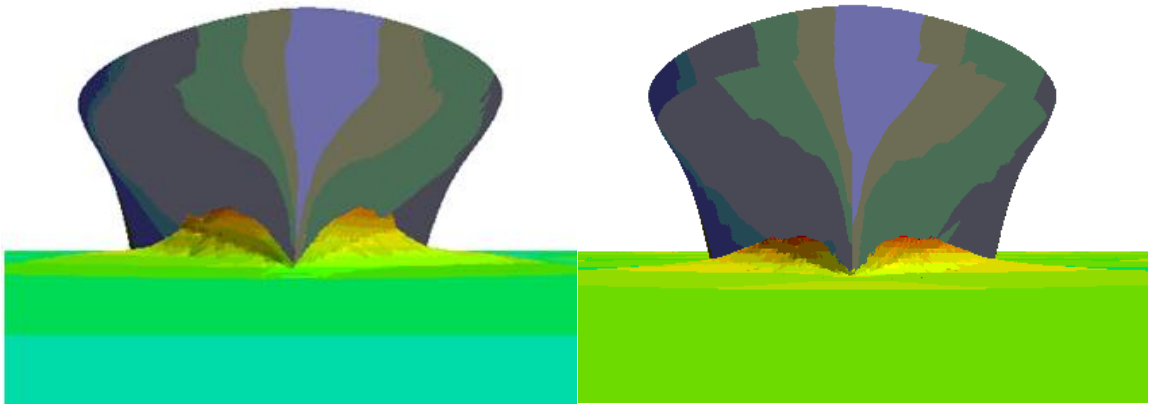

Figure n° 4.24 : CFD results for the bulbous bow optimization wave height, optimized bulbous bow (right), bulbous bow before optimization (lift).

The influence of the optimized bulbous bow on the bow wave can be clearly seen in the figure 23, 24. The optimum bulb generates a small height of wave bow comparing to the initial bulb.

The acceleration of the flow over the surface induces a low-pressure region which can extend towards the water surface. This Pronounced seen in the reduction of bow pressure wave due to the pressure field created by the bulb and the consequence the reduction of the bow wave effect further to reduction in wave making resistance.
In the figure 4.23 it seen that the optimum bulb reduces the height of the bow wave and wave stern comparing to the initial bulb.
The interference effect is considering the pure effect of the bulbous bow, if the bow and stern wave systems interact they can be phase of reinforcement or cancelation of the systems waves generated by the ship. In the case of the optimum bulb, the bulb changed the phase of the

wave and leads to the bow and stern wave systems cancel each other, and hence produce a minimum wave making resistance.

Conclusion:

This project is aimed at assessing the use of different hydrodynamic tools in hull shape optimization and in a larger ship design process. Current efforts have focused on validation, in order to provide confidence in the use of the tools, as well as the theory and method chosen for the optimization. Validation work has been performed for viscous flow analyses that are planned to use in the STARCCM+ software.

In order to optimize the ship resistance, the bulbous bow shape has been modified according to Kracht method. A demonstration of a shape optimization framework has been performed using the systematic method. The main geometrical parameters of the bulb have been modified and tested independently. The results of the shape optimization procedure demonstrated some improvements to the bow section that produced a reduction in total resistance of up to about 5.5%.

The results obtained from this optimization exposed indicate how the systematic method can be useful in design cycle as it's faster and less expensive comparing to the automatic optimization in case some guidance on the physical phenomenon is available. This is due to the fact that the guided systematic approach requires less computing time comparing to the traditional automatic optimization methods, e.g. genetic algorithms, since the solution is quickly found following the physical model provided by the guidance. Albeit that there is a deference between the results obtained from the both method systematic and automatic but in general cases is small.

The eventual goals of this effort are to be able to implement a hull form optimization strategy within the CFD technic to arrive more efficiently at an optimum solution and the determination of the influence of the geometrical parameters of the bulb on the wave making resistance then the total ship resistance which are; the length, volume (cross section area) and depth parameters of the bulb have a big effect on the efficiency of the bulb then the efficiency of the hull form.

Future work can be proposed in this field, such as a further optimization of the bulbous bow, further hull form improvement, optimization of resistance at each speed separately, with different types of bulb in order to determine which kind of bulb has a big efficiency in reducing the ship resistance.

ACKNOWLEDGMENTS:

I express my profound sense of gratitude to **Prof: Dario Boote** and **Prof: Marco Ferrando,** "University of Genova", for giving permission to undertake this project work in Hydrodynamic and optimization and for their constants guidance and encouragement in the preparation of this work.
I wish to express my sincere thanks to: Prof: E.Canippa, university of La Spezia. Ms P.Tatiana, Mr M.Davide. And many thanks for Mr F.Gelbirto, Mss.V.Giovanna and Mr S.Francesco, AZIMUT-VARRAZE, for their guidance and permitting to do the work in their office.

Reference:

[1] The maritime engineering reference book (a guide to ship design, construction and operation) edited by : ANTHONY F.MOLLAND.
[2] Chapter 7 Resistance and Powering of Ships - ITS - Open Content
[3] A study into the techniques needed to accurately predict skin friction using RANS solvers with validation against Froude's historical flat plate experimental data. by J.C.D Date and S.R.Turnock.[Ship science report no 114 University of Southampton March 1999].
[4] Hydrodynamics in ship design volume one by Harold, E.Saunders.
[5]: design of bulbous bow, *Alfred M.Kracht*
[6] USER GUIDE STAR-CCM+ Version 6.04.016
[7] Numerical Simulation of Added Resistance in Head Waves for a Container Ship Tsung-Yueh Lin , Po-Wen Wang , Jen-Shiang Kouh *Department of Engineering Science and Ocean Engineering National Taiwan University.*
[8] Lecture of Water Waves and Sea State Models for Ship Design for EMSHIP student Ecole Centrale De Nantes.
[9] Use of CFD in Design: *A Tutorial Sean M. McGu_e, P.E. Michael A. Porter, P.E. Thomas T. Hirst*